CHALMERS
UNIVERSITY OF TECHNOLOGY

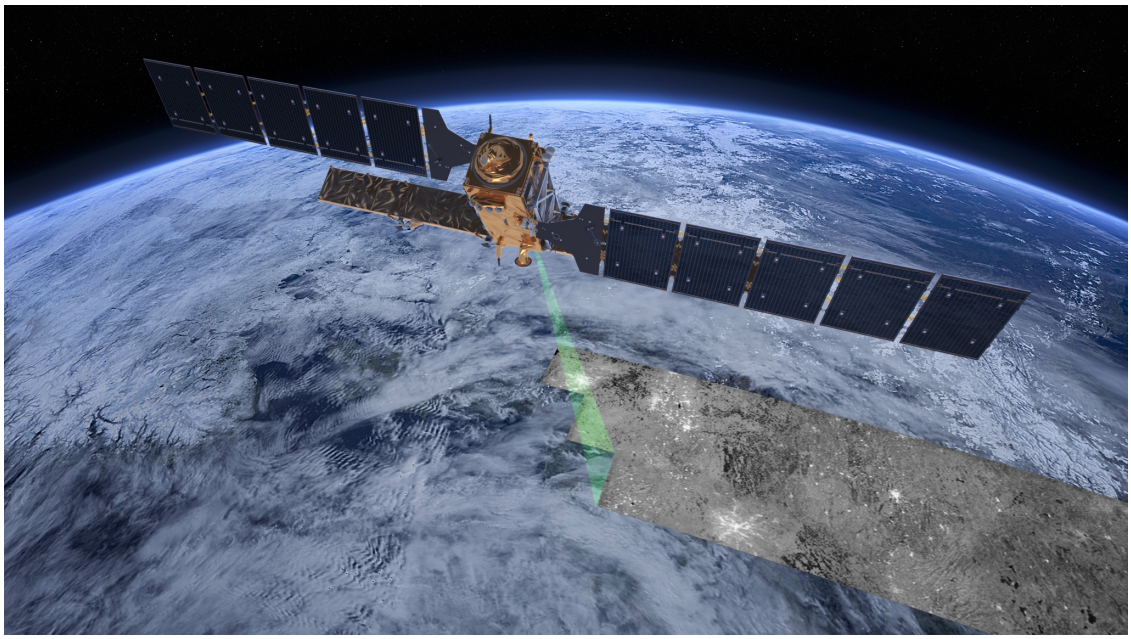

Linear and nonlinear mapping of sea surface waves imaged by synthetic aperture radar

Master's Thesis in Communication Engineering

Eltjon Qefalija

SPACE, EARTH AND ENVIRONMENT

CHALMERS UNIVERSITY OF TECHNOLOGY
Gothenburg, Sweden 2025
www.chalmers.se

Master's Thesis 2025

Linear and nonlinear mapping of sea surface waves imaged by synthetic aperture radar

Eltjon Qefalija

CHALMERS
UNIVERSITY OF TECHNOLOGY

Department of Space, Earth and Environment
Chalmers University of Technology
Gothenburg, Sweden 2025

Linear and nonlinear mapping of sea surface waves imaged by synthetic aperture radar
Eltjon Qefalija

Supervisor: Anis El Youncha, Space, Earth and Environment
Examiner: Leif Eriksson, Space, Earth and Environment

Master's Thesis 2025
Department of Space, Earth and Environment
Chalmers University of Technology
SE-412 96 Gothenburg
Sweden
Telephone +46 31 772 1000

Cover: Satellite scanning the earth's surface with the usage of Synthetic Aperture Radar.

Typeset in LaTeX
Gothenburg, Sweden 2025

Linear and nonlinear mapping of sea surface waves imaged by synthetic aperture radar

ELTJON QEFALIJA
Department of Space, Earth and Environment
Chalmers University of Technology

Abstract

Ocean observation is a powerful tool for ocean monitoring of sea surfaces. With the help of SAR it becomes easier to monitor large wave fields. The purpose of this project is to provide a simulator which when given the wind speed and wind direction, to generate the ocean wave field equivalent to those parameters, to simulate the SAR image, and finally to provide the transform for the linear, quasilinear, and nonlinear mapping. In the simulation, an analysis is performed on the validity of the three transforms, where different wind speeds, wind directions, and Slant Range-Velocity ratios β are used. The results, show that the linear and quasilinear transforms can be used when the value is β is low. On the other hand, the nonlinear transform can always be used, in many different scenarios. Remaining work to be done is an inversion algorithm to extract the ocean parameters from the SAR spectrum, an analysis of the effect of the ocean currents and finally the analysis of nonlinear waves.

Keywords: RAR, SAR, Oceanography, Simulation, Wind, radar, ocean, waves.

Acknowledgements

I would like to thank my supervisor Anis El Youncha for his continuous support and feedback throughout the whole project.

I want to also thank my examiner Leif Eriksson for his service as my examiner.

Finally, I am grateful to my family and friends for being next to me during both this semester and my whole student life.

Eltjon Qefalija, Gothenburg, August 2024

List of Acronyms

Below is the list of acronyms that have been used throughout this thesis listed in alphabetical order:

PM	Pierson Moskowitz
JONSWAP	Joint North Sea Wave Project
FFT	Fast Fourier Transform
RAR	Real Aperture Radar
SAR	Synthetic Aperture Radar
VV	Vertical Polarization
HH	Horizontal Polarization

Nomenclature

Below is the nomenclature of indices, sets, parameters, and variables that have been used throughout this thesis.

Parameters

k	Wavenumber
k_x	Azimuth Wavenumber
k_y	Range Wavenumber
ϕ	Wind direction
$V_{19.5}$	Wind speed at 19.5 meters
f	Radar frequency
λ	Radar wavelength
θ	Radar incidence angle
ρ	Spatial resolution
ρ_a	Azimuth resolution
ρ_r	Range resolution
H	Radar platform height
V	Radar platform velocity
β	Slant Range-Velocity ratio

Variables

S	Omnidirectional Spectrum
D	Spreading Function
Ψ	Directional Spectrum
A	Amplitude at index
Φ_{sea}	Fluid velocity potential

Z_{sea}	Elevation
u_r	Orbital velocity
T_k^{tilt}	Tilt modulation transfer function
T_k^{hydr}	Hydrodynamic modulation transfer function
T_k^{rb}	Range bunching modulation transfer function
T_k^{vb}	Velocity bunching modulation transfer function
T_k^u	Orbital velocity modulation transfer function (NOT DEFINED)
T_k^R	Real aperture radar modulation transfer function
T_k^S	Synthetic aperture radar modulation transfer function
σ_0	Average normalized radar cross section
ζ_k	Surface elevation in frequency domain
σ	Normalized radar cross section
$T(\cdot)$	Complex scattering function
ρ'_a	Degraded azimuth resolution
T_0	Integration time
τ_s	Coherence time
R	Range distance between the antenna and the surface
I	Intensity
I_n	Intensity with speckle noise
$f^u(r)$	Orbital velocity covariance
$f^R(r)$	RAR image covariance
$f^uR(r)$	Orbital velocity and RAR image crosscovariance
P_1^S	Linear Mapping
P_ql^S	Quasi-Linear Mapping
P^S	Non-Linear Mapping

Contents

List of Acronyms **ix**

Nomenclature **xi**

List of Figures **xvii**

List of Tables **xxi**

1 Introduction **1**
1.1 Purpose . . . 2
1.2 Limitations . . . 2
1.3 Thesis Outline . . . 2

2 Theory **3**
2.1 Ocean Waves . . . 3
2.1.1 Models . . . 3
2.1.1.1 Omnidirectional Spectra . . . 3
2.1.1.2 Spreading Functions . . . 6
2.1.2 Ocean Surface . . . 8
2.1.3 Ocean Surface Orbital Velocity . . . 9
2.2 SAR Imaging . . . 9
2.2.1 Modulation Transfer Functions . . . 10
2.2.1.1 Tilt Modulation . . . 11
2.2.1.2 Hydrodynamic Modulation . . . 11
2.2.1.3 Range Bunching . . . 11
2.2.1.4 Orbital Velocity . . . 11
2.2.1.5 Velocity Bunching . . . 11
2.2.1.6 Real Aperture Radar . . . 12
2.2.1.7 Synthetic Aperture Radar . . . 12
2.2.2 RAR Image . . . 12
2.2.3 SAR Image . . . 12
2.3 SAR Image Mapping . . . 13
2.3.1 Covariance Functions . . . 13
2.3.2 Linear Mapping of SAR Image . . . 14
2.3.3 Quasi-Linear Mapping of SAR Image . . . 14
2.3.4 Non-Linear Mapping of SAR Image . . . 14

3 Methods **15**
3.1 Parameters . . . 15
3.2 Wave Sield Simulation using The Fast Fourier Transform . . . 16
3.2.1 Ocean Surface with FFT . . . 16
3.2.2 Ocean Surface Orbital Velocity with FFT . . . 16
3.3 Verification of the ocean wave field generation . . . 17
3.4 Speckle Noise . . . 17
3.5 Simulator . . . 17
3.5.1 Environment . . . 17
3.5.2 Algorithm . . . 17

4 Results **19**
4.1 The necessity of the nonlinear mapping . . . 19
4.1.1 Case 1 . . . 20
4.1.2 Case 2 . . . 21
4.1.3 Case 3 . . . 22
4.1.4 Case 4 . . . 23
4.1.5 Case 5 . . . 24
4.1.6 Discussion . . . 25
4.2 Varying Wind Speed . . . 25
4.2.1 Case 6 . . . 25
4.2.2 Case 7 . . . 26
4.2.3 Discussion . . . 27
4.3 Varying Wind Direction . . . 27
4.3.1 Case 8 . . . 28
4.3.2 Case 9 . . . 29
4.3.3 Case 10 . . . 30
4.3.4 Discussion . . . 31
4.4 Varying β . . . 31
4.4.1 Case 11 . . . 31
4.4.2 Case 12 . . . 32
4.4.3 Discussion . . . 33

5 Conclusion **35**
5.1 Future Work . . . 35

A Appendix 1 **I**
A.1 Case A1 . . . I
A.2 Case A2 . . . II
A.3 Case A3 . . . III
A.4 Case A4 . . . IV
A.5 Case A5 . . . V
A.6 Case A6 . . . VI
A.7 Case A7 . . . VII
A.8 Case A8 . . . VIII
A.9 Case A9 . . . IX
A.10 Case A10 . . . X

A.11 Case A11 XI
A.12 Case A12 XII
A.13 Case A13 XIII
A.14 Case A14 XIV
A.15 Case A15 XV
A.16 Case A16 XVI
A.17 Case A17 XVII
A.18 Case A18 XVIII
A.19 Case A19 XIX
A.20 Case A20 XX
A.21 Case A21 XXI
A.22 Case A22 XXII
A.23 Case A23 XXIII
A.24 Case A24 XXIV
A.25 Case A25 XXV
A.26 Case A26 XXVI
A.27 Case A27 XXVII

List of Figures

2.1 Pierson Moskowitz Spectrum 5
2.2 JONSWAP Spectrum 5
2.3 Elfouhaily Spectrum 6
2.4 Simple Cosine Spreading Function 7
2.5 Longuet Higgins Spreading Function 8
2.6 Elfouhaily Spreading Function 8
2.7 SAR Setup 10
2.8 Coherence time for different wind speeds and frequencies 13

4.1 Case 1 Ocean Surface with SAR Images 20
4.2 Case 1 Plots of spectra 20
4.3 Case 2 Ocean Surface with SAR Images 21
4.4 Case 2 Plots of spectra 21
4.5 Case 3 Ocean Surface with SAR Images 22
4.6 Case 3 Plots of spectra 22
4.7 Case 4 Ocean Surface with SAR Images 23
4.8 Case 4 Plots of spectra 23
4.9 Case 5 Ocean Surface with SAR Images 24
4.10 Case 5 Plots of spectra 24
4.11 Case 6 Ocean Surface with SAR Images 25
4.12 Case 6 Plots of spectra 26
4.13 Case 7 Ocean Surface with SAR Images 26
4.14 Case 7 Plots of spectra 27
4.15 Case 8 Ocean Surface with SAR Images 28
4.16 Case 8 Plots of spectra 28
4.17 Case 9 Ocean Surface with SAR Images 29
4.18 Case 9 Plots of spectra 29
4.19 Case 10 Ocean Surface with SAR Images 30
4.20 Case 10 Plots of spectra 30
4.21 Case 11 Ocean Surface with SAR Images 31
4.22 Case 11 Plots of spectra 32
4.23 Case 12 Ocean Surface with SAR Images 32
4.24 Case 12 Plots of spectra 33

A.1 Case A1 Ocean Surface with SAR Images I
A.2 Case A1 Plots of spectra II
A.3 Case A2 Ocean Surface with SAR Images II

A.4 Case A2 Plots of spectra III
A.5 Case A3 Ocean Surface with SAR Images III
A.6 Case A3 Plots of spectra IV
A.7 Case A4 Ocean Surface with SAR Images IV
A.8 Case A4 Plots of spectra V
A.9 Case A5 Ocean Surface with SAR Images V
A.10 Case A5 Plots of spectra VI
A.11 Case A6 Ocean Surface with SAR Images VI
A.12 Case A6 Plots of spectra VII
A.13 Case A7 Ocean Surface with SAR Images VII
A.14 Case A7 Plots of spectra VIII
A.15 Case A8 Ocean Surface with SAR Images VIII
A.16 Case A8 Plots of spectra IX
A.17 Case A9 Ocean Surface with SAR Images IX
A.18 Case A9 Plots of spectra X
A.19 Case A10 Ocean Surface with SAR Images X
A.20 Case A10 Plots of spectra XI
A.21 Case A11 Ocean Surface with SAR Images XI
A.22 Case A11 Plots of spectra XII
A.23 Case A12 Ocean Surface with SAR Images XII
A.24 Case A12 Plots of spectra XIII
A.25 Case A13 Ocean Surface with SAR Images XIII
A.26 Case A13 Plots of spectra XIV
A.27 Case A14 Ocean Surface with SAR Images XIV
A.28 Case A14 Plots of spectra XV
A.29 Case A15 Ocean Surface with SAR Images XV
A.30 Case A15 Plots of spectra XVI
A.31 Case A16 Ocean Surface with SAR Images XVI
A.32 Case A16 Plots of spectra XVII
A.33 Case A17 Ocean Surface with SAR Images XVII
A.34 Case A17 Plots of spectra XVIII
A.35 Case A18 Ocean Surface with SAR Images XVIII
A.36 Case A18 Plots of spectra XIX
A.37 Case A19 Ocean Surface with SAR Images XIX
A.38 Case A19 Plots of spectra XX
A.39 Case A20 Ocean Surface with SAR Images XX
A.40 Case A20 Plots of spectra XXI
A.41 Case A21 Ocean Surface with SAR Images XXI
A.42 Case A21 Plots of spectra XXII
A.43 Case A22 Ocean Surface with SAR Images XXII
A.44 Case A22 Plots of spectra XXIII
A.45 Case A23 Ocean Surface with SAR Images XXIII
A.46 Case A23 Plots of spectra XXIV
A.47 Case A24 Ocean Surface with SAR Images XXIV
A.48 Case A24 Plots of spectra XXV
A.49 Case A25 Ocean Surface with SAR Images XXV

A.50 Case A25 Plots of spectra XXVI
A.51 Case A26 Ocean Surface with SAR Images XXVI
A.52 Case A26 Plots of spectra XXVII
A.53 Case A27 Ocean Surface with SAR Images XXVII
A.54 Case A27 Plots of spectra XXVIII

List of Tables

3.1 Ocean surface parameters 15
3.2 Radar platform parameters 15

4.1 Common Ocean surface parameters 19
4.2 Common Radar platform parameters 19
4.3 Case 1 parameters 20
4.4 Case 2 parameters 21
4.5 Case 3 parameters 22
4.6 Case 4 parameters 23
4.7 Case 5 parameters 24
4.8 Case 6 parameters 25
4.9 Case 7 parameters 26
4.10 Case 8 parameters 28
4.11 Case 9 parameters 29
4.12 Case 10 parameters 30
4.13 Case 11 parameters 31
4.14 Case 12 parameters 32

A.1 Case A1 parameters I
A.2 Case A2 parameters II
A.3 Case A3 parameters III
A.4 Case A4 parameters IV
A.5 Case A5 parameters V
A.6 Case A6 parameters VI
A.7 Case A7 parameters VII
A.8 Case A8 parameters VIII
A.9 Case A9 parameters IX
A.10 Case A10 parameters X
A.11 Case A11 parameters XI
A.12 Case A12 parameters XII
A.13 Case A13 parameters XIII
A.14 Case A14 parameters XIV
A.15 Case A15 parameters XV
A.16 Case A16 parameters XVI
A.17 Case A17 parameters XVII
A.18 Case A18 parameters XVIII
A.19 Case A19 parameters XIX

A.20 Case A20 parameters XX
A.21 Case A21 parameters XXI
A.22 Case A22 parameters XXII
A.23 Case A23 parameters XXIII
A.24 Case A24 parameters XXIV
A.25 Case A25 parameters XXV
A.26 Case A26 parameters XXVI
A.27 Case A27 parameters XXVII

1

Introduction

Knowledge of the ocean's conditions has been of high importance for millennia. Such cases are for the safety of the coastal areas, ship navigation, marine energy exploitation or weather prediction. Moreover, most of the momentum exchange between the ocean and the atmosphere is done through locally wind-generated waves. Water vapour and gases are impacted along them.

We can get to know of the ocean's conditions through ocean wave parameters which provide us with mathematical values with which the ocean waves are represented. These parameters are usually estimated through in-situ buoys and coastal radars which provide us with measured samples. While these two methods provide us with quite accurate local measurements, they are sparse. This means that it is not possible for us to measure wide areas, since they are difficult to move wherever we want. One way for us to bypass this problem is using satellite born radars. Particularly, in our case we are going to use synthetic aperture radars (SAR), which enable us to measure wide area, and without cost since they are already in use.

Satellite oceanography has been complemented by synthetic aperture radars (SAR) in the recent decades and has seen many studies. While they are helpful, it is not often possible for researchers to completely interpret the images.

There have been multiple studies on describing and modeling sea waves. Pierson and Moskowitz first tried to estimate the spectra of fully developed wind seas, but concluded that more data needed to be collected for more refinement of the accuracy [1]. Much later the Joint North Sea Wave Project (JONSWAP) gave an even more accurate description of the spectra, analyzing both long and short waves [2]. Finally, the most accurate description of both the spectra and the spreading of the sea waves came from T. Elfouhaily, B. Chapron, K. Katsaros, D. Vandemark [3].

Until the 1900s the two dimensional wave spectrum had been measured only with wave buoys inside the ocean. Monte-Carlo mapping computations were first used for nonlinear imaging of one-dimensional ocean wave fields [4]. Despite the valuable results of the simulations, many important properties of the two-dimensional ocean wave fields were missing. Two-dimensional Monte Carlo simulations had been used to compare a buoy and SAR image spectra obtained over the North Sea [5]. This change when Hasselmann provided us with complete formulas of mapping a sea surface to a SAR wave spectrum and many studies are based on those formulas [6].

1.1 Purpose

The purpose of this thesis is to develop a complete simulator which given sea condition parameters like wind speed and wind direction, and radar platform configurations like velocity and signal parameters to analyze in which conditions the linear, quasi linear and non linear mapping is valid.

1.2 Limitations

In this project, we will not look into sea currents, and non linear waves.

1.3 Thesis Outline

In Chapter 2, all relevant background knowledge needed for understanding the thesis is presented. Chapter 3, presents the methods used in the thesis and the way the work was implemented. The results are shown in Chapter 4, and finally the conclusions are in Chapter 5. More results, which are not discussed are presented in Appendix 1.

2
Theory

In this chapter, necessary theory behind concepts used or discussed in the following chapters are introduced.

2.1 Ocean Waves

2.1.1 Models

Ocean waves are created by winds. Longer and stronger winds, result in bigger waves. There exist various models that take input the wind speed and the wind direction and describe ocean waves. For this purpose, we are going to look into omnidirectional spectra, and spreading functions, which when combined generate an ocean wave field.

2.1.1.1 Omnidirectional Spectra

Omnidirectional spectra give us the distribution of the wave energy over wave numbers. In other words, for each wave number, we can see what is the amplitude of the wave for a specific wind speed. There exist two sea states: (i) Fully developed sea, in which the waves are fully developed and will not increase anymore and (ii) developing sea, in which the waves will continue to grow [7].
In this project we will look into the following spectra: Pierson-Moskowitz , JONSWAP and Elfouhaily.
The Pierson-Moskowitz spectrum is an empirical model for a fully developed sea state and was done through measurements [1].

$$S_{PM}(k) = \frac{a}{2k^3} \exp\left[-\beta \left(\frac{g}{k}\right)^2 \frac{1}{V_{19.5}^4}\right] \tag{2.1}$$

where $a = 0.0081$ is a Phillips constant, $\beta = 0.74$, g is the gravitational acceleration, and $V_{19.5}$ is the wind speed at 19.5 m above the surface.

The Joint North Sea Wave Project (JONSWAP) spectrum describes a developing sea state [2]

$$S_J(k) = \frac{a}{2} k^{-3} \exp\left[-1.25 \left(\frac{k}{k_p}\right)^2\right] \exp\left\{ln\gamma \exp\left[-\frac{\left(\sqrt{k/k_p} - 1\right)^2}{2\sigma^2}\right]\right\} \tag{2.2}$$

Lastly, the Elfouhaily spectrum combines short and long waves [3]

$$S_E(k) = k^{-3}(B_l + B_h) \tag{2.3}$$

where the long waves part is

$$B_l = \frac{1}{2} a_p \frac{c_p}{c} L_{PM} J_p \exp\left[-\frac{\Omega}{\sqrt{10}} \left(\sqrt{\frac{k}{k_p}} - 1 \right) \right] \tag{2.4}$$

where a_p is the Philips equilibrium range parameter for long waves, c_p is the phase speed of the dominant long wave, k_p is the wavenumber of the spectral peak and Ω is the inverse wave age.

The short waves part is

$$B_h = \frac{1}{2} a_m \frac{c_m}{c} L_{PM} J_p \exp\left[-\frac{1}{4} \left(\frac{k}{k_m} - 1 \right)^2 \right] \tag{2.5}$$

where a_m is the Philips equilibrium range parameter for long waves, c_m is the phase speed of the dominant short wave, and k_m is the wavenumber of the short wave peak.

L_{PM} is the Pierson-Moskowitz shape spectrum and J_p is the peak enhancement factor [8].

In Figures 2.1, 2.2 and 2.3 there are different elevations for different wind speeds for the three models. In the plots, we can see the elevation of the surface for each wavenumber. Low wavenumbers are equivalent to high wavelengths. We can see that long wave have bigger elevation that short wave for a specific wind speed.

Moreover, we can see the difference of the elevation for different wind speeds. Higher wind speeds not only have higher elevation for the same wavenumber, but also they push the peak towards lower wavenumbers. For wavenumbers greater and equal than one, the elevation remains the same for all values of wind speeds. The Elfouhaily model is an exception, as for very high wavenumbers, the elevation differs.

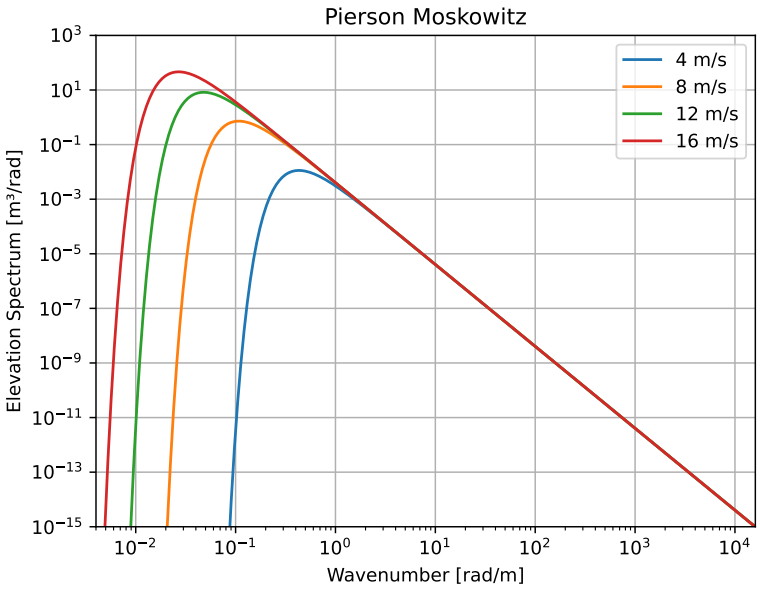

Figure 2.1: Pierson Moskowitz Spectrum

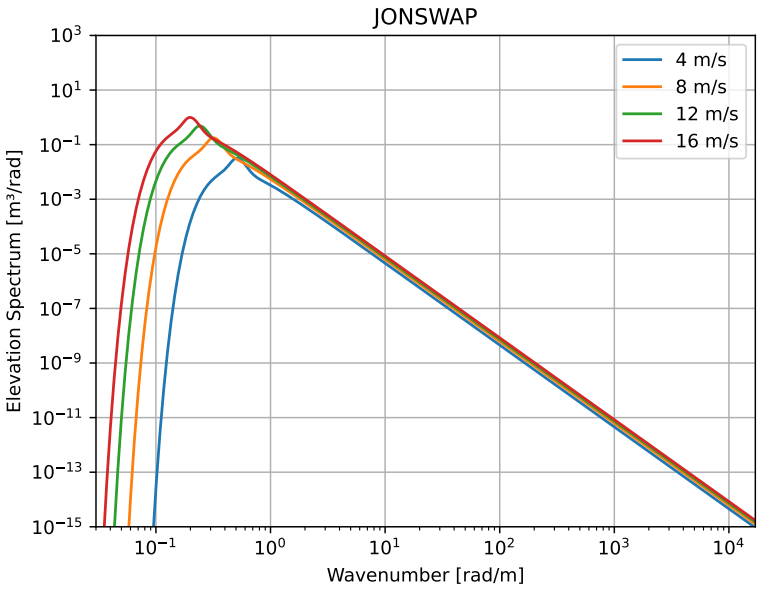

Figure 2.2: JONSWAP Spectrum

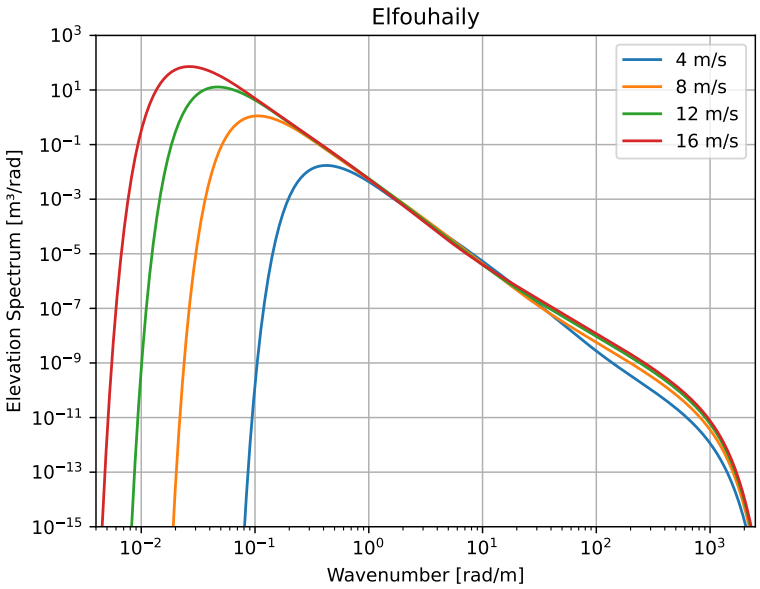

Figure 2.3: Elfouhaily Spectrum

2.1.1.2 Spreading Functions

The frequency spectrum $S(k)$ by itself is not enough to describe the propagation of wave on the x-y plane. Thus, spreading functions are needed. In this project we will look into the following models: Simple Cosine, Longuet Higgins and Elfouhaily.

The simple cosine model is

$$D(\phi) = \frac{2}{\pi} \cos^n \phi \tag{2.6}$$

This model has limitations and can not describe a real world propagation since it does not depend on frequencies or wind speed.
The Longuet Higgins model is a model that is based on empirical measurements with pitch-and-roll buoys[7].

$$D(\phi) = \frac{\Gamma(S+1)}{\Gamma(S+0.5)2\sqrt{\pi}} \cos^{2S}\left(\frac{\phi}{2}\right) \tag{2.7}$$

where $\Gamma(\cdot)$ is the Gamma function, and S controls the width of the function and depends on k [7].

Finally, the Elfouhaily function is described by [3]

$$D(\phi) = \frac{1}{2\pi}\left[1 + \tanh\left(a_0 + a_p\left(\frac{c}{c_p}\right)^{2.5} + a_m\left(\frac{c_m}{c}\right)^{2.5}\right)\cos 2\phi\right] \tag{2.8}$$

where $a_0 = \frac{\ln 2}{4}$ and a_m and a_p are functions of the phase speeds and the wind speed.

In Figures 2.4, 2.5 and 2.6 there are different spreading functions presented in polar coordinates.

The simple cosine model is dependent on n. High values of n make the waves more directive.

The Longuet Higgins model is dependent on S. With increasing values of S the angular range over which the model maintains high values increases. When S equals one, the models creates a cardioid shape.

Finally, the Elfouhaily model, creates a double direction spreading. For $k = 0.1$ the angular range for the orthogonal directions is 0, but for other bands the range is higher.

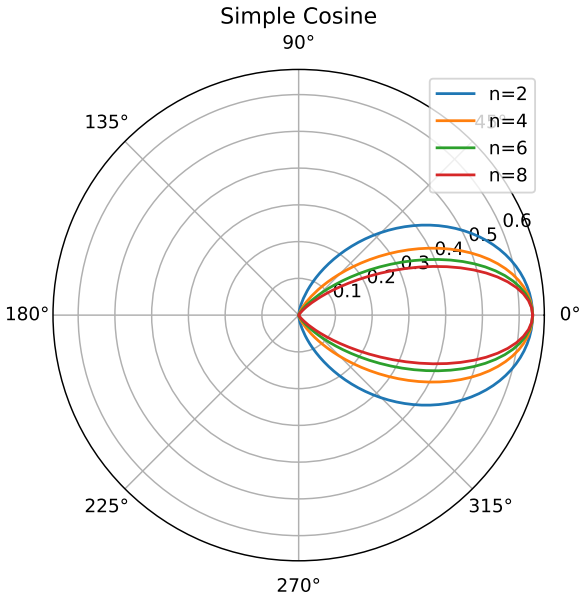

Figure 2.4: Simple Cosine Spreading Function

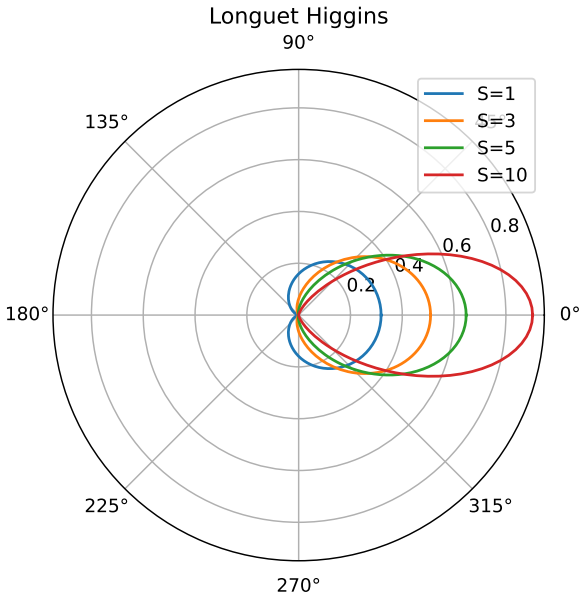

Figure 2.5: Longuet Higgins Spreading Function

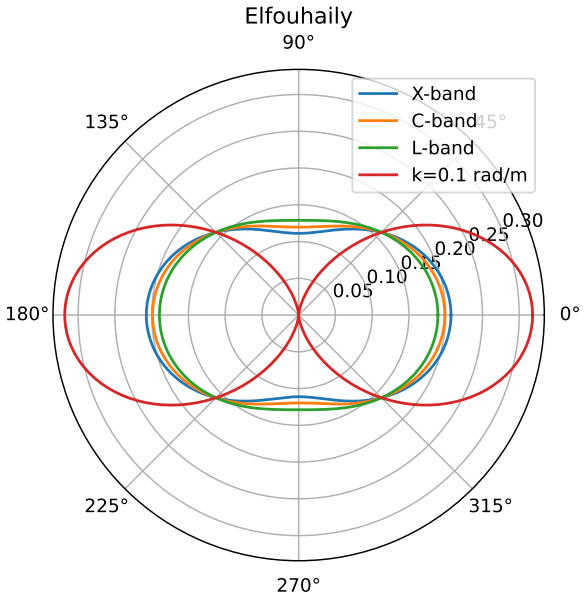

Figure 2.6: Elfouhaily Spreading Function

2.1.2 Ocean Surface

Linear wave theory has been used for describing ocean waves for many years. In this theory, water is assumed to have no resistance and be incompressible, with nonrotational motion [7]. The elevation of a ocean wave field can be described as the summation of many harmonic waves which propagate on the x-y plane with a direction ϕ_j, amplitude A which is estimated from the omnidirectional spectrum

and the spreading function, and a uniformly distributed random phase $\epsilon \in (0, 2\pi)$ [7].

The fluid velocity potential is

$$\Phi_{sea}(x, y, z, t) = g \sum_i \sum_j \frac{A_{ij}}{\omega_i} e^{k_i z} sin\left[k_i \left(x \cos\phi_j + y \sin\phi_j\right) - \omega_i t + \epsilon_{ij}\right] \tag{2.9}$$

From this equation the surface elevation formula can be derived

$$Z_{sea} = -\frac{1}{g} \frac{\partial \Phi_{sea}}{\partial t}\bigg|_{z=0} \tag{2.10}$$

$$Z_{sea}(x, y, z, t) = \sum_i \sum_j A_{ij} \cos\left[k_i \left(x \cos\phi_j + y \sin\phi_j\right) - \omega_i t + \epsilon_{ij}\right] \tag{2.11}$$

where ω is the dispertion relation

$$\omega = \sqrt{gk}$$

and A is the amplitude

$$A = \sqrt{2S(k)D(k, \phi)\Delta k \Delta \phi} \tag{2.12}$$

where Δk is the wavenumber spacing and $\Delta\phi$ is the angle spacing.

2.1.3 Ocean Surface Orbital Velocity

During the SAR imaging, the simulation needs the orbital velocity of the surface. That can be found with two ways.
The first method comes from the following analytic formula [9]

$$u_r = u_z cos\theta - sin\theta \left(u_x sin\phi + u_y cos\phi\right) \tag{2.13}$$

where ϕ is the angle between the wind direction and the radar flight direction, θ is the radar incidence angle and the orbital velocity components are derived by [7]

$$u_x = \frac{\partial \Phi(x, y, 0)}{\partial x} \tag{2.14}$$

$$u_z = \frac{\partial \Phi(x, y, 0)}{\partial y} \tag{2.15}$$

$$u_z = \frac{\partial \Phi(x, y, 0)}{\partial z} \tag{2.16}$$

2.2 SAR Imaging

The scattering of electromagnetic waves from a sea surface is a complex process, and relies on the surface conditions, the radar platform, and the signal properties. From these parameters, only the radar platform and the signal properties can be configured [7].

A picture of a setup with the satellite and some parameters are shown in Figure 2.7.

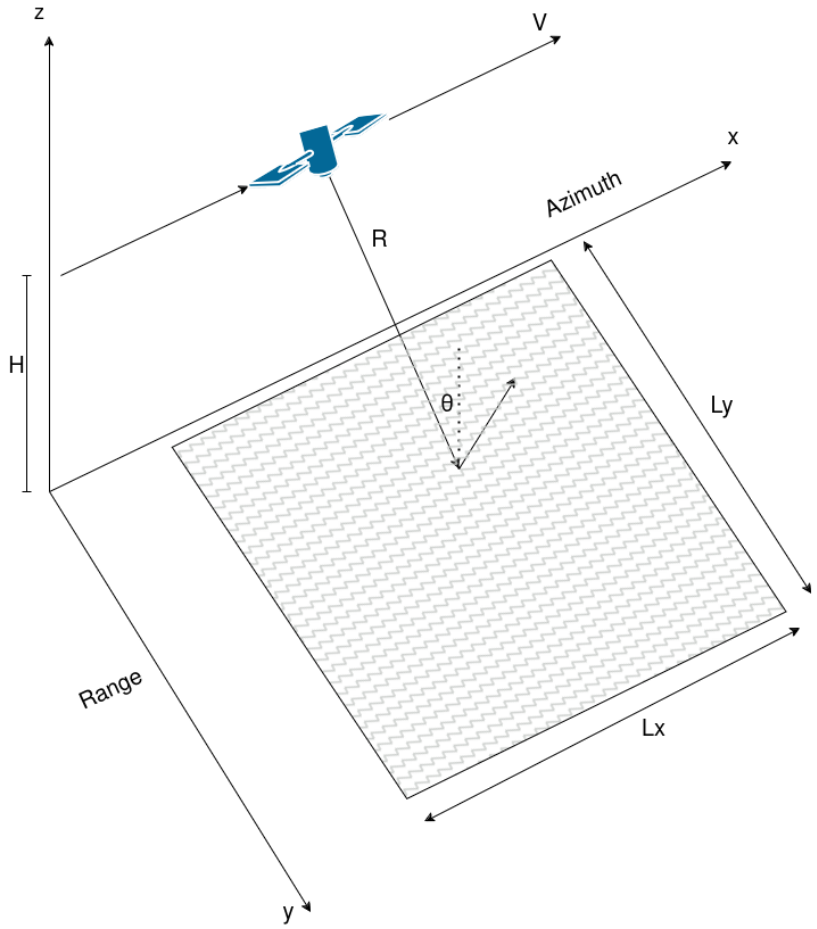

Figure 2.7: SAR Setup

In this project, we are looking into SAR imaging. Due to the movement of the radar platform in the azimuth direction, we can achieve higher resolution.
There exists two types of scattering, which are the Bragg scattering and the non-Bragg scattering [7]. In this project, we will look only into Bragg scattering, since SAR mainly operates in wavelengths in the centimeters to decimeters range, and incidence angles between $20° \sim 70°$ [7].

2.2.1 Modulation Transfer Functions

Detection of capillary waves is possible through Bragg scattering, while the long waves can be detected by the modulation of the capillary waves by the long waves [10].

Real aperture radar (RAR) modulation is attributed to tilt modulation, hydrodynamic modulation and range bunching modulation, while SAR modulation is attributed to the previous with the addition of velocity bunching modulation.

In the next sections, the modulation will be explained and their transfer functions will be presented for a SAR looking in the range direction.

2.2.1.1 Tilt Modulation

The tilt modulation appears to be due to the effect of the long waves tilting the capillary wave which affects the local incidence angle and shifts the wave by $\frac{\pi}{2}$ deg towards the radar[11].

The transfer function for the tilt modulation is

$$T_k^{tilt} = -\frac{4ik_y cot\theta}{1+\sin^2\theta} \tag{2.17}$$

where θ is the radar incidence angle.

2.2.1.2 Hydrodynamic Modulation

The interactions between the long waves and the capillary waves causes divergence and convergence and results in modulation of the energy [11], and its transfer function is

$$T_k^{hydr} = 4.5\omega\frac{k_y^2(\omega - i\mu)}{|k|\,(\omega^2+\mu^2)} \tag{2.18}$$

where ω is the dispertion relation and μ is the hydrodynamic relaxation rate which is 0.5 s^{-1} [6].

2.2.1.3 Range Bunching

Surface slopes caused by long waves and short wave, result in an uneven surface. The radar signal reflected on an uneven surface results in a modulation of the backscatter. This is called range bunching, which has the following transfer function [10]

$$T_k^{rb} = -ik_y\frac{cos\theta}{sin\theta} \tag{2.19}$$

2.2.1.4 Orbital Velocity

The orbital velocity transfer function is defined by

$$T_k^u = -\omega\left(\frac{k_y}{k}sin\theta + icos\theta\right) \tag{2.20}$$

2.2.1.5 Velocity Bunching

Velocity bunching occurs due to the azimuthal displacements of the reflected signal due to the orbital velocity. The modulation transfer function is

$$T_k^{vb} = -i\beta k_x T_k^u \tag{2.21}$$

where T_k^u is the orbital velocity modulation transfer function.

2.2.1.6 Real Aperture Radar

As noted previously, the tilt, hydrodynamic and range bunching modulations result in the RAR modulation with transfer function [6]

$$T_k^R = T_k^{tilt} + T_k^{hydr} + T_k^{rb} \tag{2.22}$$

2.2.1.7 Synthetic Aperture Radar

The SAR modulation, is defined by the RAR modulation in addition to the velocity bunching modulation [6]

$$T_k^S = T_k^R + T_k^{vb} \tag{2.23}$$

2.2.2 RAR Image

To simulate the SAR image, the radar cross section which gives the RAR image is needed [7]

$$\sigma(x,y) = \sigma_0 \left[1 + 2 \int T_k^R \zeta_k \exp\{ikx\} dk\right] \tag{2.24}$$

where T_k^R is the RAR modulation transfer function, ζ_k is the surface elevation in the frequency domain and σ_0 is the average normalized radar cross-section

$$\sigma_0(x,y) = 8\pi k_e^4 \cos^4\theta W(k_{Bx}, k_{By}) |T(\cdot)|^2 \tag{2.25}$$

where $k_e = 2\pi/\lambda$ is the radar electromagnetic wavenumber, λ is the signal wavelength, $W(\cdot)$ is the spectrum of the Bragg Wavenumbers, and $T(\cdot)$ is the complex scattering function [9].

2.2.3 SAR Image

The SAR image is affected by variables like azimuth resolution, the satellite height, satellite velocity and orbital velocity. The formula is [7][11]

$$I(x_i, y_i) = \frac{\pi T_0^2 \rho_a}{2} \int\int \delta(y_i - y) \frac{\sigma(x,y)}{\rho_a'} \exp\{-\pi^2 \left[\frac{x_i - x - \beta u_r(x,y)}{\rho_a'}\right]^2\} dxdy \tag{2.26}$$

where T_0 is the SAR integration time, ρ_a is the azimuth resolution and δ is the Dirac function. β is defined by

$$\beta = \frac{R}{V} \tag{2.27}$$

which $R = H/cos\theta$ being the slant range of the satellite radar, H is the height of the satellite, V is the velocity of the satellite and ρ_a' is the degraded azimuth resolution

$$\rho_a' = \rho_a \sqrt{1 + \frac{T_0^2}{\tau_s^2}} \tag{2.28}$$

where τ_s is the coherence time [12]

$$\tau_s = 3 \frac{\lambda}{V_{19.5}} erf^{-1/2}\left(2.7 \frac{\rho_a}{V_{19.5}^2}\right) \tag{2.29}$$

where the integration time T_0 is

$$T_0 = \frac{\lambda\beta}{2\rho_a} \tag{2.30}$$

In Figure 2.8 Coherence time for different wind speeds and frequencies is shown. We can see that with higher wind speeds, the coherence time decreases. When the wind speed is higher than 10 m/s, the coherence time remains constant. Moreover, the radar signal frequency affects the coherence time. Higher frequencies results in smaller coherence time.

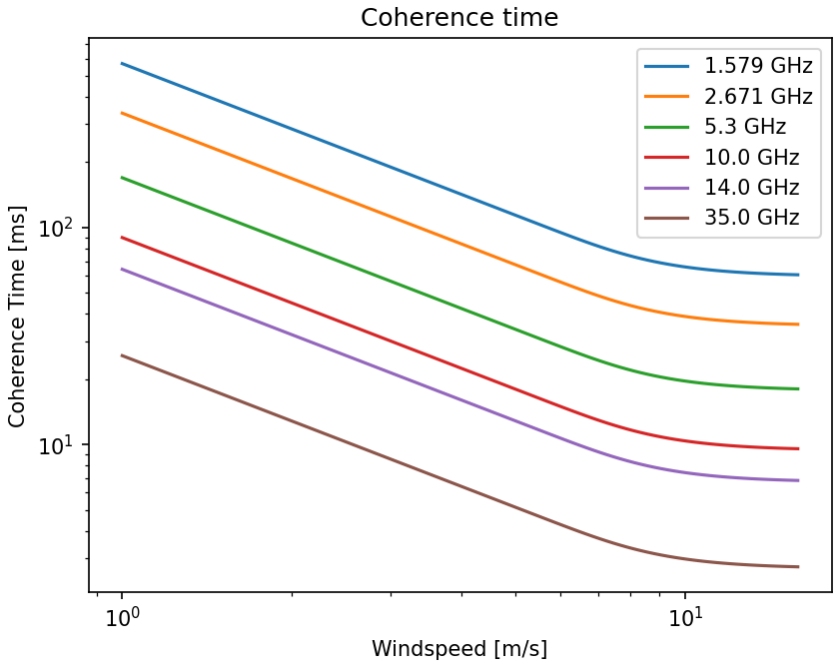

Figure 2.8: Coherence time for different wind speeds and frequencies

2.3 SAR Image Mapping

In the same way that the wave spectrum describes a wave field, the spectrum of a SAR image should describe the SAR image of the wave field. This is done with the help of the modulation transfer functions that were described in the previous sections. There are three cases of SAR image mapping: linear, quasi linear and non-linear [6], and the optimal choice depends on the condition of both the sea surface and the radar platform.

2.3.1 Covariance Functions

Before defining the mapping functions, the covariance functions need to be explained. They explain how the spectrum can change according to the orbital velocities and the RAR intensity.

The orbital velocity auto-covariance function is [6]

$$f^u(r) = \int F_k |T_k^u|^2 \exp\{ikr\} dk \tag{2.31}$$

the RAR image auto-covariance function is [6]

$$f^R(r) = 0.5 \int \{F_k |T_k^R|^2 + F_{-k} |T_{-k}^R|^2\} \exp\{ikr\} dk \tag{2.32}$$

and the RAR image and orbital velocity auto-covariance function is [6]

$$f^{uR}(r) = 0.5 \int \{F_k T_k^R (T_k^u)^* + F_{-k} (T_{-k}^R)^* T_{-k}^u\} \exp\{ikr\} dk \tag{2.33}$$

2.3.2 Linear Mapping of SAR Image

The linear mapping, while effective under calm sea conditions and low values of β, is the least accurate for harsh sea conditions and high values of β [6].

$$P_1^S = 0.5(|T_k^S|^2 F_k + |T_{-k}^S|^2 F_{-k}) \tag{2.34}$$

2.3.3 Quasi-Linear Mapping of SAR Image

This is a bit more complex form of SAR image mapping. In addition to the linear form, it include the factor β which depends on the satellite velocity. [6]

$$P_{ql}^S = \exp[-k_x^2 \beta^2 f^u(0)] P_1^S \tag{2.35}$$

2.3.4 Non-Linear Mapping of SAR Image

The non linear form comes from a series expansion and the degree of the non linearity can be selected manually [6]

$$P^S = \exp[-k_x^2 \beta^2 f^u(0)](P_1^S + P_2^S + ... + P_{n-1}^S + P_n^S) \tag{2.36}$$

Where $P_1, P_2, ..., P_n$ are the nonlinear terms and n indicates the nonlinearity order and

$$P_n^S = P_{n,2n}^S + P_{n,2n-1}^S + P_{n,2n-2}^S \tag{2.37}$$

where

$$P_{n,2n} = \Omega_n \{\frac{f^u(r)^n}{n!}\} \tag{2.38}$$

$$P_{n,2n-1} = \Omega_n \{\frac{i[f^{uR}(r) - f^{uR}(-r)] f^u(r)^{n-1}}{(n-1)!}\} \tag{2.39}$$

$$\begin{aligned} P_{n,2n-2} = \Omega_n \{\frac{1}{(n-1)!} f^R(r) f^{uR}(r)^{n-1} + \\ \frac{1}{(n-2)!} [f^{uR}(r) - f^{uR}(0)][f^{uR}(-r) - f^{uR}(0)] f^R(r)^{n-2}\} \end{aligned} \tag{2.40}$$

where Ω_n is the Fourier Transform

$$\Omega_n = (2\pi)^{-2} \int dr \exp(-ikr) \tag{2.41}$$

3
Methods

This chapter describes the main parts of the implementation of the simulator.

3.1 Parameters

This projects does not use any data, but produces everything by itself. Thus, the parameters need to be specified.

Parameter	Description
spectrum	$Pierson\_Moskowitz$ | $JONSWAP$ | $Elfouhaily$
spreading	$Simple\_Cosine$ | $Longuet\_Higgins$ |$Elfouhaily$
n	Simple Cosine Power
S	Longuet_Higgins width
length_x	Wave field azimuth length
length_y	Wave field range length
N_x	Number of azimuth points
N_y	Number of range points
wind_speed	Wind Speed
wind_direction	Direction of wind relative to radar platform flight direction
fetch	Ocean fetch

Table 3.1: Ocean surface parameters

Moreover, the parameters of the radar platform need to also be specified

Parameter	Description
polarization	Radar signal polarization
frequency	Radar signal frequency
incidence_angle	Incidence angle of the signal
range_resolution	Range resolution
azimuth_resolution	Azimuth resolution
H	Radar platform height
V	Radar platform velocity
β	Sland Range to Velocity Ratio (optional)

Table 3.2: Radar platform parameters

In Table 3.2 the parameter β is optional. Meaning that if the value is equal to zero, then the real β will be used.

3.2 Wave Sield Simulation using The Fast Fourier Transform

3.2.1 Ocean Surface with FFT

While the previous method discussed in Chapter 2 for generating an ocean wave field has been used for many years, the complexity of the formula is high, which makes it extremely slow for simulation of big fields. In recent years, there has been an increased need for simulating ocean fields in movies and computer games. Movies and computer games require not only one instance of the wave field but many, as they need to generate a continuous representation of the ocean surface. Consequently, the computational demands for generating such simulations have become even more challenging, requiring algorithms that can efficiently handle large-scale wave simulations while maintaining real-time performance.

Jerry Tessendord presents a method that uses the FFT to generate an ocean field [13].

$$Z_{sea}(x,t) = \sum_k \tilde{h}(k,t) \exp(ik \cdot x) \tag{3.1}$$

where t is the time and k is a two dimensional vector with components $k = (k_x, k_y)$, $k_x = \frac{2\pi n}{L_x}$, $k_y = \frac{2\pi m}{L_y}$ and n and m are integers with bounds $-\frac{N}{2} \leq n < \frac{N}{2}$ and $-\frac{M}{2} \leq m < \frac{M}{2}$. The parameters N and M are integers that define resolution of the surface on each axis. $\tilde{h}(k,t)$ is the height amplitude Fourier component

$$\tilde{h}(k,t) = \tilde{h_0}(k) \exp\{i\omega(k)t\} + \tilde{h_0^*}(-k) \exp\{-i\omega(k)t\} \tag{3.2}$$

and

$$\tilde{h_0}(k) = \frac{1}{\sqrt{2}} (\xi_r + i\xi_i) A \tag{3.3}$$

where A is the amplitude as equation 2.12, ξ_r and ξ_i are random numbers drawn from a Gaussian distribution with mean 0 and standard deviation 1.

3.2.2 Ocean Surface Orbital Velocity with FFT

Besides the approach discussed in Subsection 2.1.3, a FFT approach exists [11]

$$u_r(\mathbf{x},t) = 2\Re(\sum_k T_k^u \zeta_k \exp(-i(kx - \omega t))) \tag{3.4}$$

where ζ_k is the surface elevation in the frequency domain, T_k^u is the orbital velocity transfer function and $\Re$ refers to the real part of the component.

3.3 Verification of the ocean wave field generation

To verify that the previous methods have been correctly implemented, the following formulas need to be true

$$\sigma^2_{surface} = \iint \Psi(k, \phi)\, dk\, d\phi \tag{3.5}$$

and

$$\sigma^2_{slope_x} + \sigma^2_{slope_y} = \iint k^2 \Psi(k, \phi)\, dk\, d\phi \tag{3.6}$$

where

$$\Psi(k, \phi) = S(k)D(k, \phi) \tag{3.7}$$

and $\sigma^2_{surface}$ is the variance of the ocean surface, $\sigma^2_{slope_x}$ is the variance of the azimuth slopes of the surface, and $\sigma^2_{slope_y}$ is the variance of the range slopes of the surface.

3.4 Speckle Noise

Speckle noise is an interference that inherently affects SAR images, particularly in oceanographic applications. This type of noise arises due to the coherent nature of SAR imaging, where multiple scatterers within a single resolution cell interfere with each other, causing random fluctuations in the returned signal intensity. Since in the real world it is impossible to get a crystal clear image from a satellite, speckle noise needs to be added manually [7].

$$I_n(x_i, y_i) = I(x_i, y_i)N(x_i, y_i) \tag{3.8}$$

In this case the noise follows an exponential distribution with PDF $P(N) = exp(-N)$.

3.5 Simulator

3.5.1 Environment

In this project the Python programming language was used. The *numpy* library was extensively used for fast matrix calculations and the *FFT* and *IFFT* functions were used for fast transformations between the time and frequency domains. In addition the *special* module from *scipy* was also used for the *erf* function. Finally, the *matplotlib* library was used for plotting.

3.5.2 Algorithm

In this section, a high level description of the algorithms is presented. Algorithm 1 is for the surface generation, Algorithm 2 is for the SAR imaging, and Algorithm 3 is for the SAR mapping.

Algorithm 1 Ocean Surface Generation Algorithm

procedure OCEAN(`params`)
- $n \leftarrow -\frac{N}{2}, ..., \frac{N}{2}$
- $m \leftarrow -\frac{M}{2}, ..., \frac{M}{2}$
- $k_x \leftarrow \frac{2\pi n}{L_x}$
- $k_y \leftarrow \frac{2\pi m}{L_y}$
- $k \leftarrow \sqrt{k_x^2 + k_y^2}$
- $S(k) \leftarrow$ `Omnidirectional_Spectrum(params)`
- $D(k, \phi) \leftarrow$ `Spreading_Function(params)`
- $\omega = \sqrt{g * k}$ ▷ g is the Gravitational acceleration
- $\Psi \leftarrow S(k)D(k, \phi)$
- $A = \sqrt{2\Psi(k, \phi)\Delta k \Delta \phi}$
- `random` $\leftarrow \frac{1}{\sqrt{2}}($`normal_dist`$(N, M) + 1j *$ `normal_dist`$(N, M))$
- `coefficients` $= N * M * A *$ `random` $* \exp(-1j\omega t)$
- `surface` $\leftarrow$ `IFFT2`$\{$`coefficients`$\}$

Algorithm 2 SAR Imaging Algorithm

procedure SAR IMAGING(`params,surface`)
- `rar_mtf` $\leftarrow$ `tilt_mtf` $+$ `hydrodynamic_mtf` $+$ `range_bunching_mtf`
- $\sigma \leftarrow \sigma_0 * (1 + 2 *$ `IFFT2`$\{rar\_mtf *$ `FFT2`$\{surface\}\})$
- $u_r \leftarrow 2 *$ `IFFT2`$\{$`orbital_velocity_mtf` $*$ `FFT2`$\{surface\}\}$
- **for** $i \leftarrow 0$ to N **do**
  - **for** $j \leftarrow 0$ to M **do**
    - `img[i,j]` $\leftarrow \frac{\pi T_0^2 \rho_a}{2} *$ `trapz` $\left(\frac{\sigma[i,:]}{\rho'_a} \exp\{-\left(\frac{\pi^2}{\rho'^2_a}\right)^2 (x[i,j] - x[i,:] - \beta * u_r[i,:])\}\right)$
- `speckle` $\leftarrow$ `exponential_dist()`
- `img_noise` $\leftarrow$ `img` $*$ `speckle`

Algorithm 3 SAR Mapping Algorithm

procedure SAR MAPPING(`params,surface`)
- `sar_mtf` $\leftarrow$ `rar_mtf` $+$ `velocity_bunching_mtf`
- $F_k \leftarrow \Psi(k, \phi) * \frac{2\pi}{d_x} * \frac{2\pi}{d_y}$
- `linear_mapping` $\leftarrow$ `abs(sar_mtf)`$^2 * F_k$
- `quasilinear_mapping` $\leftarrow \exp\{-kx^2 * \beta^2 * f_v[0,0]\} *$ `linear_mapping`
- **for** $i \leftarrow 1$ to $nonlinear\_order$ **do**
  - $nonlinear\_terms+ =\leftarrow (2\pi)^{-2} *$ `FFT2`$\{\frac{1}{(i-1)!} * f_r * f_v^(i-1) + \frac{1}{(i-2)!} * (f_{rv} - f_{rv}[0,0]) * (rot180(f_{rv}) - f_{rv}[0,0]) * f_r^{(i-2)}\}$
- `nonlinear_mapping`

4

Results

In Chapter 4, the results of the thesis are presented. Simulations of different cases have been run, and all of them will be shown. In Tables 4.1 and 4.2, the common parameters used are presented

Parameter	Value
spectrum	$Elfouhaily$
spreading	$Longuet\_Higgins$
S	12
length_x	5000 m
length_y	5000 m
N_x	1024
N_y	1024
fetch	200000 m

Table 4.1: Common Ocean surface parameters

Parameter	Value
Polarization	Vertical
Frequency	5 GHz
Incidence Angle	30°
Range Resolution	5 m
Azimuth Resolution	5 m

Table 4.2: Common Radar platform parameters

The results will show cases for different wind speeds, wind directions, and slant range to velocity ratios. In all of the following cases, the nonlinear mapping has been plotted with nonlinearity order three.
In total 38 cases have been simulated but only 12 will be presented in the next sections. More results, which are not discussed can be found in Appendix 1.

4.1 The necessity of the nonlinear mapping

In this section, we are demonstrating the results for simulations for varying β but with calm sea conditions. This is to show the need for the nonlinear mapping. In the next sections we will show varying β for harsh sea conditions.

4.1.1 Case 1

Parameter	Value
Wind Speed	5 m/s
Wind Direction	45°
beta	1 s

Table 4.3: Case 1 parameters

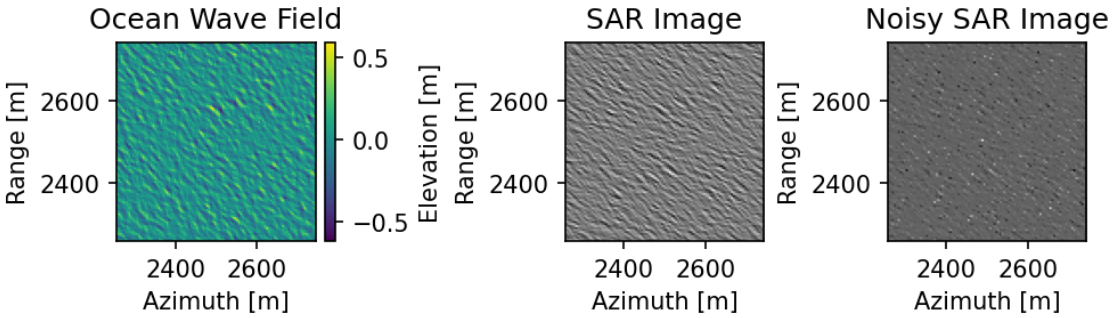

Figure 4.1: Case 1 Ocean Surface with SAR Images

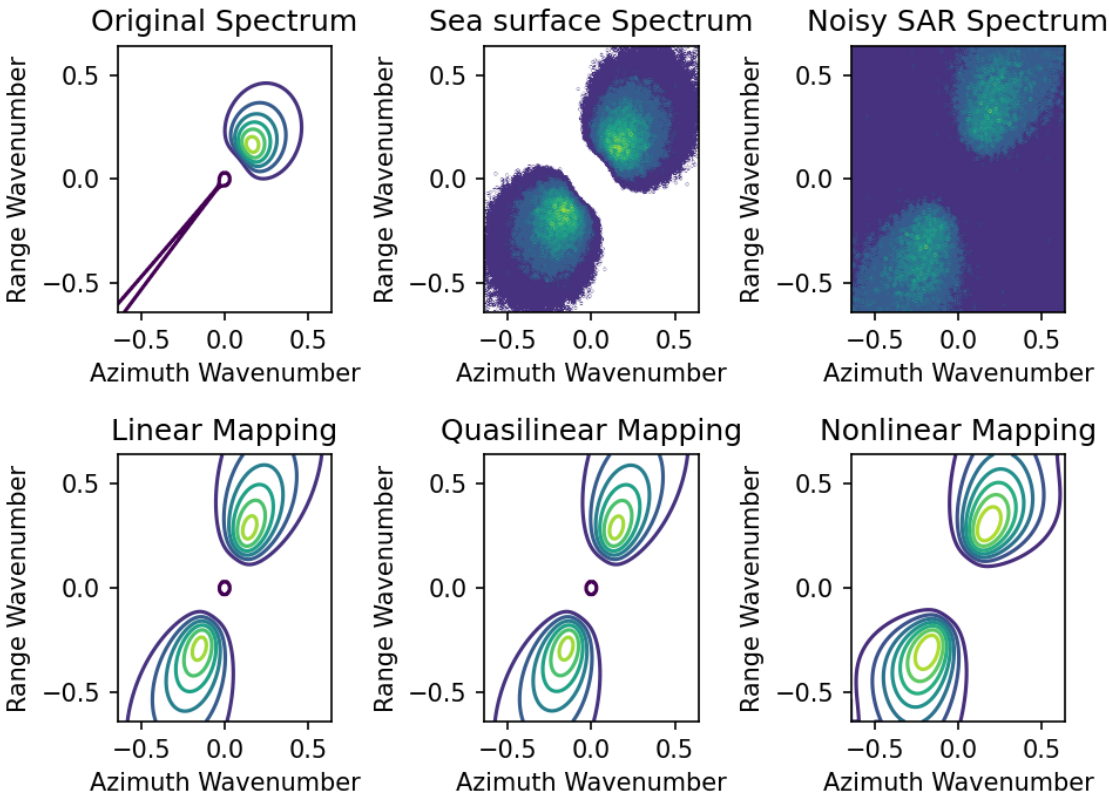

Figure 4.2: Case 1 Plots of spectra

4.1.2 Case 2

Parameter	Value
Wind Speed	5 m/s
Wind Direction	45°
beta	10 s

Table 4.4: Case 2 parameters

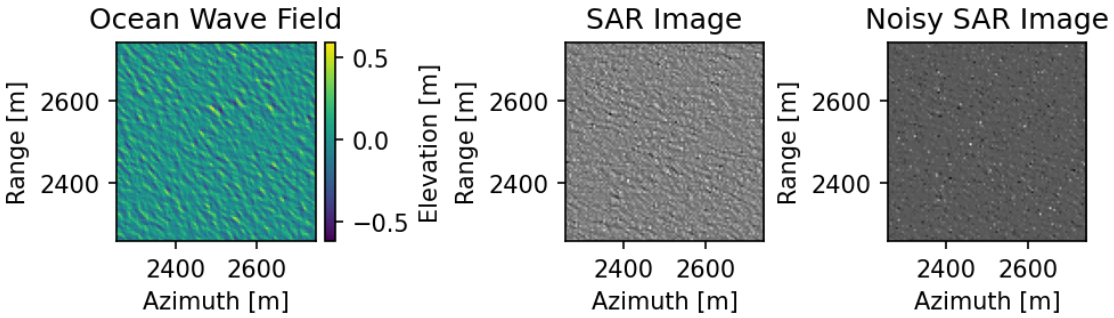

Figure 4.3: Case 2 Ocean Surface with SAR Images

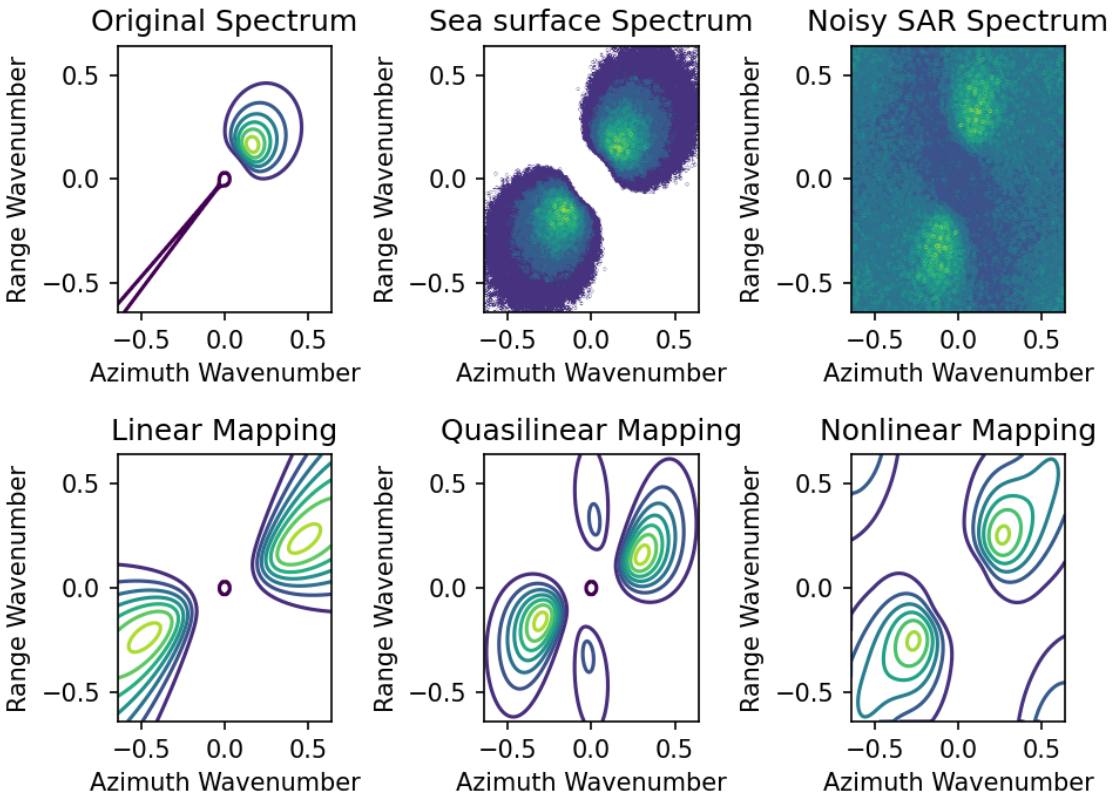

Figure 4.4: Case 2 Plots of spectra

4.1.3 Case 3

Parameter	Value
Wind Speed	5 m/s
Wind Direction	45°
beta	30 s

Table 4.5: Case 3 parameters

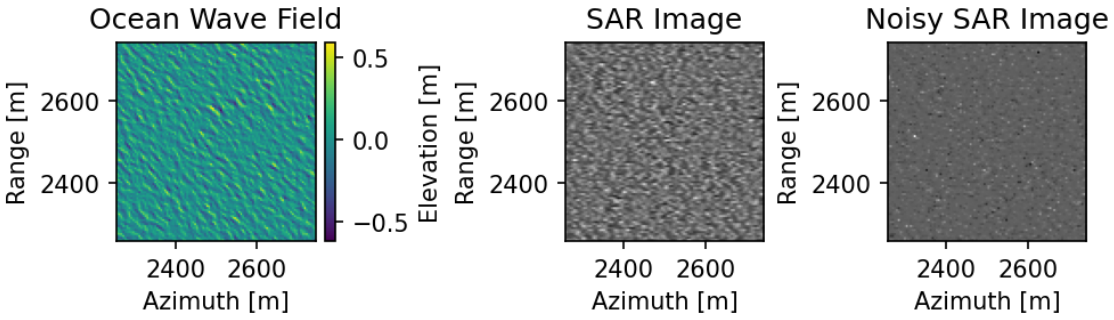

Figure 4.5: Case 3 Ocean Surface with SAR Images

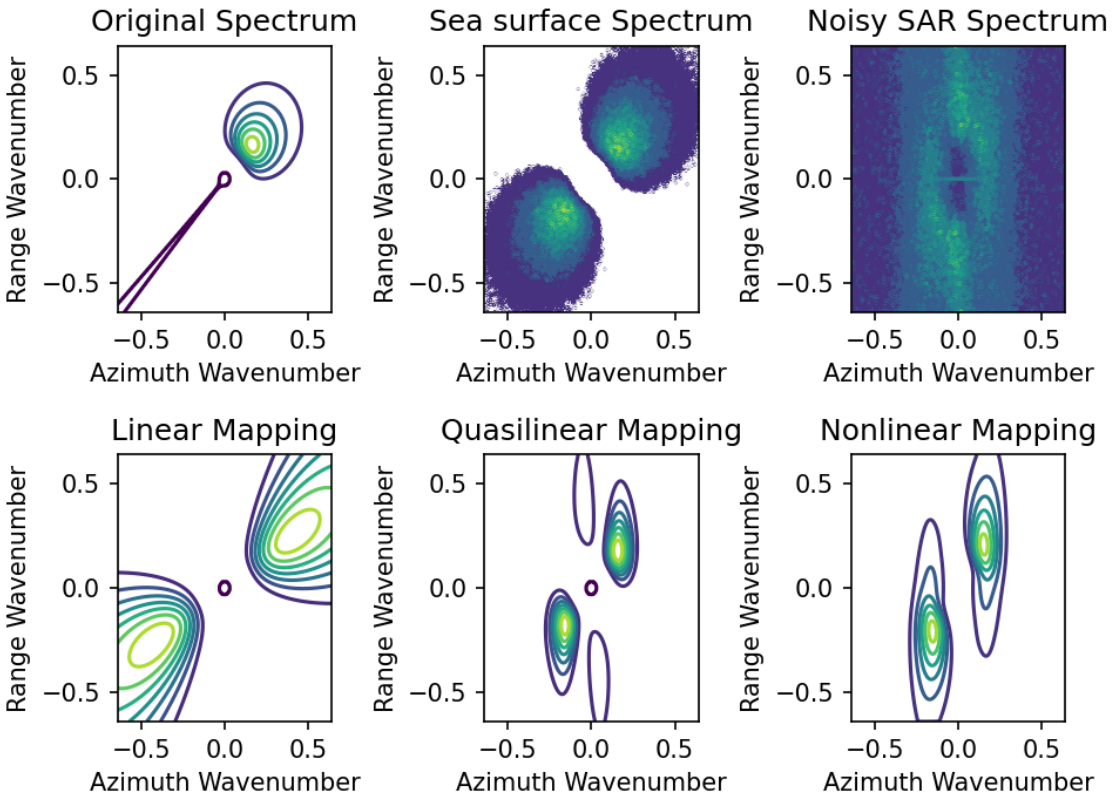

Figure 4.6: Case 3 Plots of spectra

4.1.4 Case 4

Parameter	Value
Wind Speed	5 m/s
Wind Direction	45°
beta	70 s

Table 4.6: Case 4 parameters

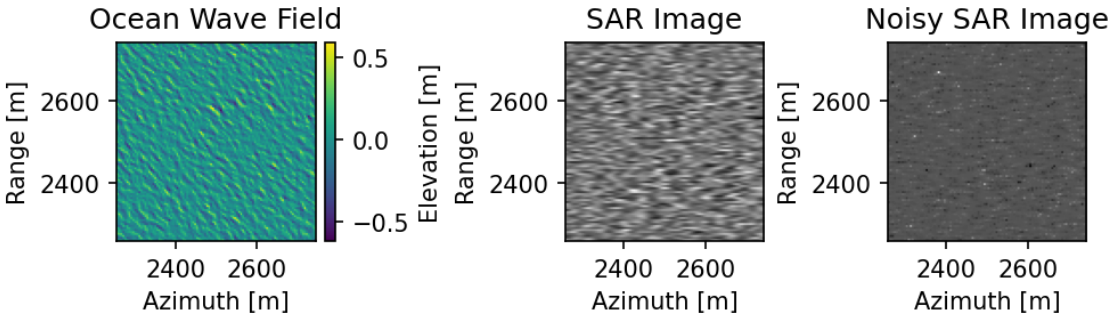

Figure 4.7: Case 4 Ocean Surface with SAR Images

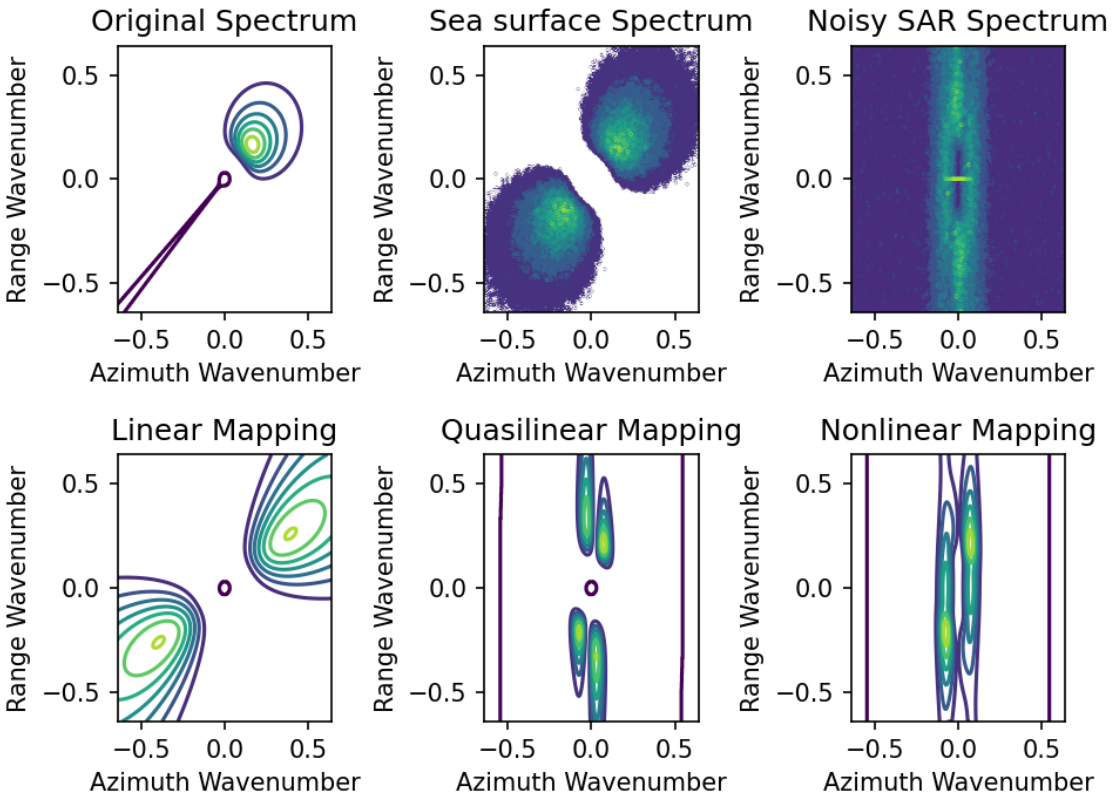

Figure 4.8: Case 4 Plots of spectra

4.1.5 Case 5

Parameter	Value
Wind Speed	5 m/s
Wind Direction	45°
beta	100 s

Table 4.7: Case 5 parameters

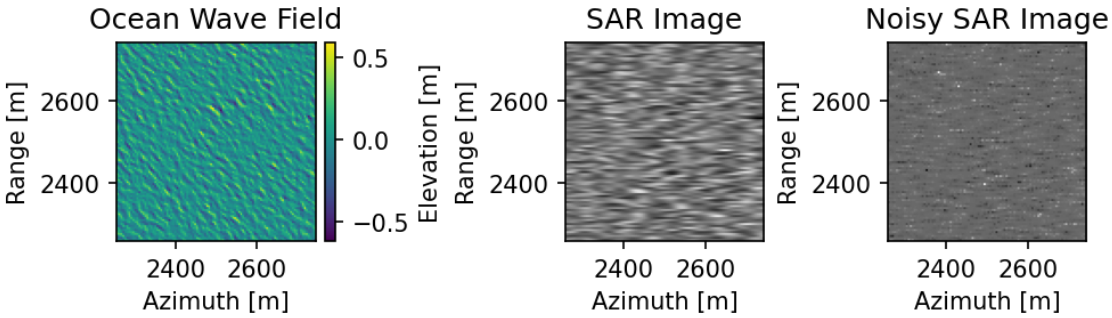

Figure 4.9: Case 5 Ocean Surface with SAR Images

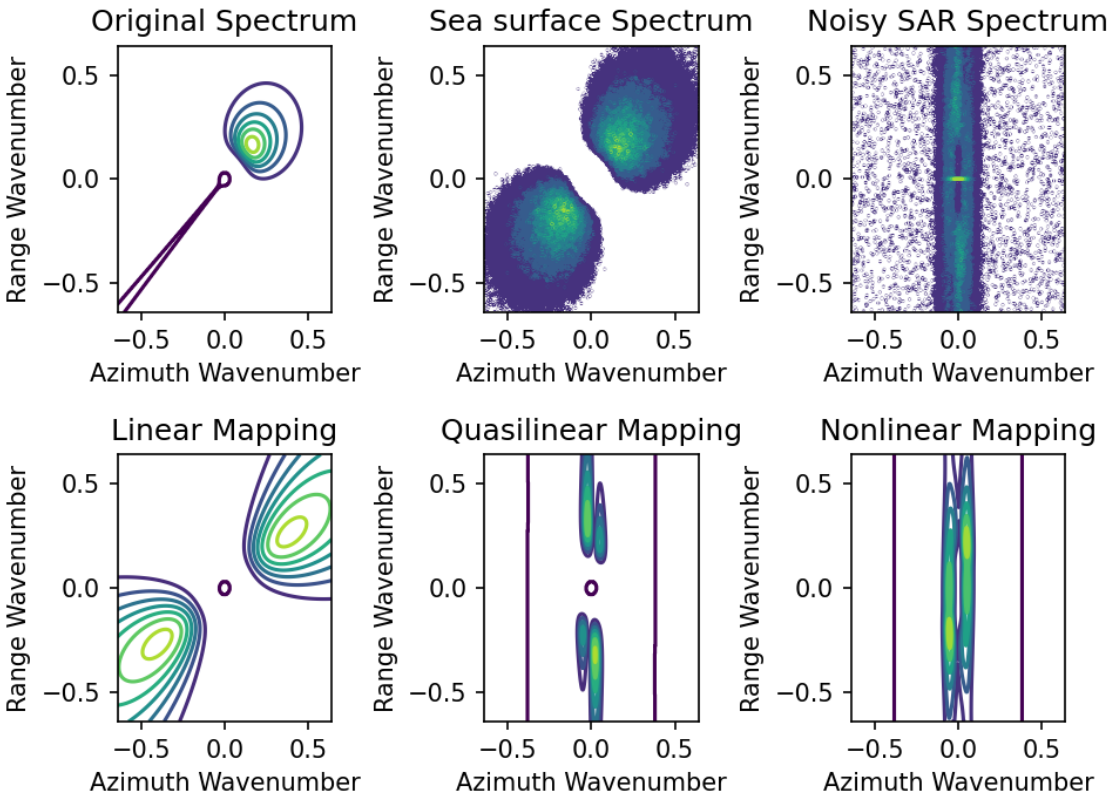

Figure 4.10: Case 5 Plots of spectra

4.1.6 Discussion

In the previous plots, we have done simulations, with low wind speed and varying β. By using a low value for the wind speed we can focus only on the effect of β. For low value of β the wave SAR image in traveling on the same direction as the ocean wave. But as we increase β the direction shifts towards to the SAR platform. In the first case of low β the linear, quasilinear and nonlinear mappings are the same and they math the SAR spectrum. But as the value of β is increased, the SAR spectrum converges towards the middle of the azimuth wavenumbers because of the velocity bunching effect. The linear mappings does not changed. The quasilinear mapping changes because it depends on the value of β. For the high values of β only the nonlinear mapping matches the SAR spectrum.

4.2 Varying Wind Speed

In this section, we are demonstrating the results for simulations for varying wind speeds.

4.2.1 Case 6

Parameter	Value
Wind Speed	5 m/s
Wind Direction	45°
beta	50 s

Table 4.8: Case 6 parameters

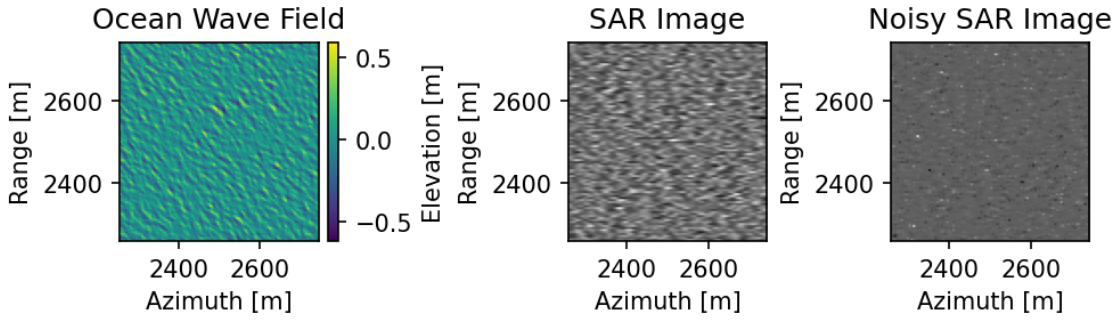

Figure 4.11: Case 6 Ocean Surface with SAR Images

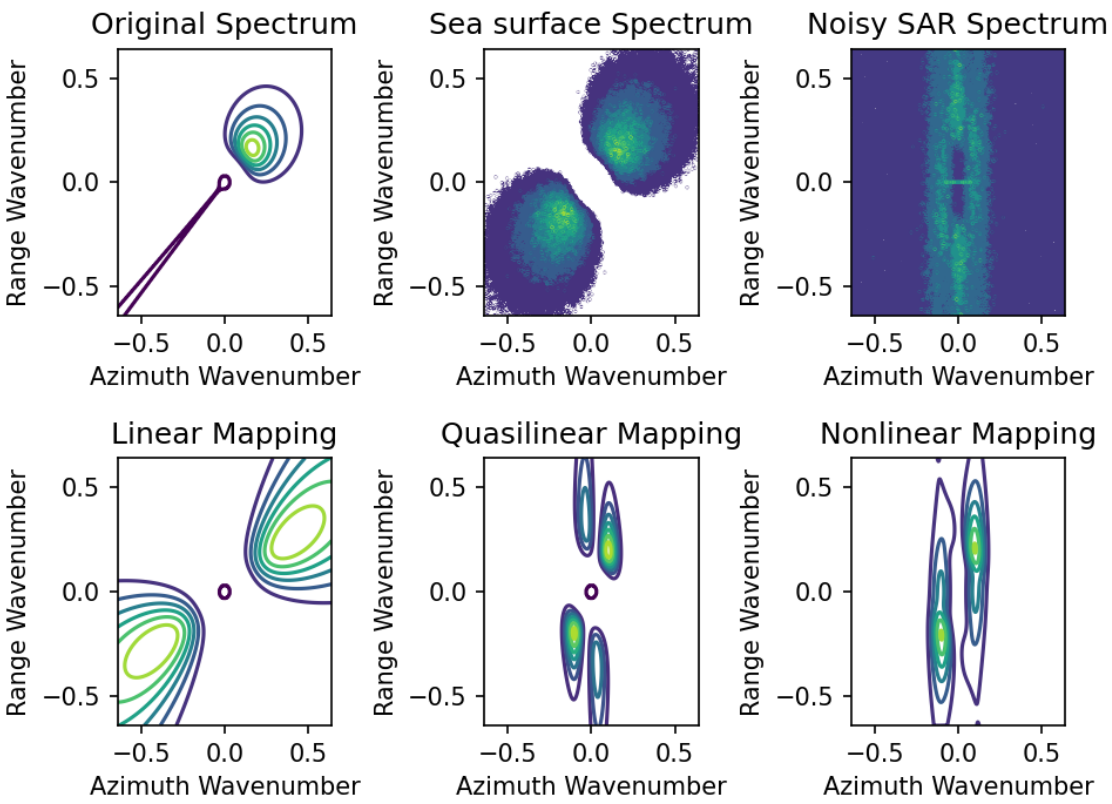

Figure 4.12: Case 6 Plots of spectra

4.2.2 Case 7

Parameter	Value
Wind Speed	15 m/s
Wind Direction	45°
beta	50 s

Table 4.9: Case 7 parameters

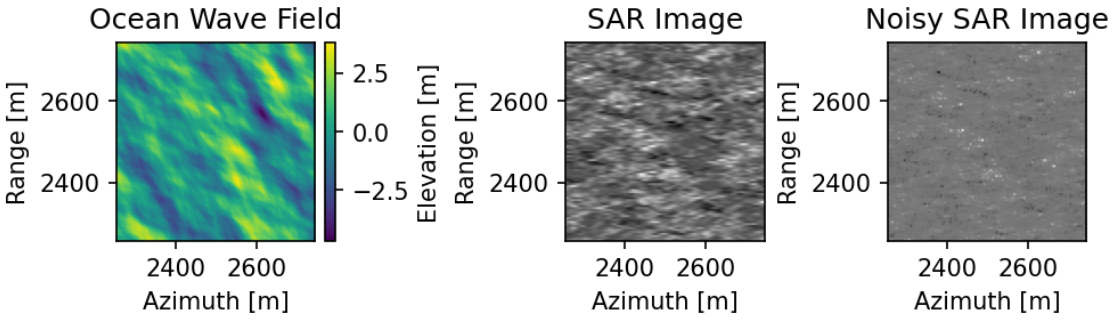

Figure 4.13: Case 7 Ocean Surface with SAR Images

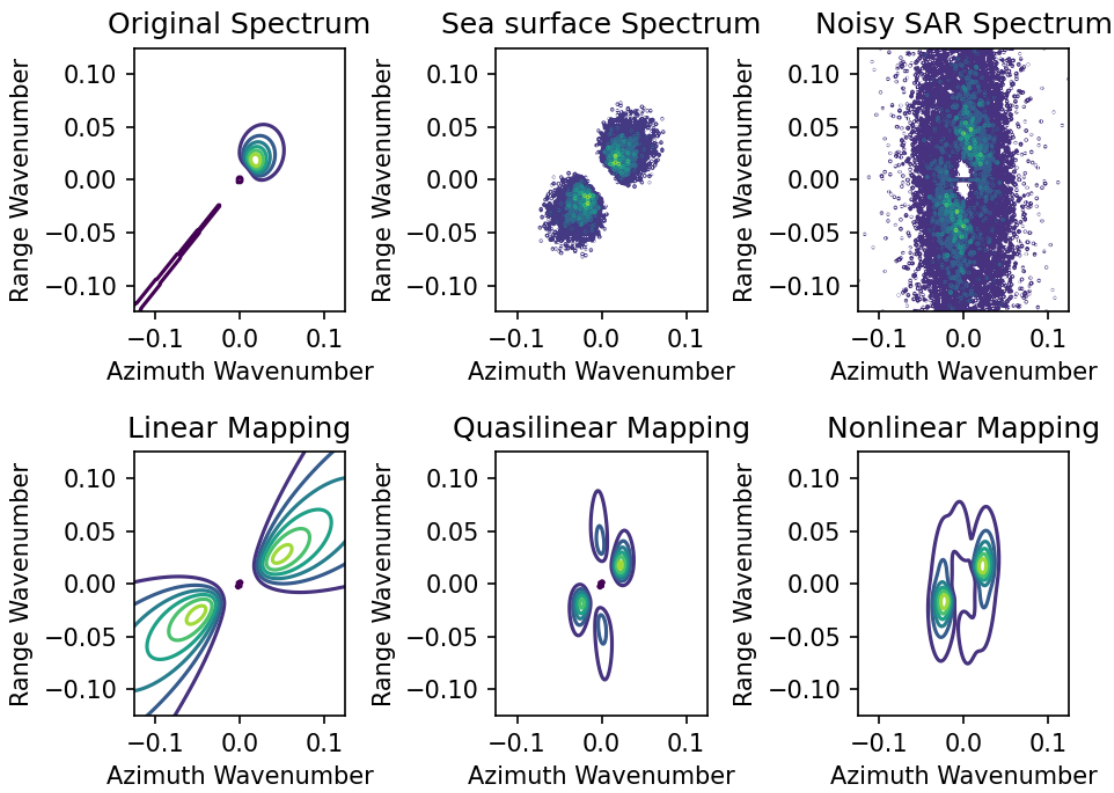

Figure 4.14: Case 7 Plots of spectra

4.2.3 Discussion

In the previous plots, we have done simulations for varying wind speeds. As we can see in the original spectrum, higher wind speeds result in a smaller spread. We can also see this in the sea surface and the SAR spectra. This is because the high wavenumber, or low wavelength waves are negligible to the long waves.

For the low wind speed, we can see that the linear mapping does not match the SAR spectrum. In this case both the quasilinear and nonlinear mappings have achieved matching the SAR spectrum.

On the high wind speed case, the SAR spectrum has rotated counterclockwise. In this case we can see that the quasilinear mapping does not match the SAR spectrum, but the nonlinear mapping has achieved matching it.

4.3 Varying Wind Direction

In this section, we are demonstrating the results for simulations for varying wind directions.

4.3.1 Case 8

Parameter	Value
Wind Speed	10 m/s
Wind Direction	0°
beta	50 s

Table 4.10: Case 8 parameters

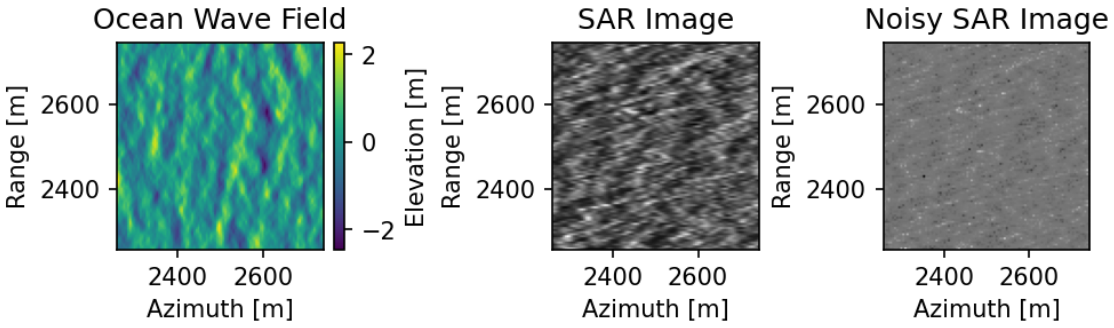

Figure 4.15: Case 8 Ocean Surface with SAR Images

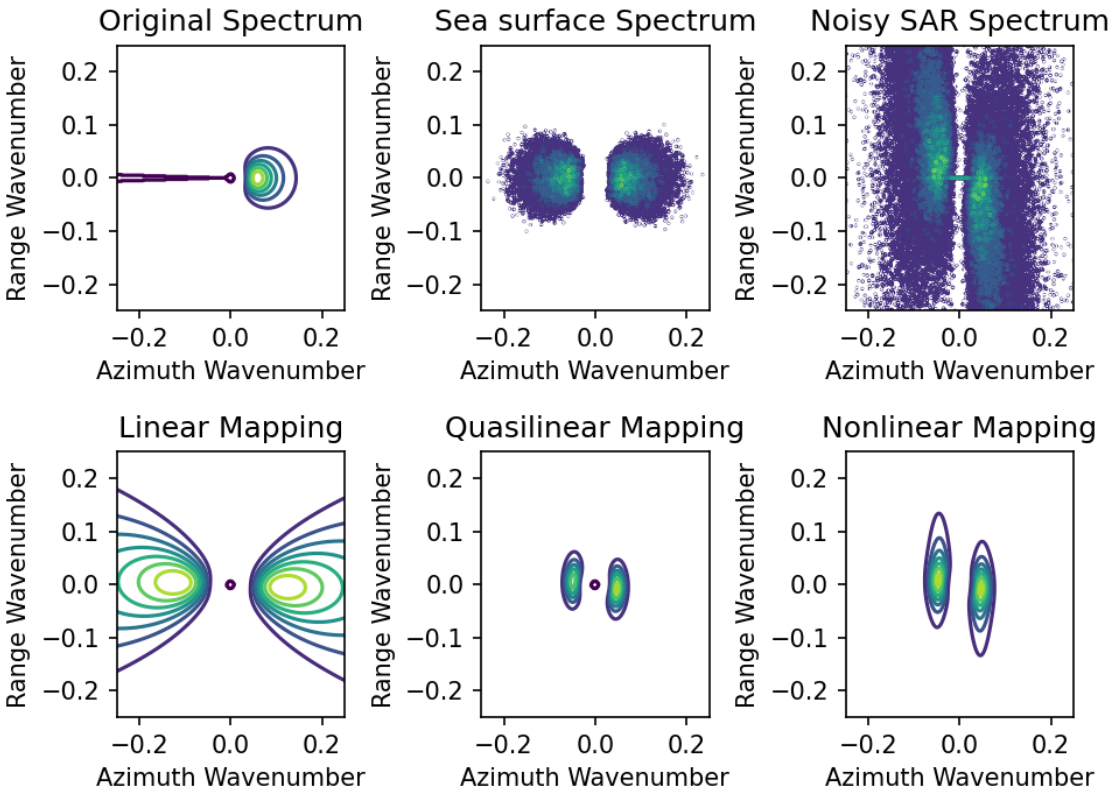

Figure 4.16: Case 8 Plots of spectra

4.3.2 Case 9

Parameter	Value
Wind Speed	10 m/s
Wind Direction	45°
beta	50 s

Table 4.11: Case 9 parameters

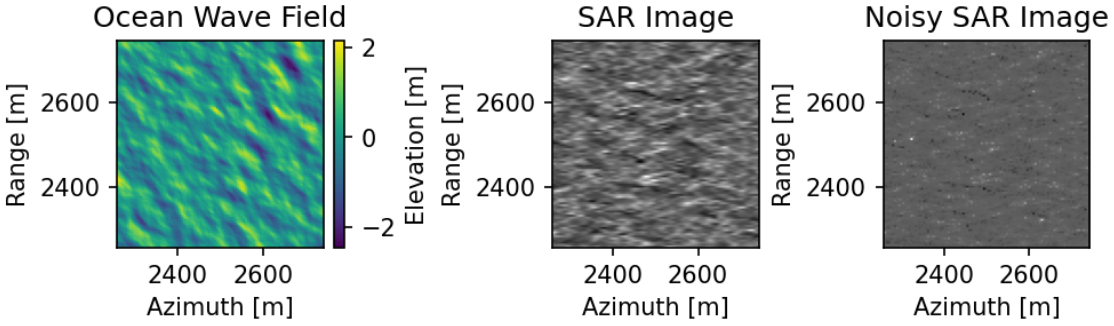

Figure 4.17: Case 9 Ocean Surface with SAR Images

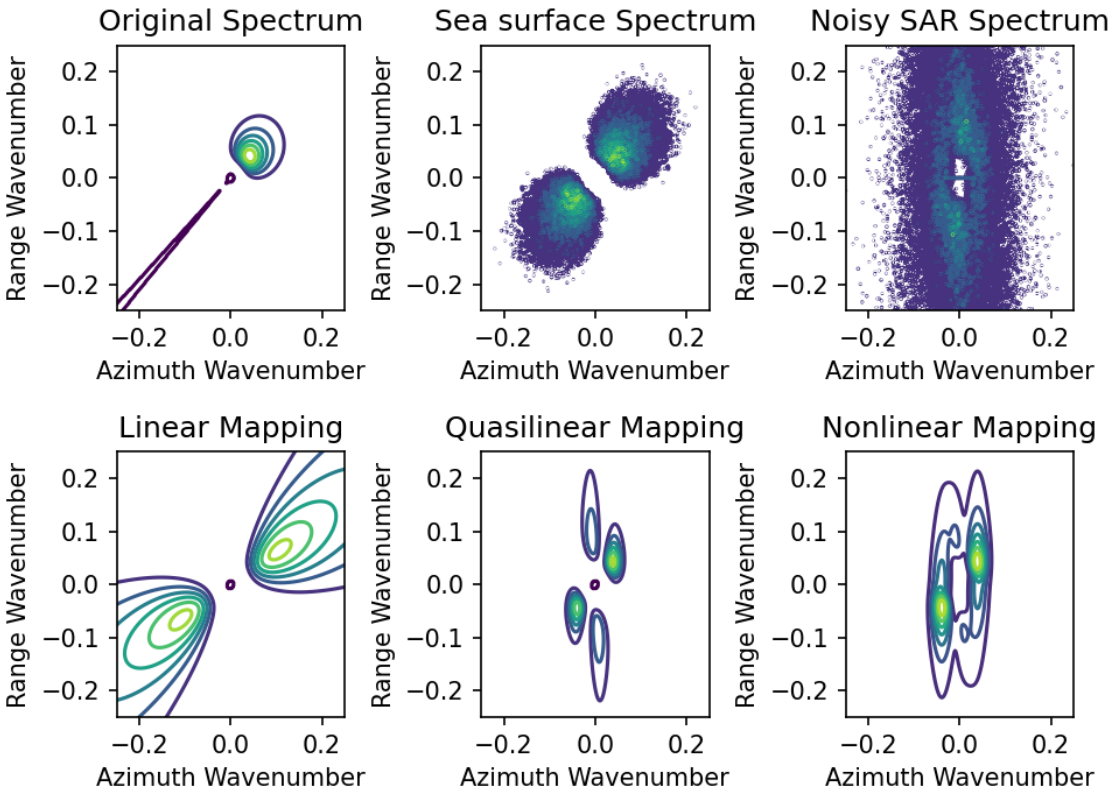

Figure 4.18: Case 9 Plots of spectra

4.3.3 Case 10

Parameter	Value
Wind Speed	10 m/s
Wind Direction	90°
beta	50 s

Table 4.12: Case 10 parameters

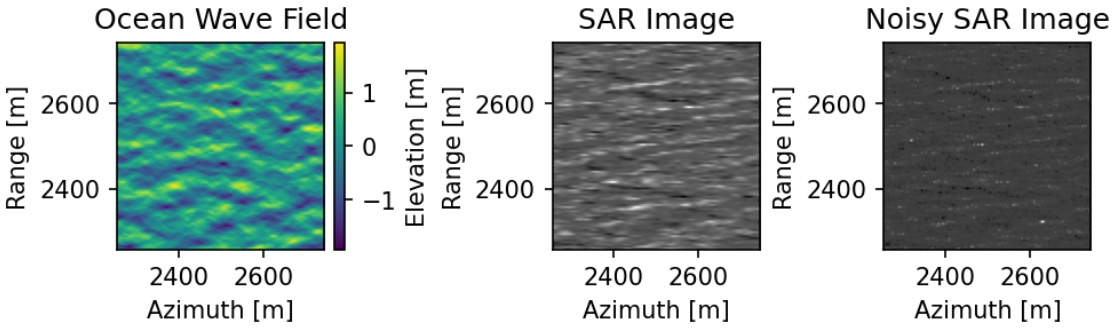

Figure 4.19: Case 10 Ocean Surface with SAR Images

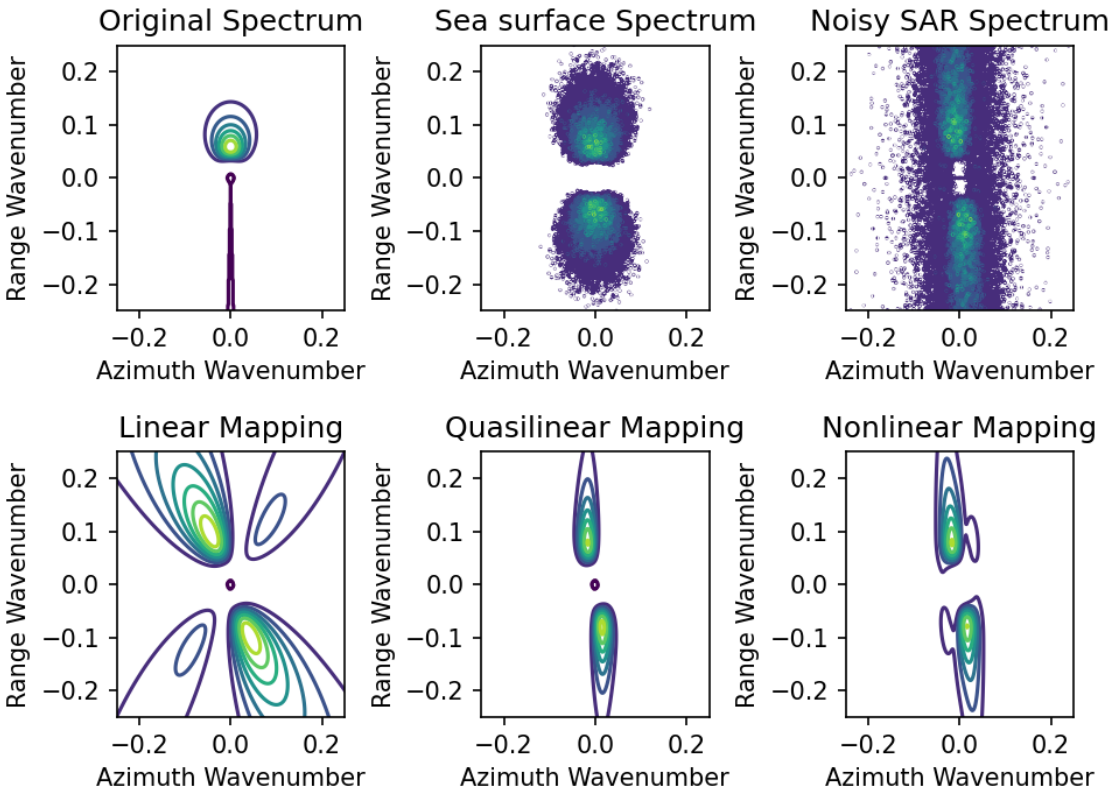

Figure 4.20: Case 10 Plots of spectra

4.3.4 Discussion

In the previous plots, we have done simulations for varying wind directions.
In the case that the ocean wave propagates in the azimuth direction, we can see that the SAR spectrum is both converging to the low azimith wavenumbers, and is shifting towards the high range wavenumbers. The linear mapping does not match the the SAR spectrum. The quasilinear mapping is close to the SAR spectrum, but does not shift towards the high range wavenumbers. Finally, the nonlinear mapping has achieved matching the SAR spectrum.
In the case that the ocean wave propagates with an angle of 45°, the SAR spectrum is concentrated around the zero azimuthal wavenumber. Again the linear mapping does not match the SAR spectrum, The quasilinear mapping has a double peak which is non connected, so it does not match the SAR spectrum. Finally, the nonlinear mapping, also has a double peak, but they are connected, and the spectrum matches the SAR spectrum.
In the case that the ocean wave propagates in the range directions the SAR spectrum is again concetrated around the zero azimuthal wavenumber, but with a small counterclockwise rotation. The linear mapping does not match the SAR spectrum. The quasilinear matches the shift towards the zero azimuthal wavenumber, but does not match the rotation. Finally, the nonlinear mapping matches the SAR spectrum, with an addition of the double peak.

4.4 Varying β

4.4.1 Case 11

In this section, we are demonstrating the results for simulations for varying β.

Parameter	Value
Wind Speed	10 m/s
Wind Direction	45°
beta	10 s

Table 4.13: Case 11 parameters

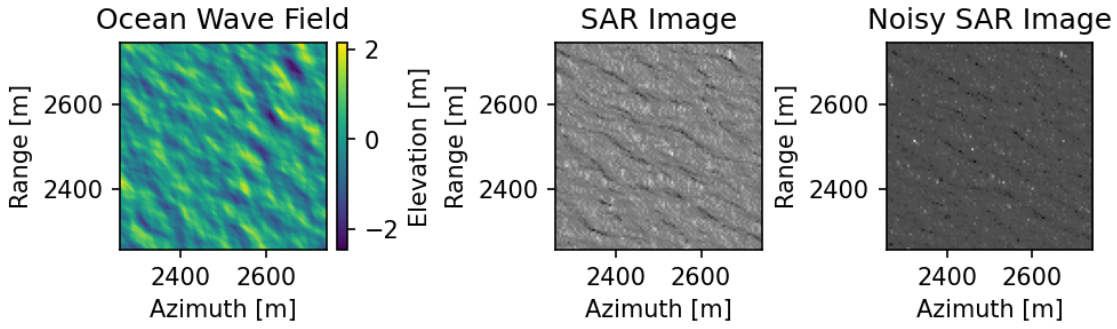

Figure 4.21: Case 11 Ocean Surface with SAR Images

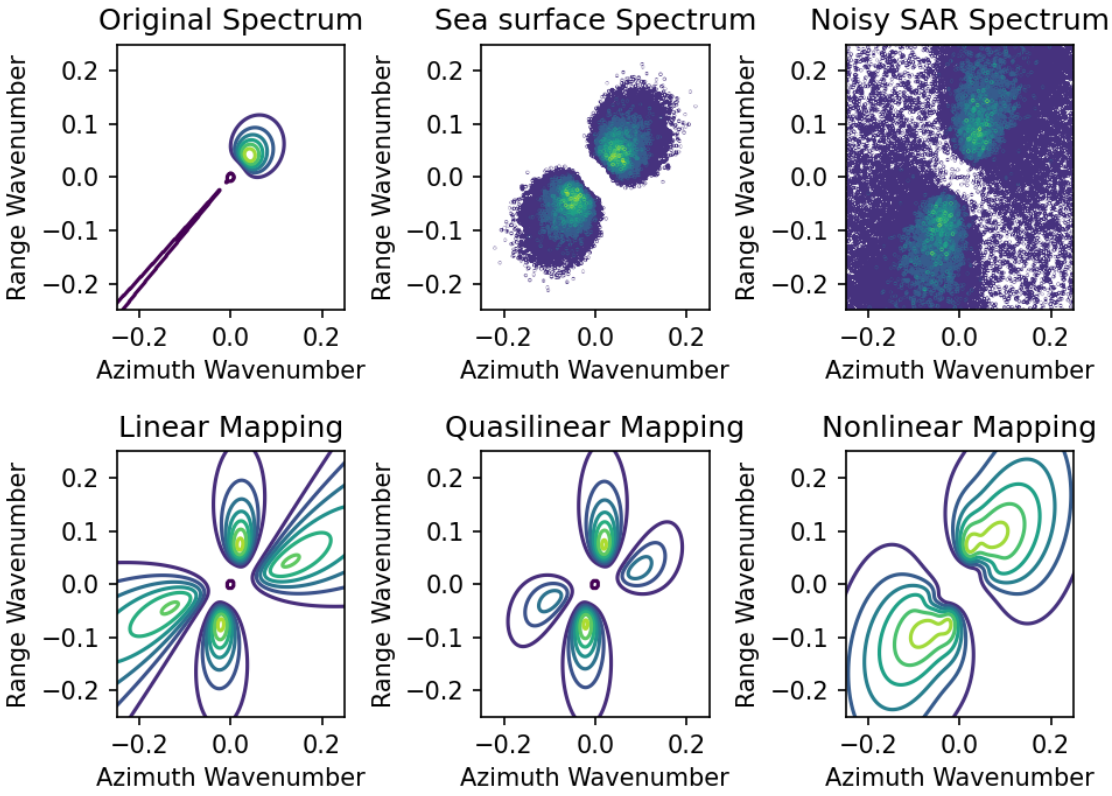

Figure 4.22: Case 11 Plots of spectra

4.4.2 Case 12

Parameter	Value
Wind Speed	10 m/s
Wind Direction	45°
beta	100 s

Table 4.14: Case 12 parameters

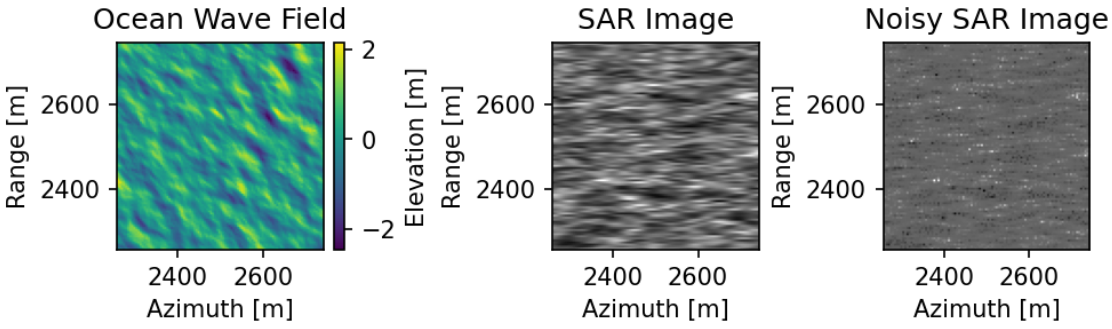

Figure 4.23: Case 12 Ocean Surface with SAR Images

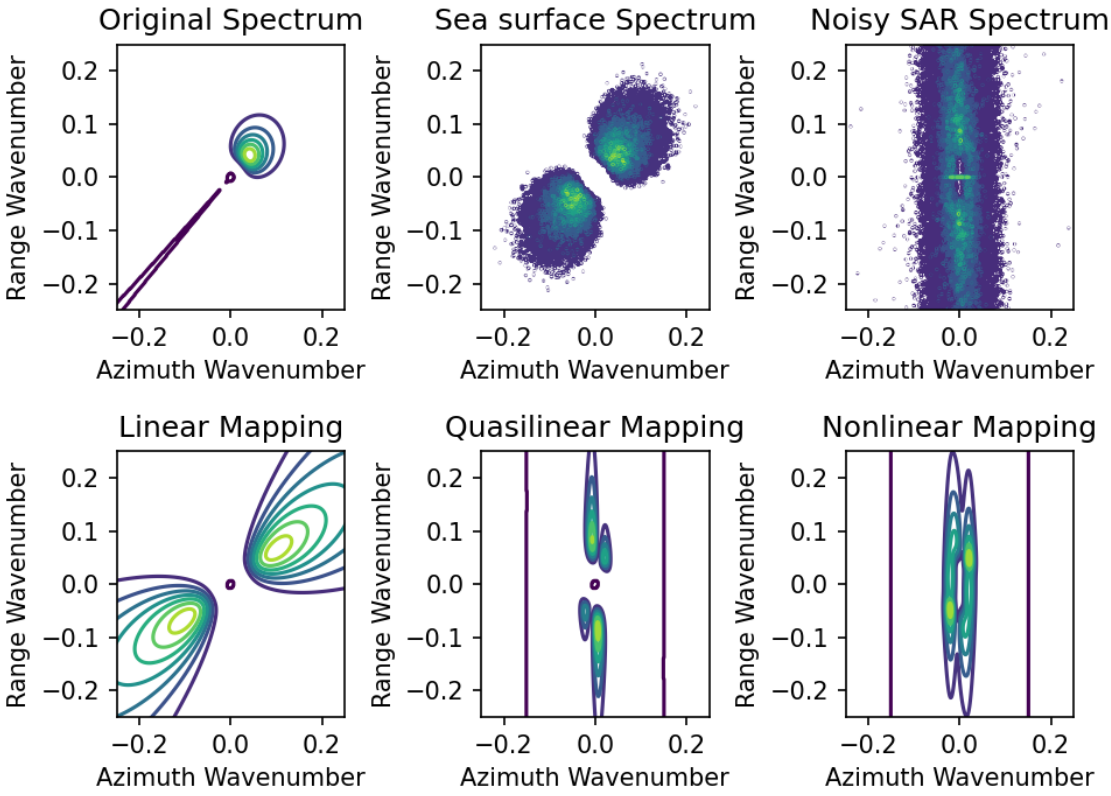

Figure 4.24: Case 12 Plots of spectra

4.4.3 Discussion

In the previous plots, we have done simulations for varying β.
In the case with low value of β we can see that the SAR spectrum is simular to the original spectrum. The linear mapping has a big double peak, so it does not match the SAR spectrum. The quasilinear mapping is similar to the linear mapping but with a smaller double peak. Moreover, the strong peak is shifted towards the zero azimuthal wavenumber more than the peak of the SAR spectrum. Finally, the nonlinear mapping has achieved matching of the SAR spectrum.
In the case of the high value of β we can see that the SAR spectrum is completely on the zero azimuthal wavenumber. The linear mapping does not match the SAR spectrum. The quasilinear mapping is closely aligned with the SAR spectrum, but one peak is smaller than the other, making the spectra stronger counterclockwise. Finally, the nonlinear mapping matches the SAR spectrum.

5
Conclusion

In this project, we aimed to create a simulator, which given wind parameters can generate an ocean wave field and transform it to a SAR image. During this process, we evaluated the possibility of using the *Fast Fourier Transform* for faster calculations, which resulted in statistically results. Finally, we have implemented the linear, quasilinear and nonlinear mapping to the SAR spectrum. Our results, present different cases which show the effect of wind speed, wind direction and β on the mapping.
For the evaluation of the results, we have compared the linear, quasilinear and nonlinear mappings and found out that the nonlinear mapping always achieves good similarity to the SAR spectrum. Moreover, the results agree with Brunning's simulations [14]. This means the the nonlinear mapping can be accurately be used in all cases, while the linear and quasilinear can not always achieve the mapping.

5.1 Future Work

Althouth, this simulator was developed in a limited scope, we believe in can be extended into a complete simulator, with the addition of ocean currents, and the transformation of the linear waves, to nonlinear ones.
An interesting test for evaluation, is using real world SAR data, but this type of data is often proprietery and are not easily obtainable

Bibliography

[1] Willard J Pierson Jr and Lionel Moskowitz. A proposed spectral form for fully developed wind seas based on the similarity theory of sa kitaigorodskii. *Journal of geophysical research*, 69(24):5181–5190, 1964.

[2] Mikhail B Kanevsky. *Radar imaging of the ocean waves*. Elsevier, 2008.

[3] Tanos Elfouhaily, Bertrand Chapron, Kristina Katsaros, and Douglas Vandemark. A unified directional spectrum for long and short wind-driven waves. *Journal of Geophysical Research: Oceans*, 102(C7):15781–15796, 1997.

[4] Werner Alpers. Monte carlo simulations for studying the relationship between ocean wave and synthetic aperture radar image spectra. *Journal of Geophysical Research: Oceans*, 88(C3):1745–1759, 1983.

[5] Werner Alpers, Claus Bruening, and Karl Richter. Comparison of simulated and measured synthetic aperture radar image spectra with buoy-derived ocean wave spectra during the shuttle imaging radar b mission. *IEEE Transactions on Geoscience and Remote Sensing*, (4):559–566, 1986.

[6] Klaus Hasselmann and Susanne Hasselmann. On the nonlinear mapping of an ocean wave spectrum into a synthetic aperture radar image spectrum and its inversion. *Journal of Geophysical Research: Oceans*, 96(C6):10713–10729, 1991.

[7] Igor G Rizaev, Oktay Karakuş, S John Hogan, and Alin Achim. Modeling and sar imaging of the sea surface: A review of the state-of-the-art with simulations. *ISPRS Journal of Photogrammetry and Remote Sensing*, 187:120–140, 2022.

[8] Klaus Hasselmann, Tim P Barnett, E Bouws, H Carlson, David E Cartwright, K Enke, JA Ewing, A Gienapp, DE Hasselmann, P Kruseman, et al. Measurements of wind-wave growth and swell decay during the joint north sea wave project (jonswap). *Ergaenzungsheft zur Deutschen Hydrographischen Zeitschrift, Reihe A*, 1973.

[9] Gregory Zilman, Anatoli Zapolski, and Moshe Marom. On detectability of a ship's kelvin wake in simulated sar images of rough sea surface. *IEEE Transactions on Geoscience and Remote Sensing*, 53(2):609–619, 2014.

[10] Xiao-Ming Li. *Ocean surface wave measurements using SAR wave mode data*. PhD thesis, University of Hamburg, 2010.

[11] Johannes Schulz-Stellenfleth. *Ocean wave measurements using complex synthetic aperture radar data*. PhD thesis, Staats-und Universitätsbibliothek Hamburg Carl von Ossietzky, 2003.

[12] Stephen J Frasier and Adriano J Camps. Dual-beam interferometry for ocean surface current vector mapping. *IEEE Transactions on geoscience and remote sensing*, 39(2):401–414, 2001.

[13] Jerry Tessendorf et al. Simulating ocean water. *Simulating nature: realistic and interactive techniques. SIGGRAPH*, 1(2):5, 2001.

[14] Claus Brüning, Werner Alpers, and Klaus Hasselmann. Monte-carlo simulation studies of the nonlinear imaging of a two dimensional surface wave field by a synthetic aperture radar. *Remote Sensing*, 11(10):1695–1727, 1990.

A

Appendix 1

A.1 Case A1

Parameter	Value
Wind Speed	5 m/s
Wind Direction	0°
beta	10 s

Table A.1: Case A1 parameters

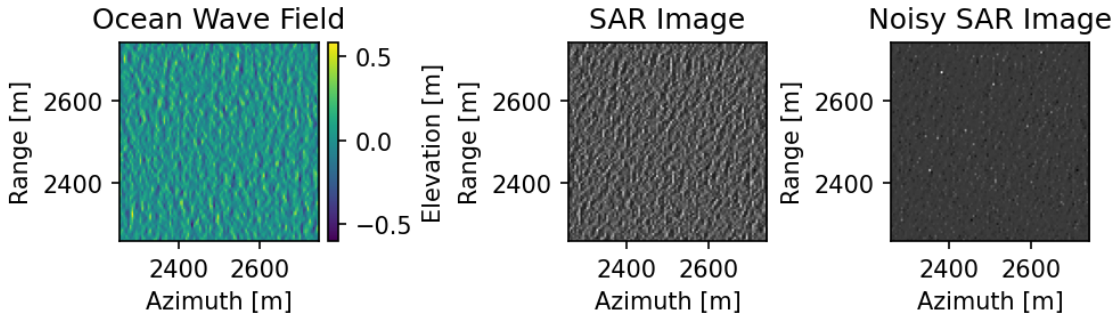

Figure A.1: Case A1 Ocean Surface with SAR Images

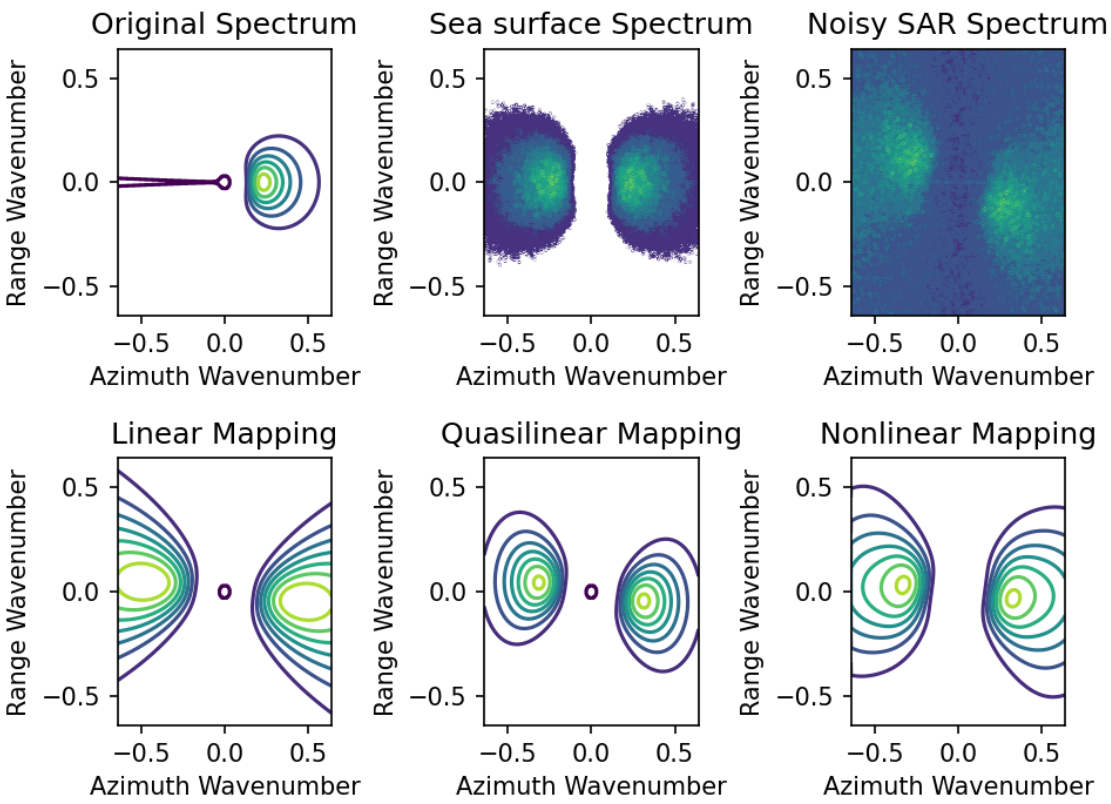

Figure A.2: Case A1 Plots of spectra

A.2 Case A2

Parameter	Value
Wind Speed	5 m/s
Wind Direction	0°
beta	50 s

Table A.2: Case A2 parameters

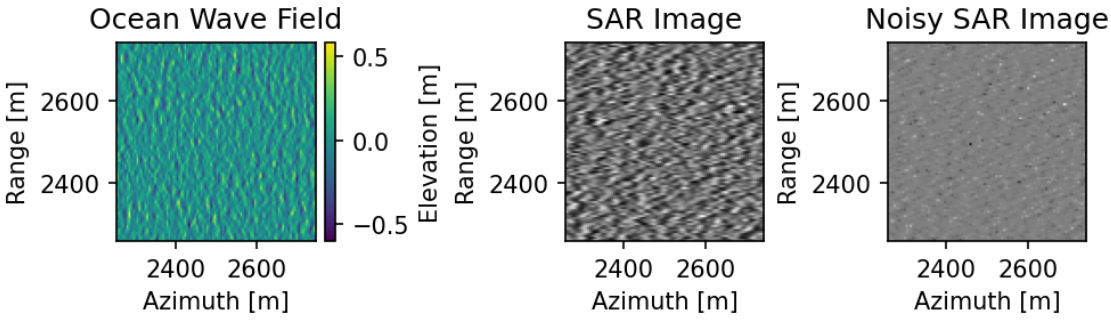

Figure A.3: Case A2 Ocean Surface with SAR Images

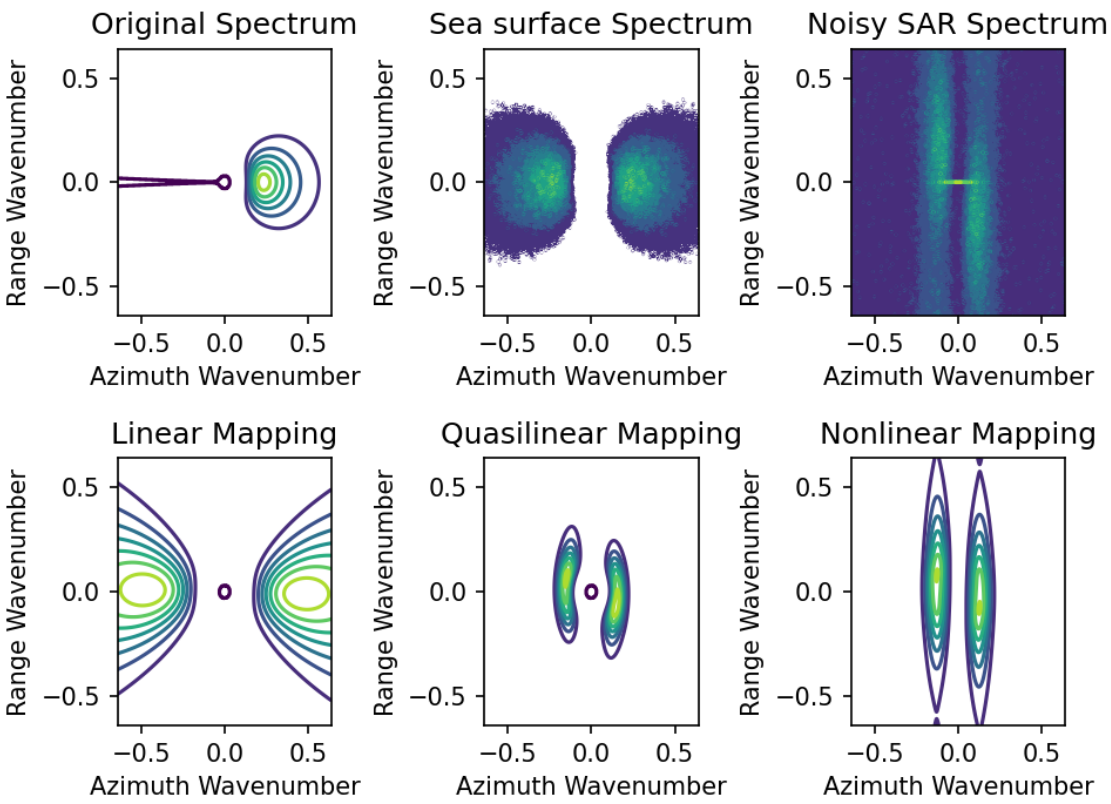

Figure A.4: Case A2 Plots of spectra

A.3 Case A3

Parameter	Value
Wind Speed	5 m/s
Wind Direction	0°
beta	100 s

Table A.3: Case A3 parameters

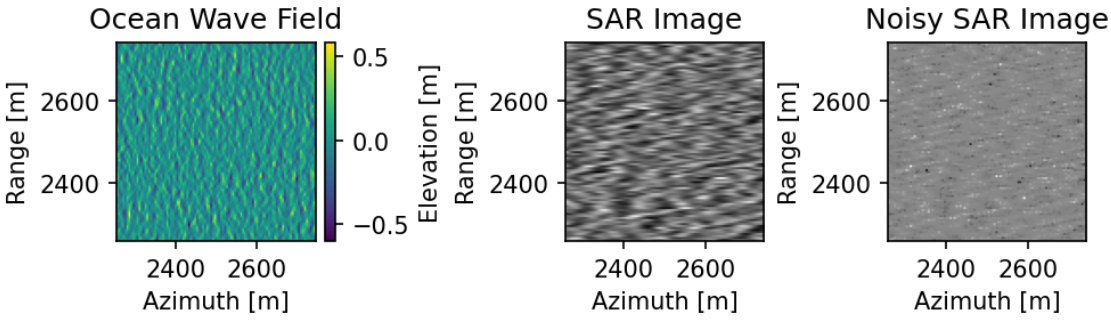

Figure A.5: Case A3 Ocean Surface with SAR Images

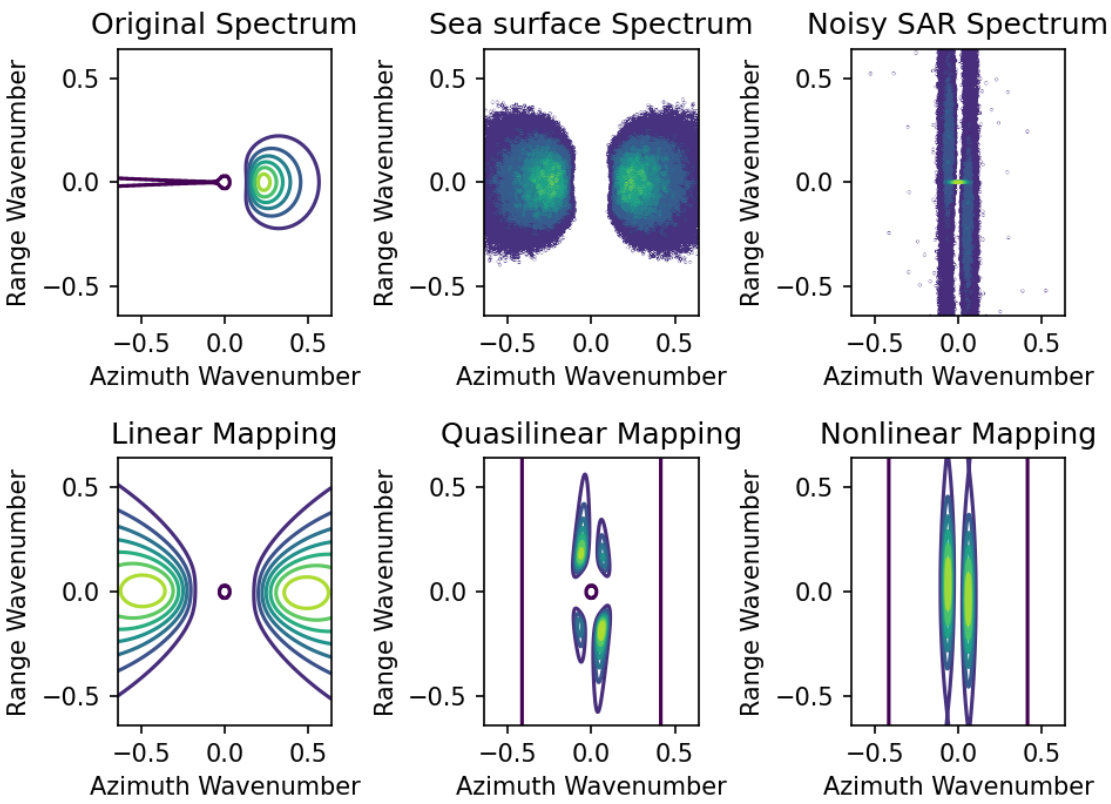

Figure A.6: Case A3 Plots of spectra

A.4 Case A4

Parameter	Value
Wind Speed	5 m/s
Wind Direction	45°
beta	10 s

Table A.4: Case A4 parameters

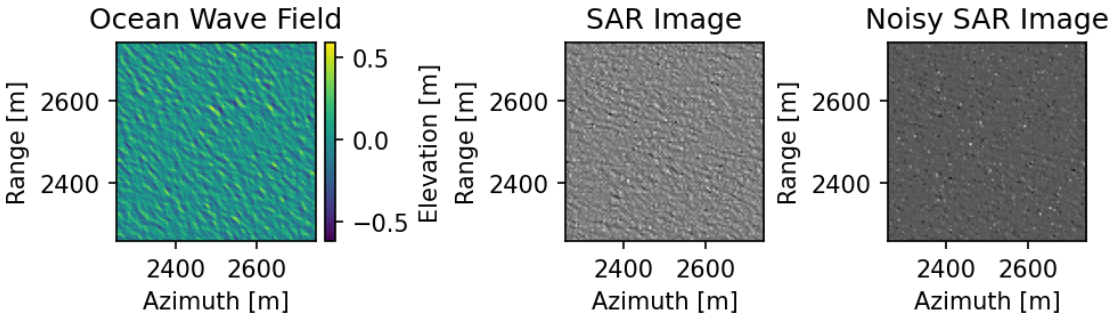

Figure A.7: Case A4 Ocean Surface with SAR Images

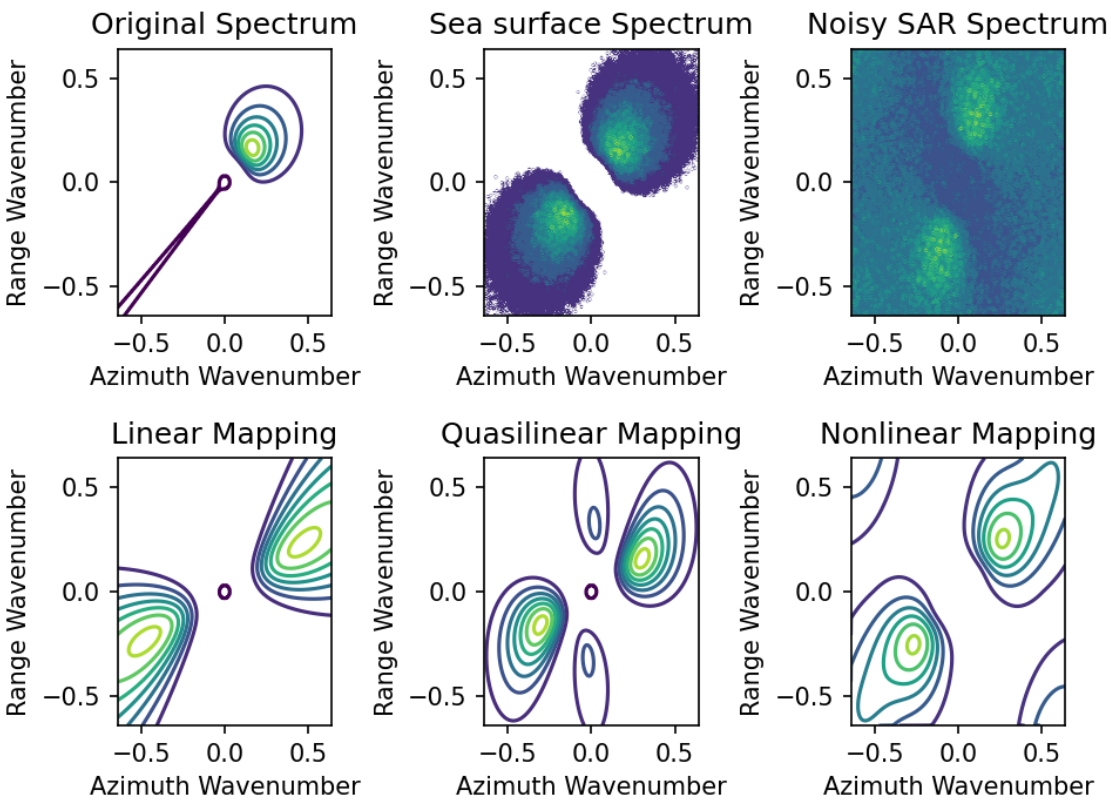

Figure A.8: Case A4 Plots of spectra

A.5 Case A5

Parameter	Value
Wind Speed	5 m/s
Wind Direction	45°
beta	50 s

Table A.5: Case A5 parameters

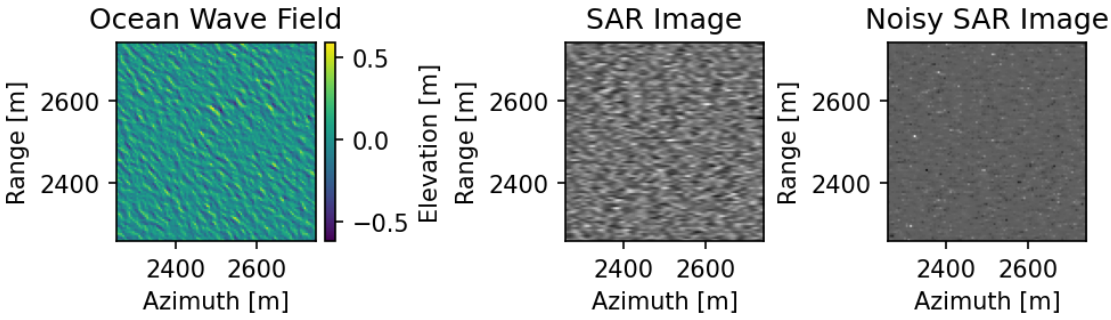

Figure A.9: Case A5 Ocean Surface with SAR Images

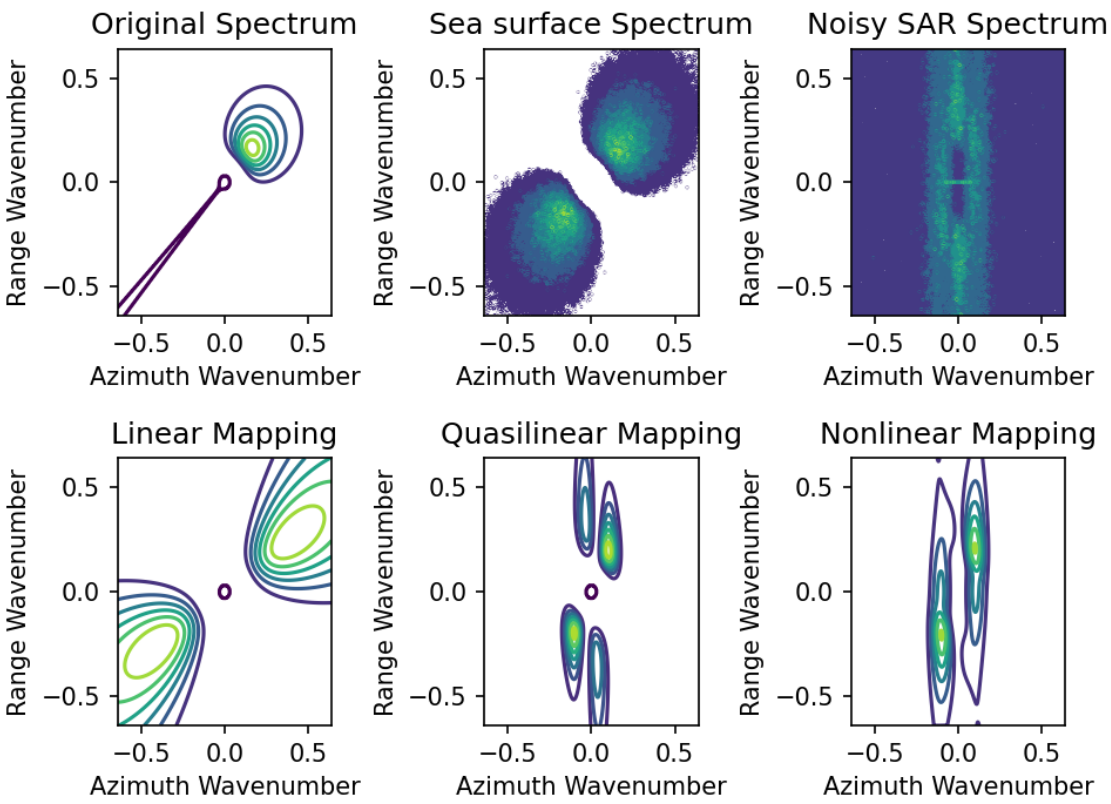

Figure A.10: Case A5 Plots of spectra

A.6 Case A6

Parameter	Value
Wind Speed	5 m/s
Wind Direction	45°
beta	100 s

Table A.6: Case A6 parameters

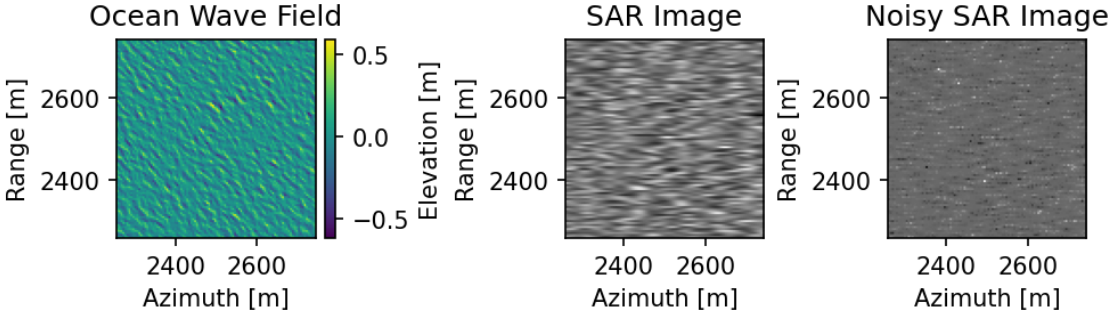

Figure A.11: Case A6 Ocean Surface with SAR Images

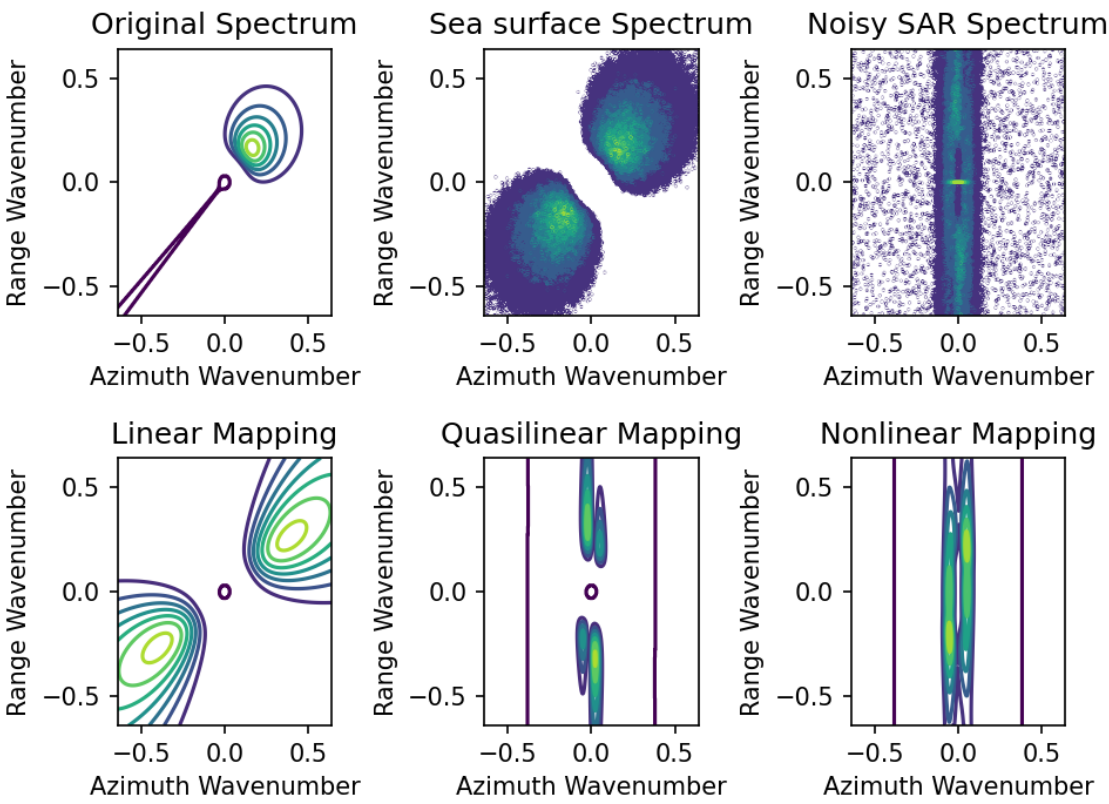

Figure A.12: Case A6 Plots of spectra

A.7 Case A7

Parameter	Value
Wind Speed	5 m/s
Wind Direction	90°
beta	10 s

Table A.7: Case A7 parameters

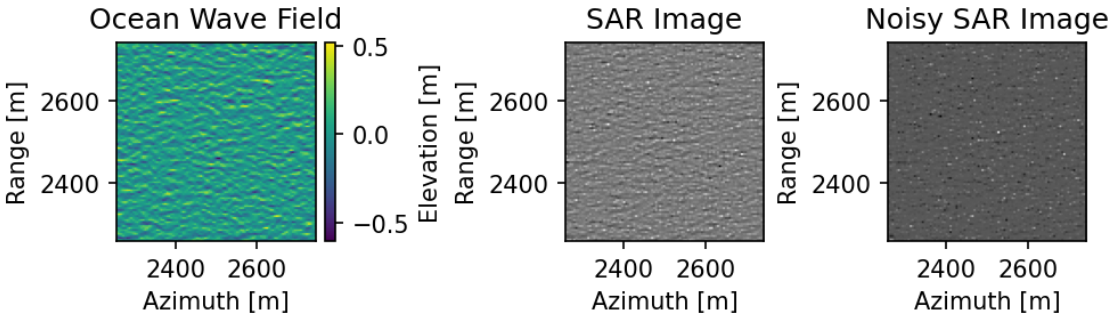

Figure A.13: Case A7 Ocean Surface with SAR Images

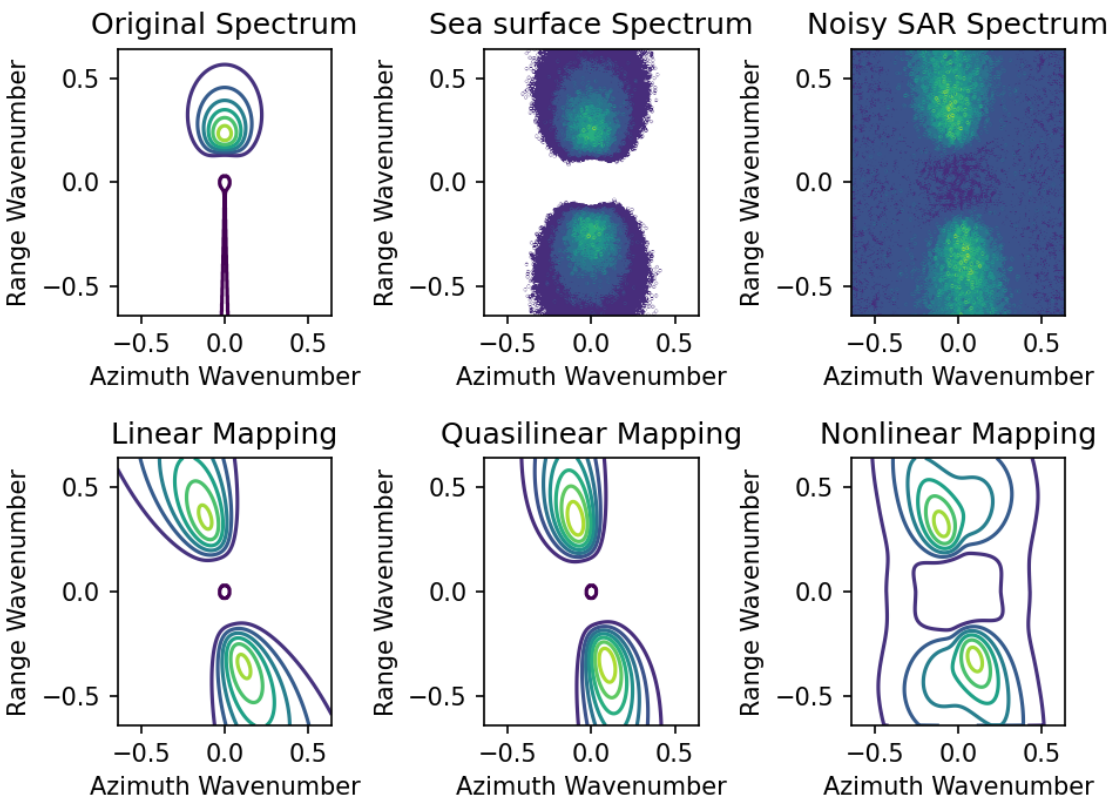

Figure A.14: Case A7 Plots of spectra

A.8 Case A8

Parameter	Value
Wind Speed	5 m/s
Wind Direction	90°
beta	50 s

Table A.8: Case A8 parameters

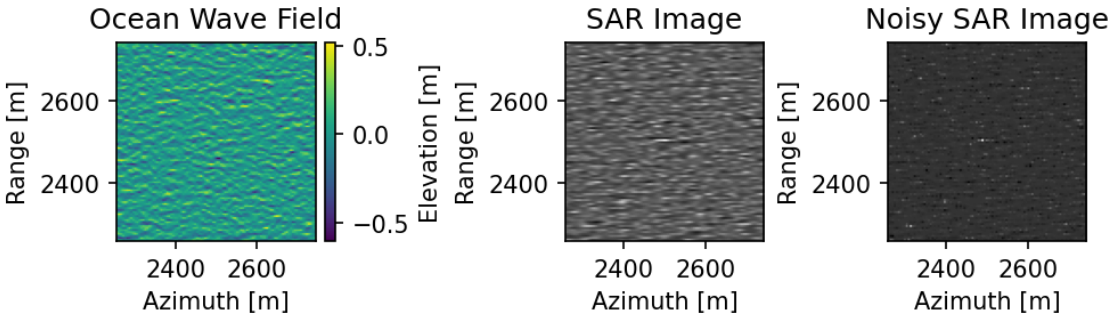

Figure A.15: Case A8 Ocean Surface with SAR Images

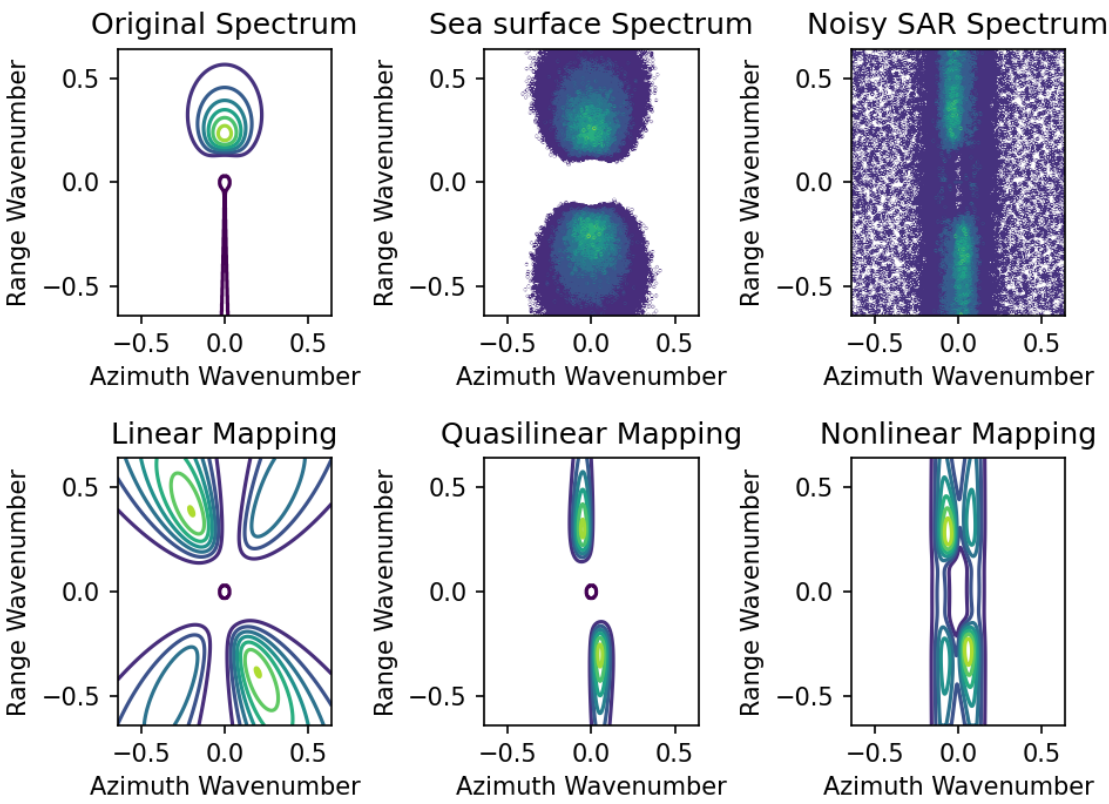

Figure A.16: Case A8 Plots of spectra

A.9 Case A9

Parameter	Value
Wind Speed	5 m/s
Wind Direction	90°
beta	100 s

Table A.9: Case A9 parameters

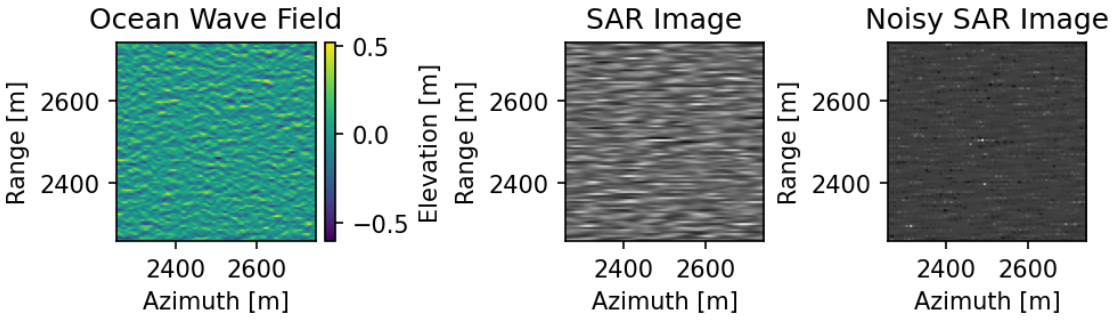

Figure A.17: Case A9 Ocean Surface with SAR Images

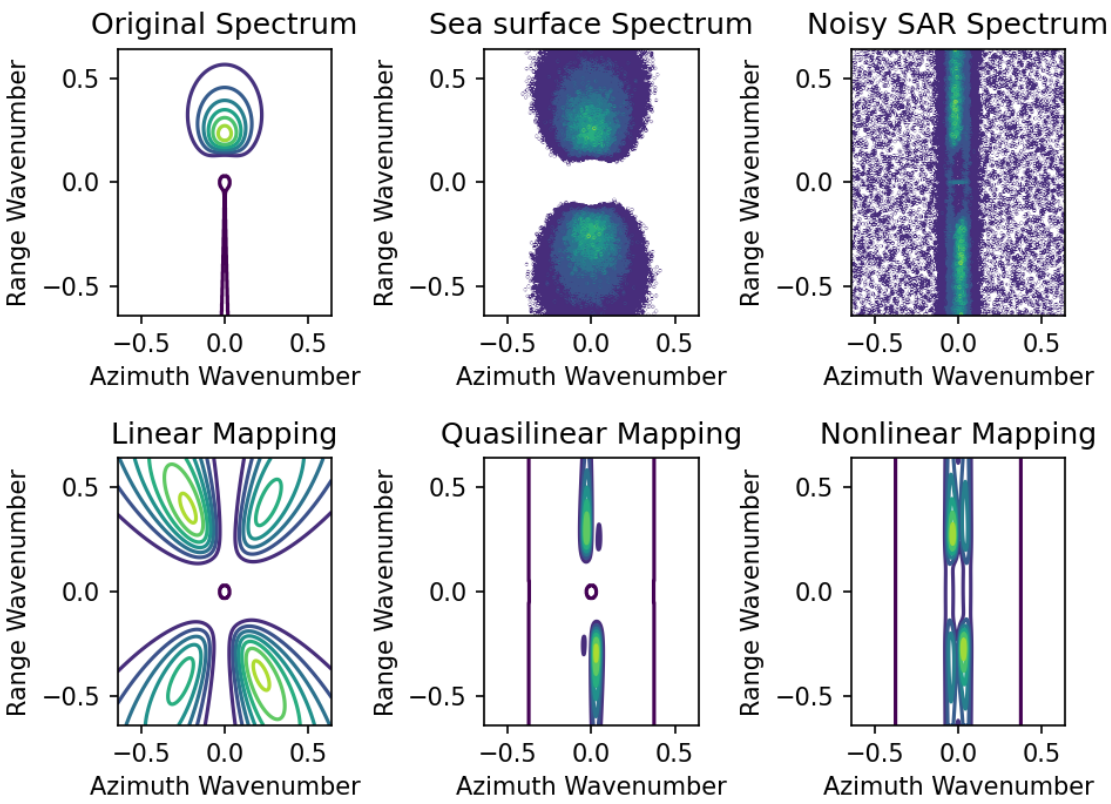

Figure A.18: Case A9 Plots of spectra

A.10 Case A10

Parameter	Value
Wind Speed	10 m/s
Wind Direction	0°
beta	10 s

Table A.10: Case A10 parameters

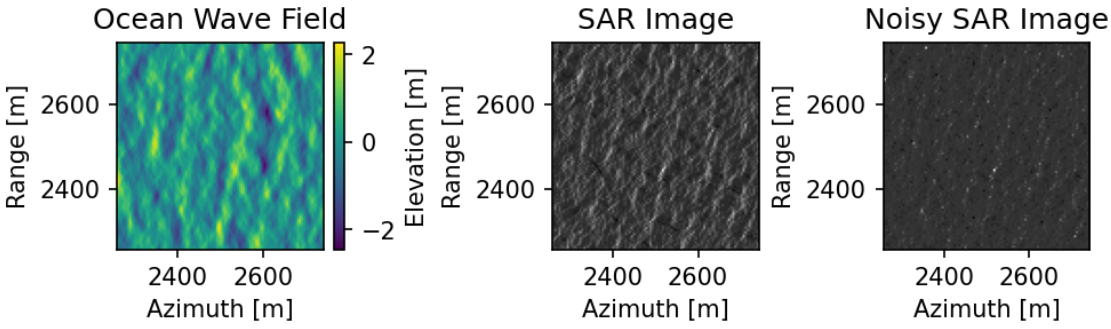

Figure A.19: Case A10 Ocean Surface with SAR Images

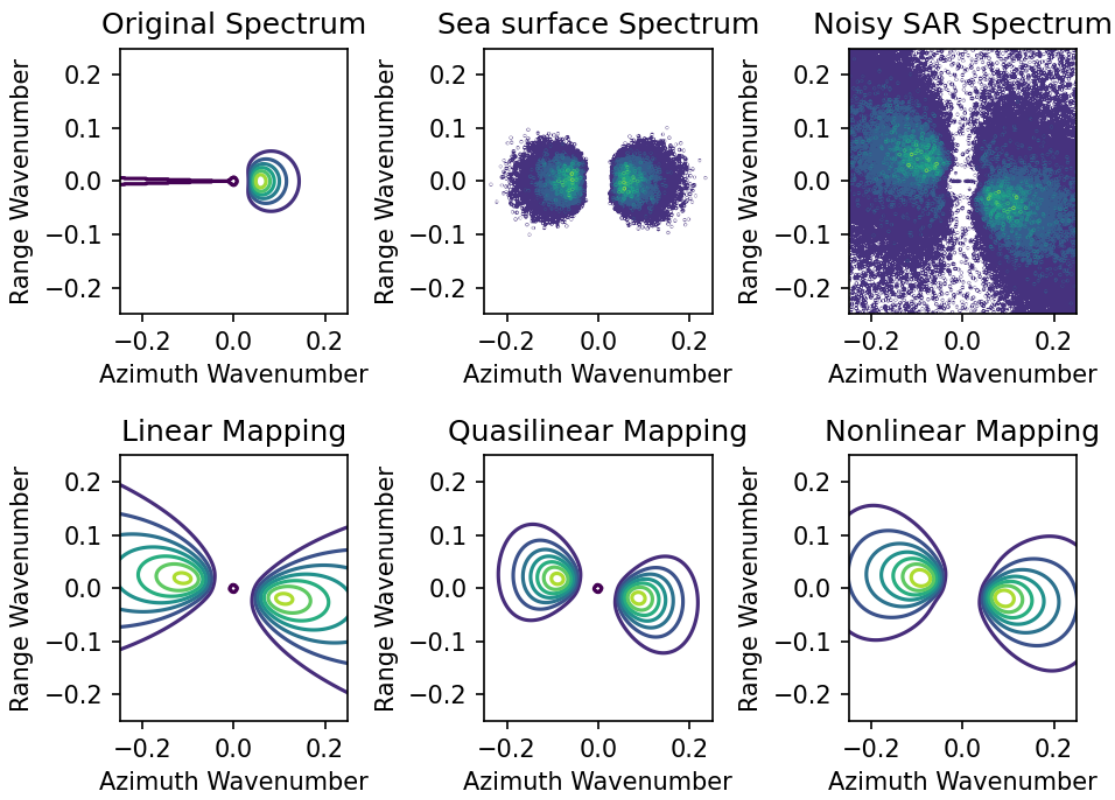

Figure A.20: Case A10 Plots of spectra

A.11 Case A11

Parameter	Value
Wind Speed	10 m/s
Wind Direction	0°
beta	50 s

Table A.11: Case A11 parameters

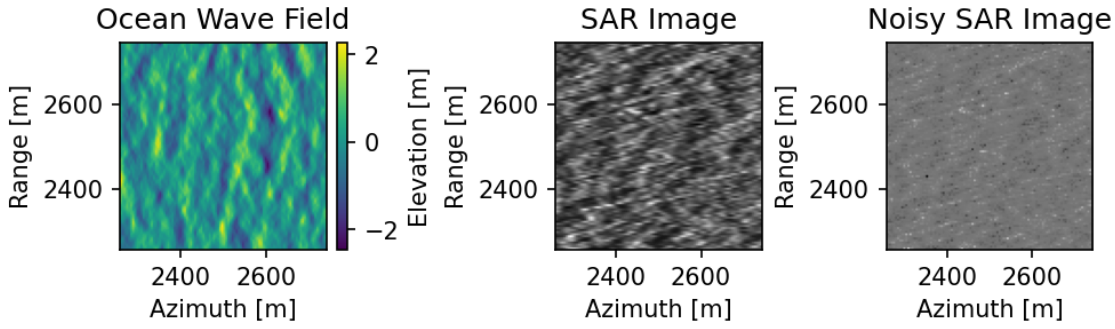

Figure A.21: Case A11 Ocean Surface with SAR Images

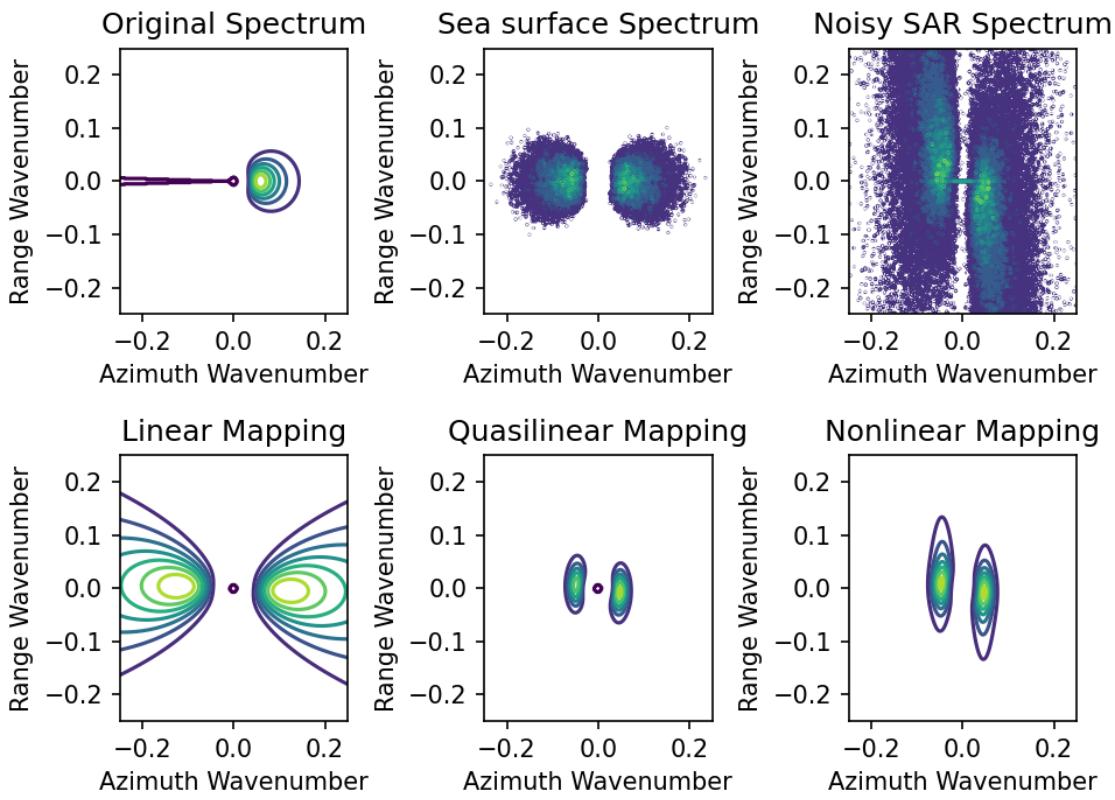

Figure A.22: Case A11 Plots of spectra

A.12 Case A12

Parameter	Value
Wind Speed	10 m/s
Wind Direction	0°
beta	100 s

Table A.12: Case A12 parameters

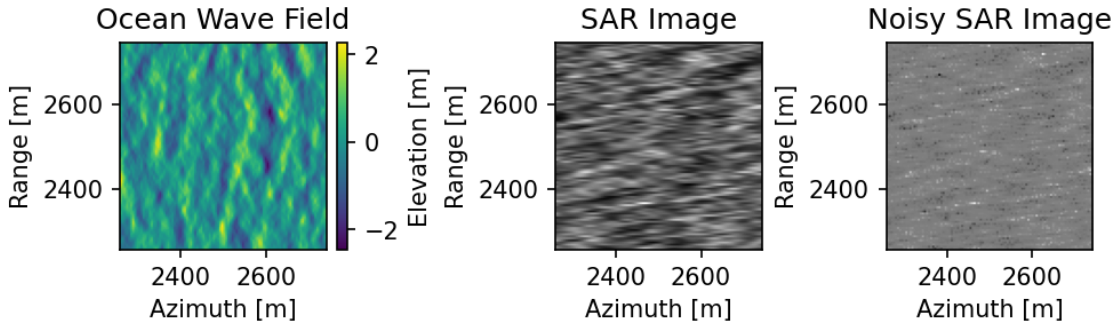

Figure A.23: Case A12 Ocean Surface with SAR Images

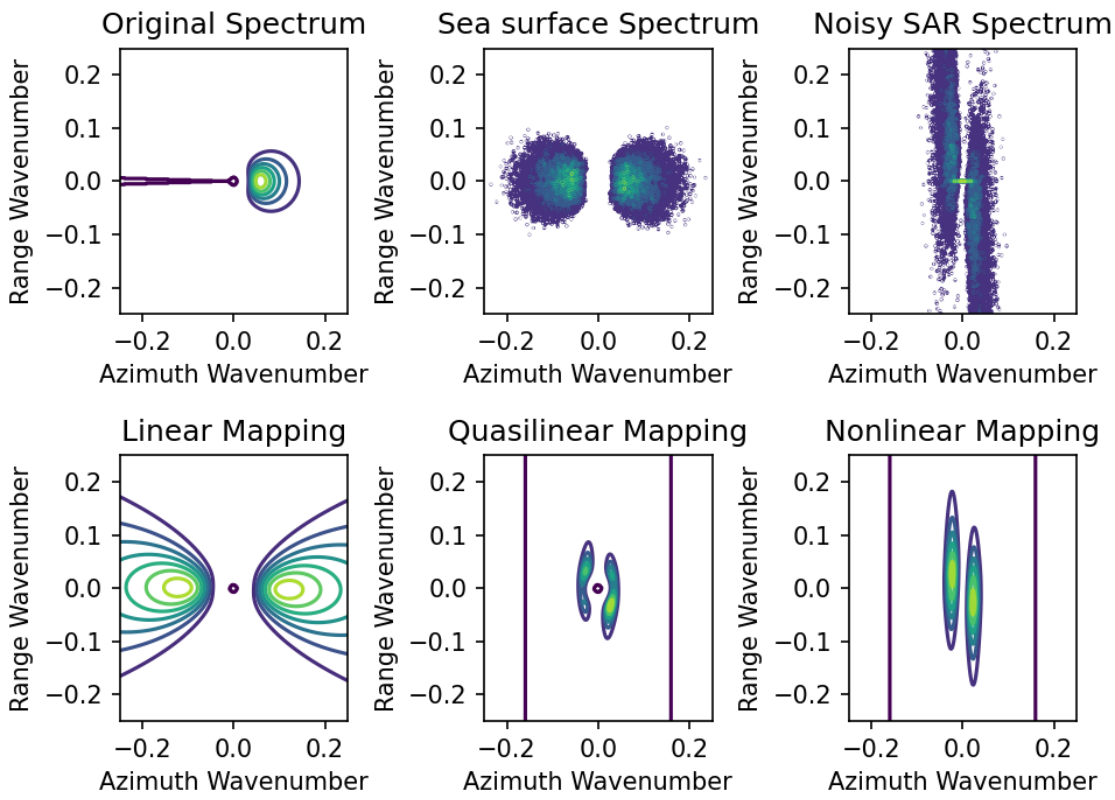

Figure A.24: Case A12 Plots of spectra

A.13 Case A13

Parameter	Value
Wind Speed	10 m/s
Wind Direction	45°
beta	10 s

Table A.13: Case A13 parameters

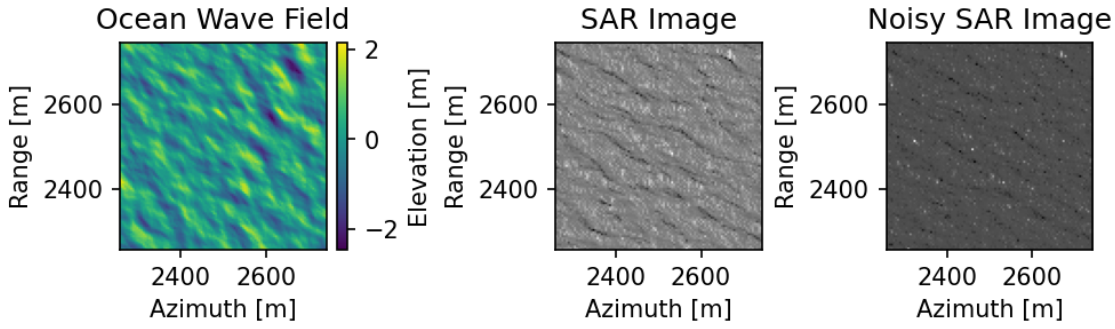

Figure A.25: Case A13 Ocean Surface with SAR Images

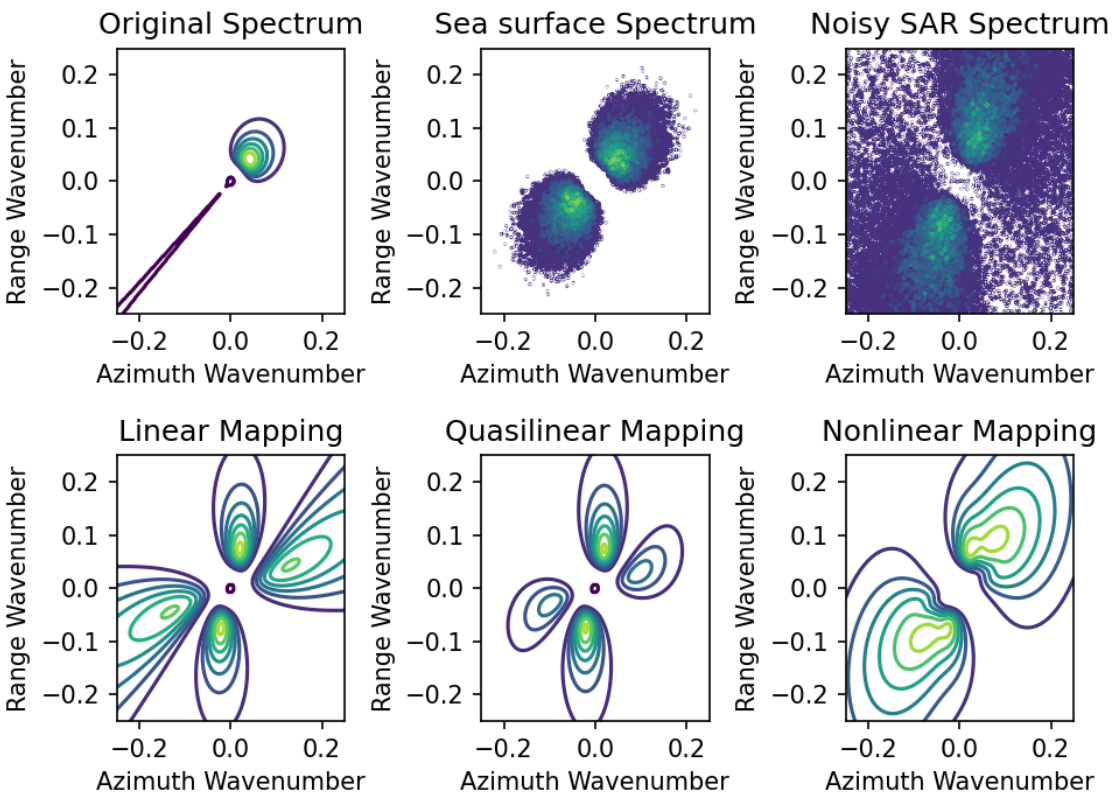

Figure A.26: Case A13 Plots of spectra

A.14 Case A14

Parameter	Value
Wind Speed	10 m/s
Wind Direction	45°
beta	50 s

Table A.14: Case A14 parameters

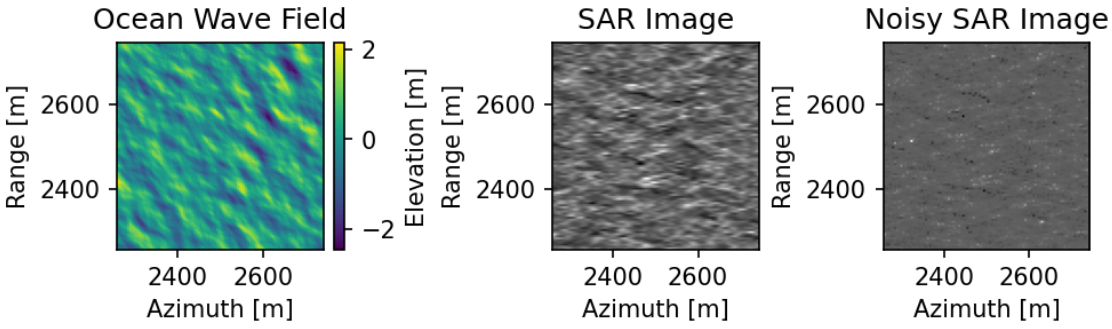

Figure A.27: Case A14 Ocean Surface with SAR Images

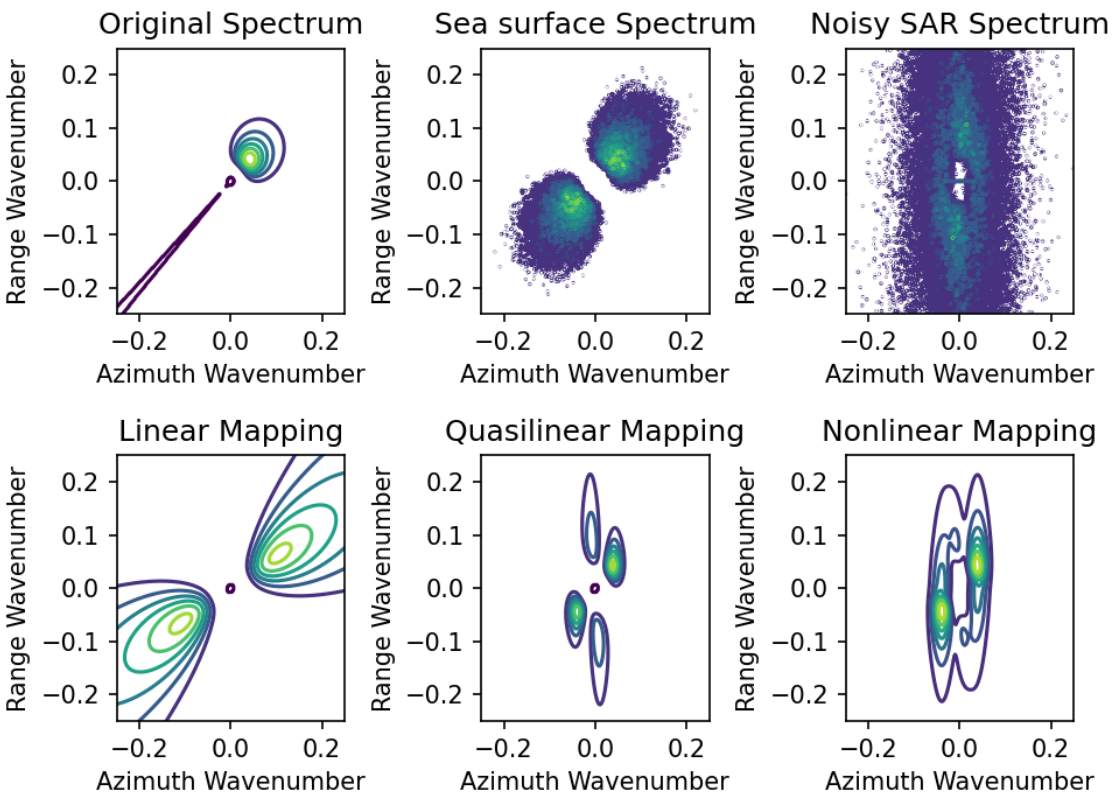

Figure A.28: Case A14 Plots of spectra

A.15 Case A15

Parameter	Value
Wind Speed	10 m/s
Wind Direction	45°
beta	100 s

Table A.15: Case A15 parameters

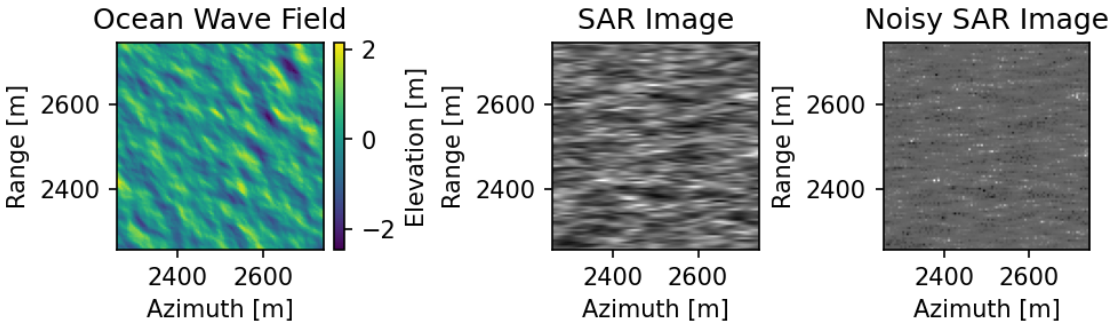

Figure A.29: Case A15 Ocean Surface with SAR Images

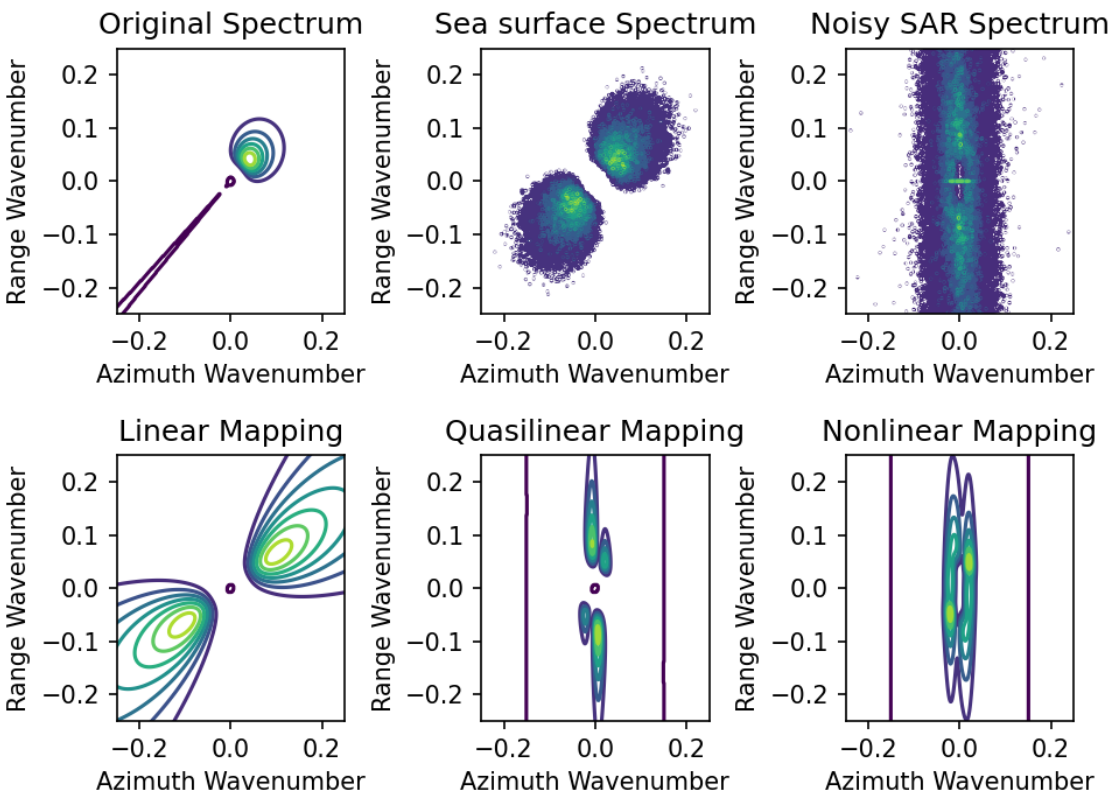

Figure A.30: Case A15 Plots of spectra

A.16 Case A16

Parameter	Value
Wind Speed	10 m/s
Wind Direction	90°
beta	10 s

Table A.16: Case A16 parameters

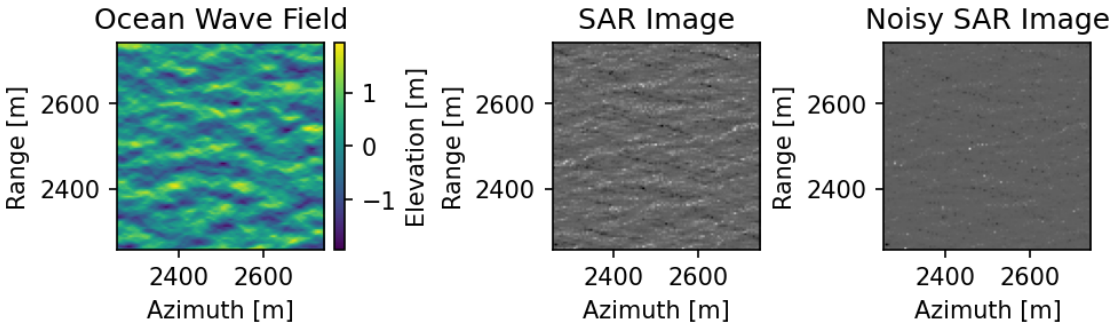

Figure A.31: Case A16 Ocean Surface with SAR Images

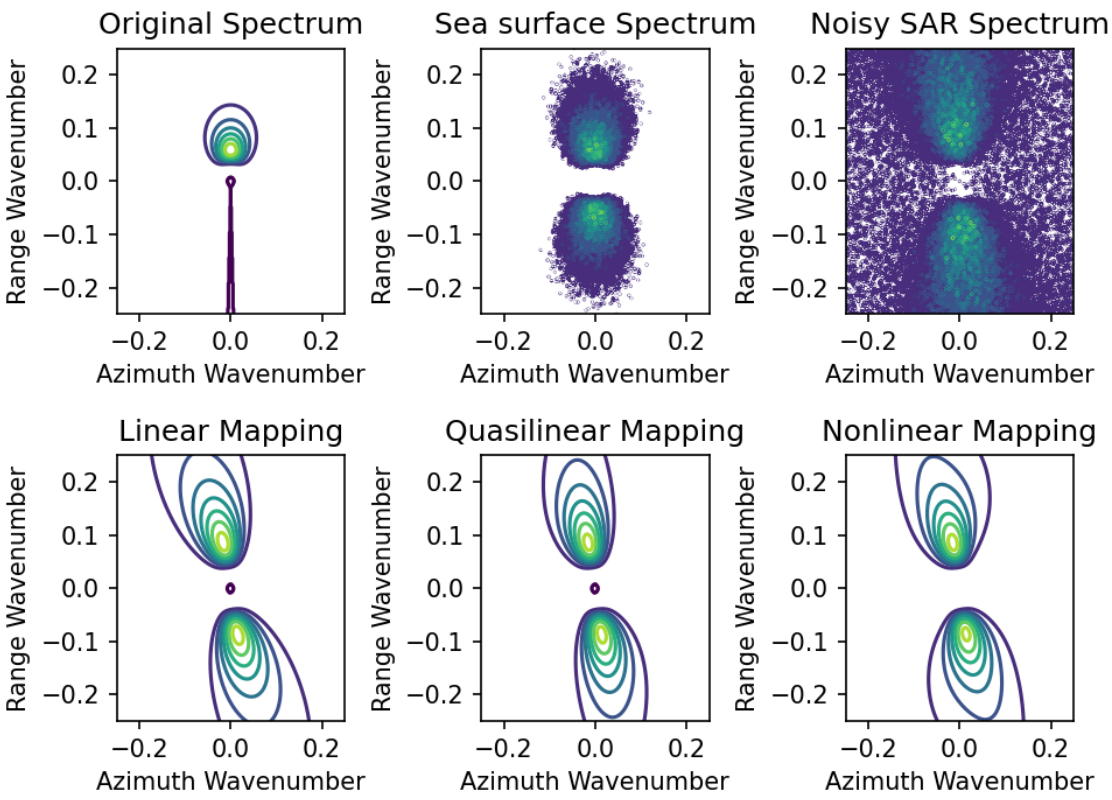

Figure A.32: Case A16 Plots of spectra

A.17 Case A17

Parameter	Value
Wind Speed	10 m/s
Wind Direction	90°
beta	50 s

Table A.17: Case A17 parameters

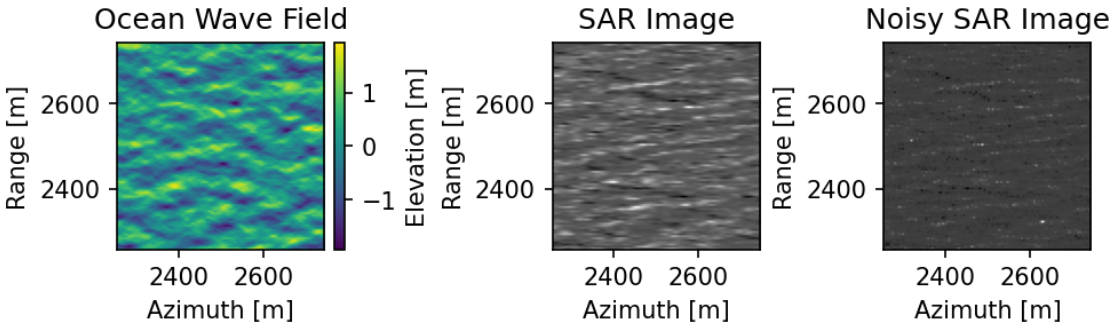

Figure A.33: Case A17 Ocean Surface with SAR Images

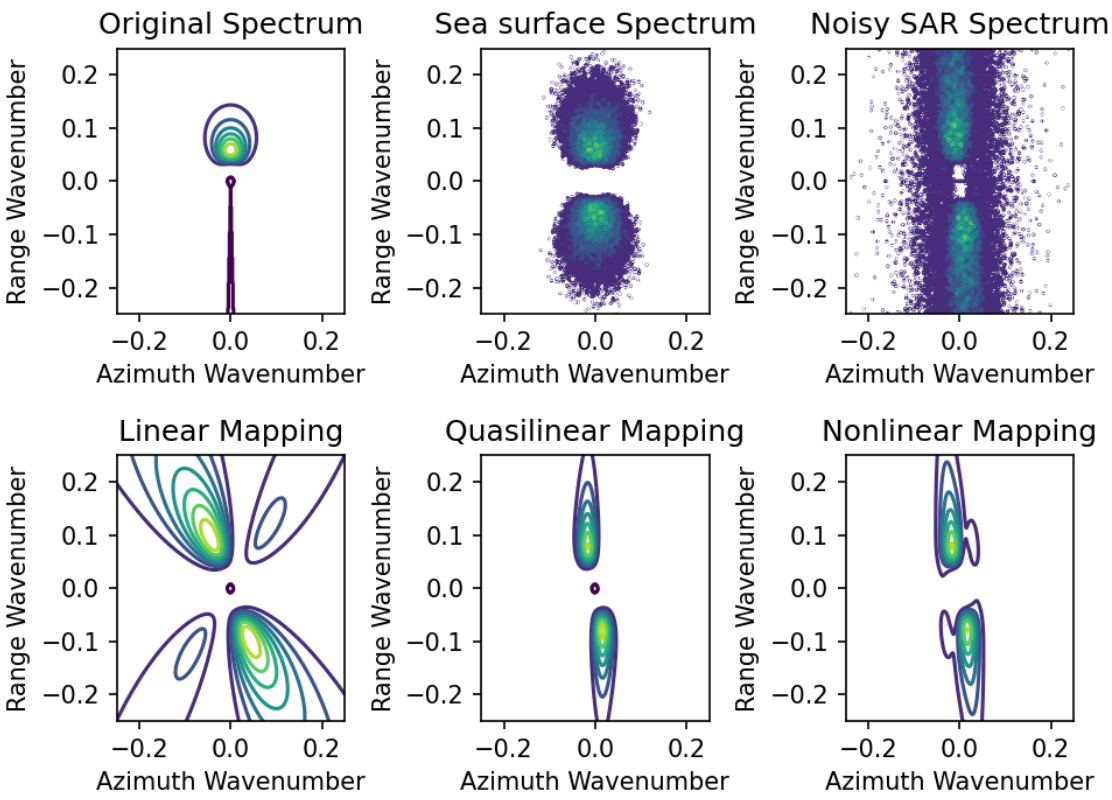

Figure A.34: Case A17 Plots of spectra

A.18 Case A18

Parameter	Value
Wind Speed	10 m/s
Wind Direction	90°
beta	100 s

Table A.18: Case A18 parameters

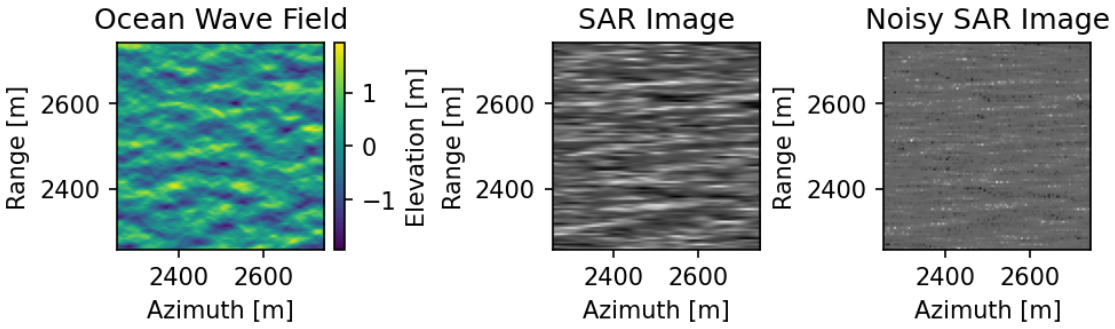

Figure A.35: Case A18 Ocean Surface with SAR Images

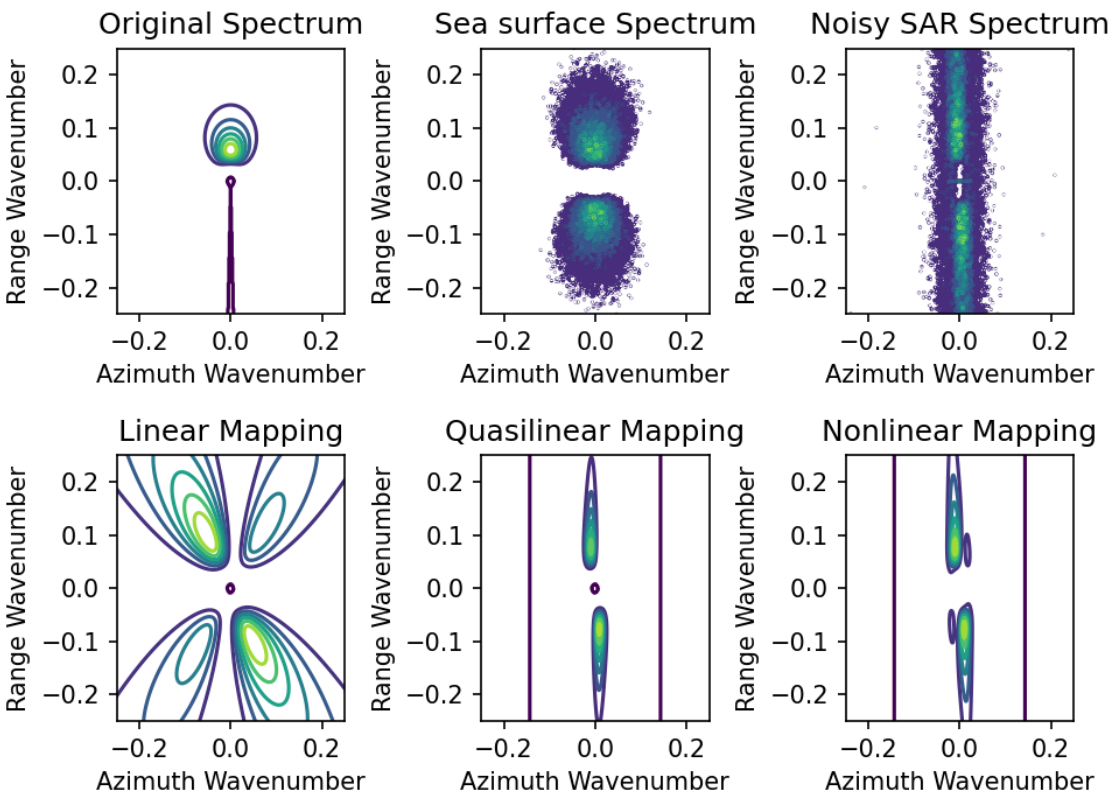

Figure A.36: Case A18 Plots of spectra

A.19 Case A19

Parameter	Value
Wind Speed	15 m/s
Wind Direction	0°
beta	10 s

Table A.19: Case A19 parameters

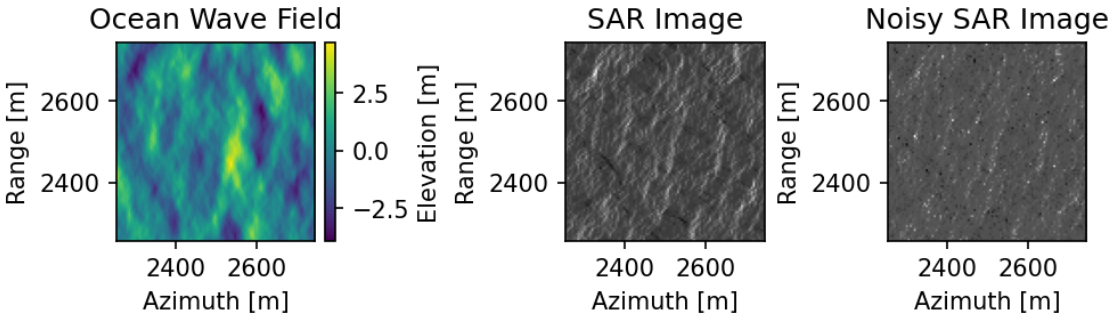

Figure A.37: Case A19 Ocean Surface with SAR Images

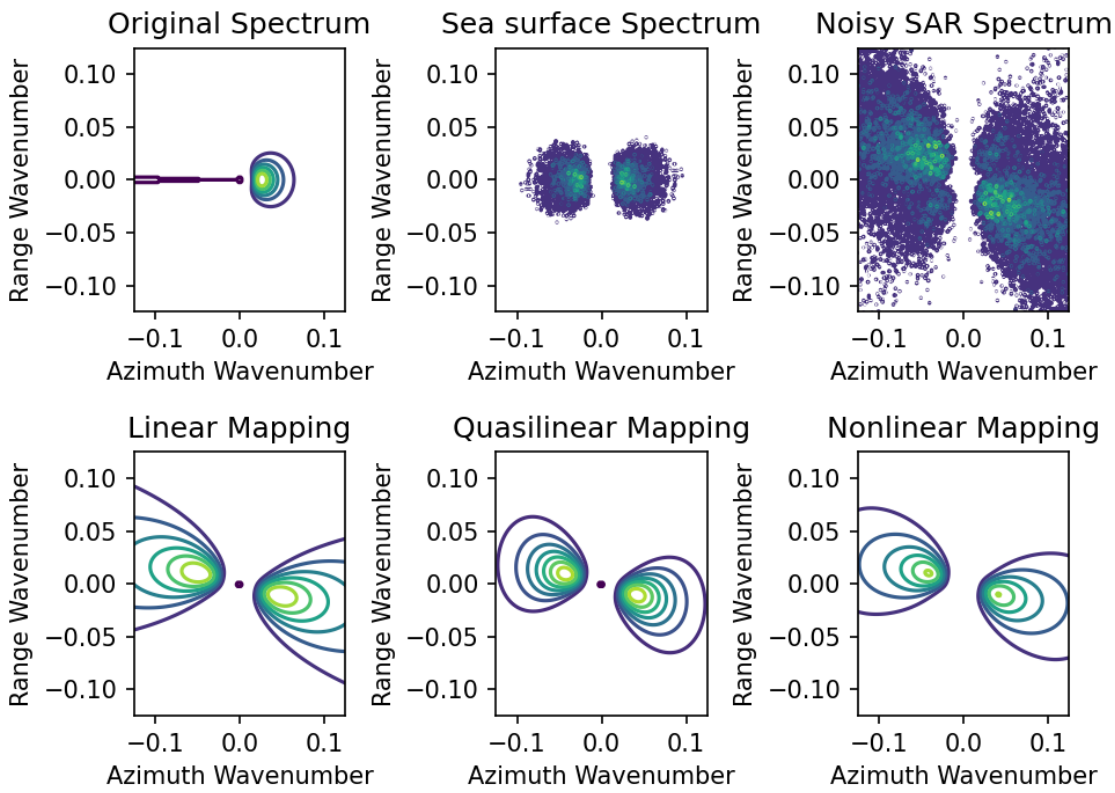

Figure A.38: Case A19 Plots of spectra

A.20 Case A20

Parameter	Value
Wind Speed	15 m/s
Wind Direction	0°
beta	50 s

Table A.20: Case A20 parameters

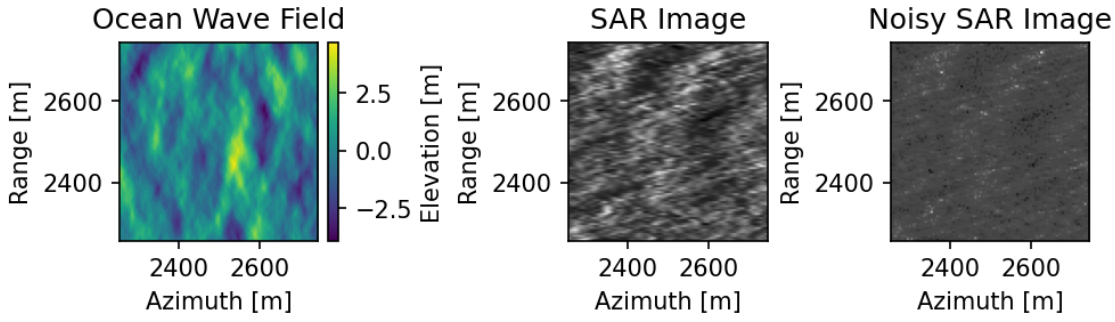

Figure A.39: Case A20 Ocean Surface with SAR Images

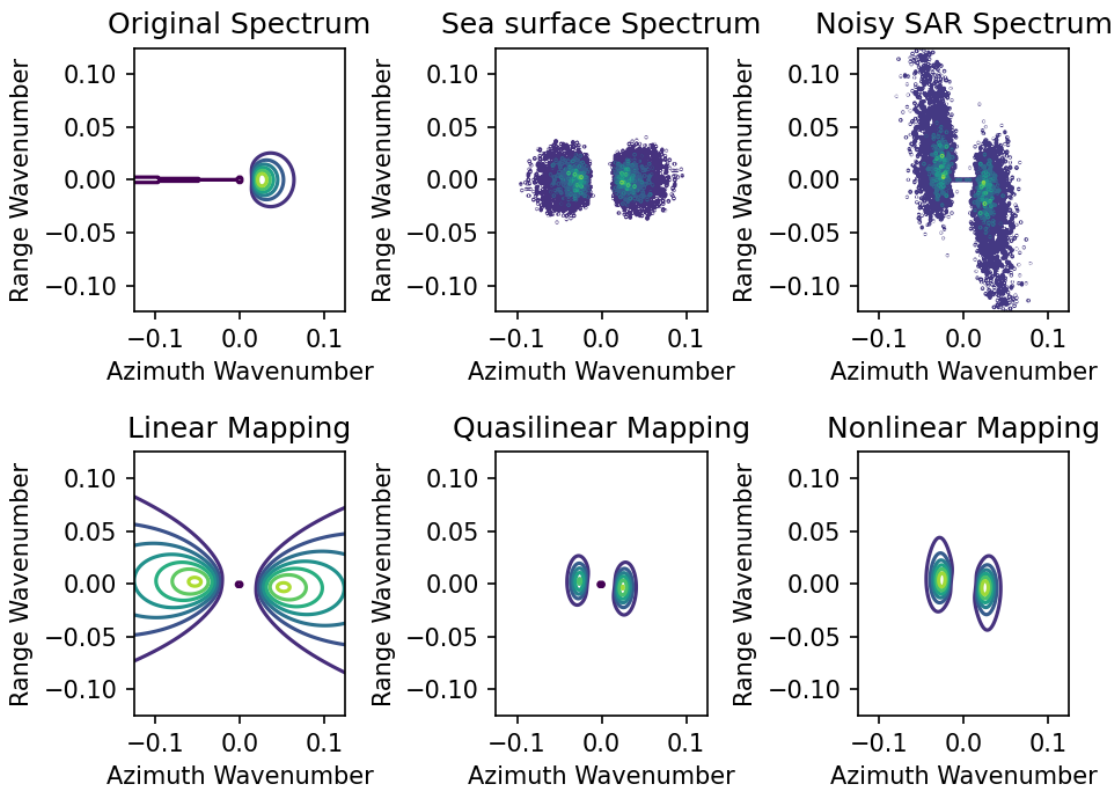

Figure A.40: Case A20 Plots of spectra

A.21 Case A21

Parameter	Value
Wind Speed	15 m/s
Wind Direction	0°
beta	100 s

Table A.21: Case A21 parameters

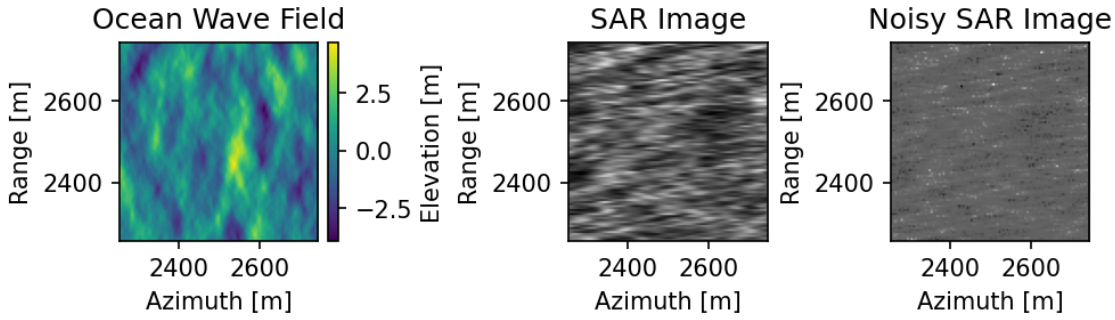

Figure A.41: Case A21 Ocean Surface with SAR Images

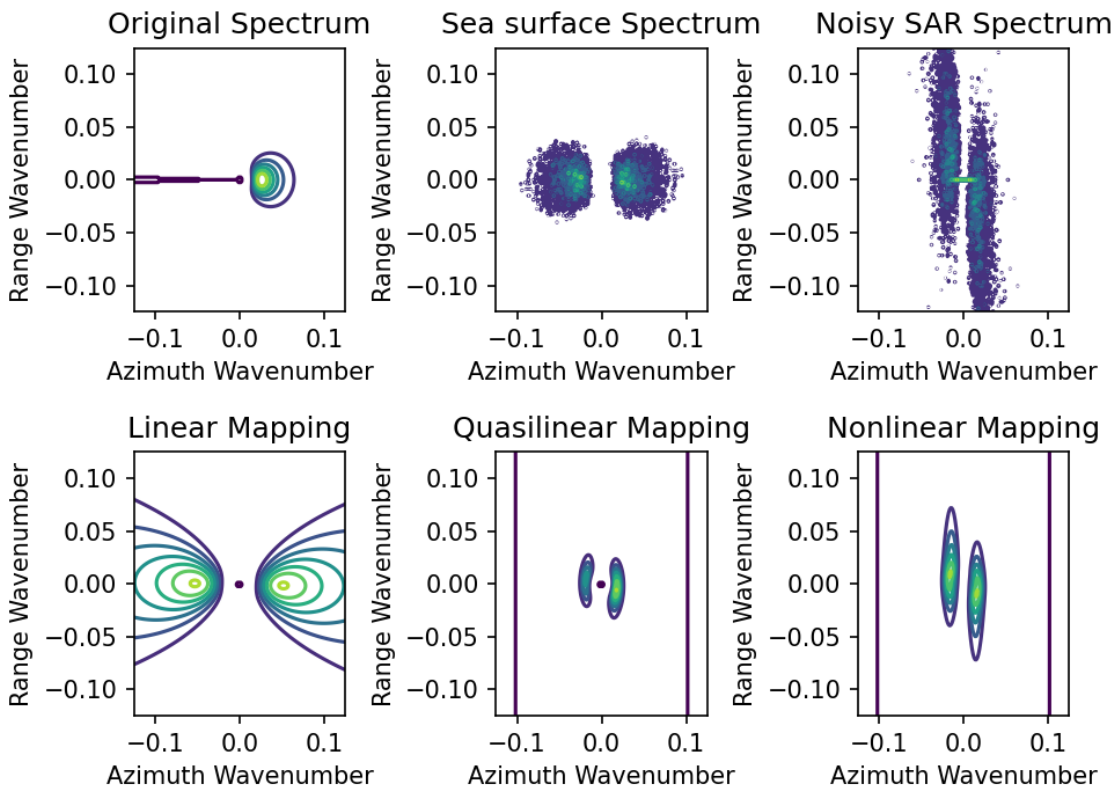

Figure A.42: Case A21 Plots of spectra

A.22 Case A22

Parameter	Value
Wind Speed	15 m/s
Wind Direction	45°
beta	10 s

Table A.22: Case A22 parameters

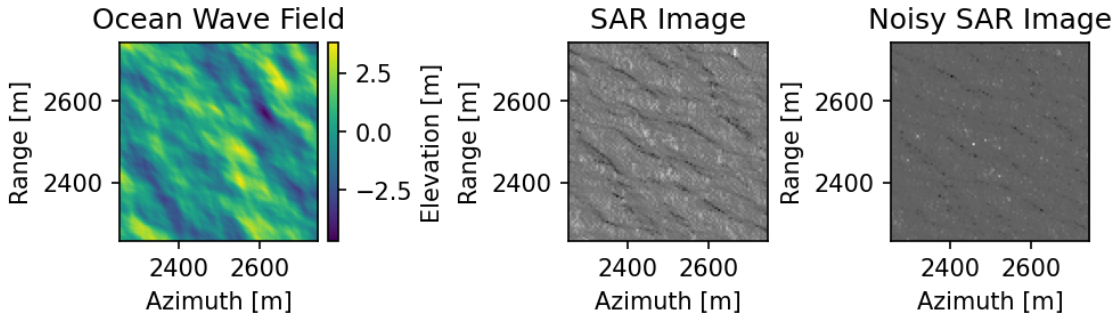

Figure A.43: Case A22 Ocean Surface with SAR Images

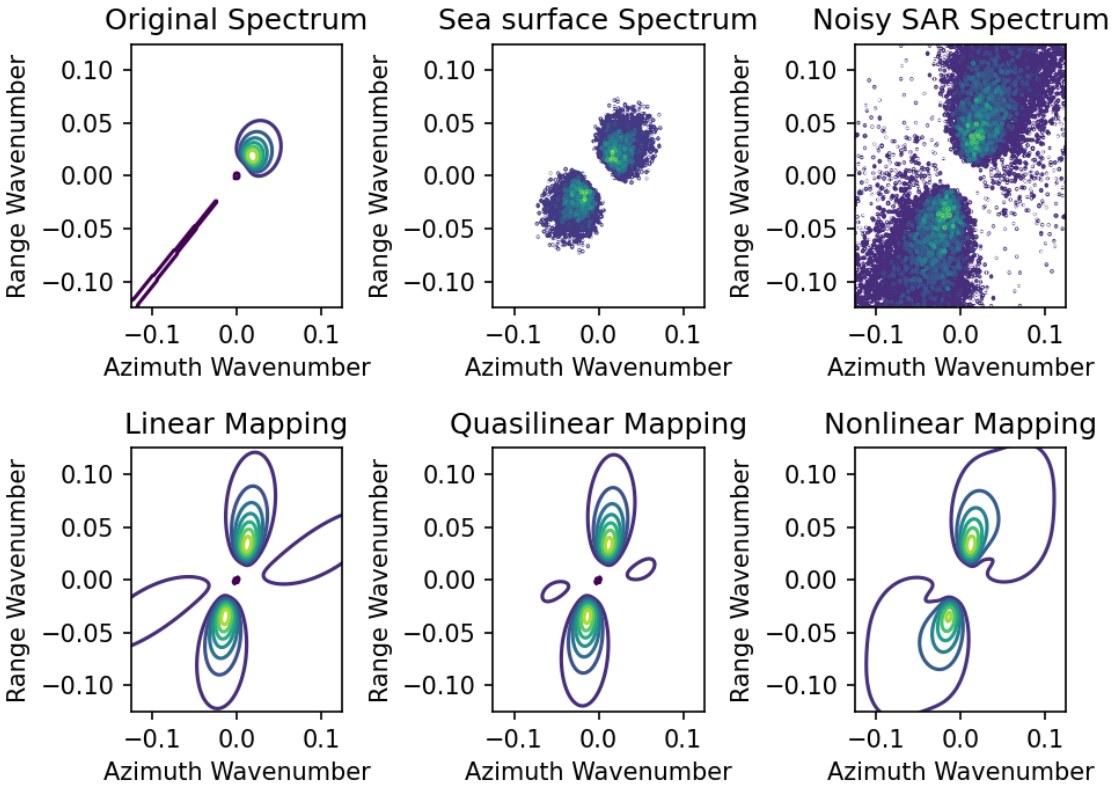

Figure A.44: Case A22 Plots of spectra

A.23 Case A23

Parameter	Value
Wind Speed	15 m/s
Wind Direction	45°
beta	50 s

Table A.23: Case A23 parameters

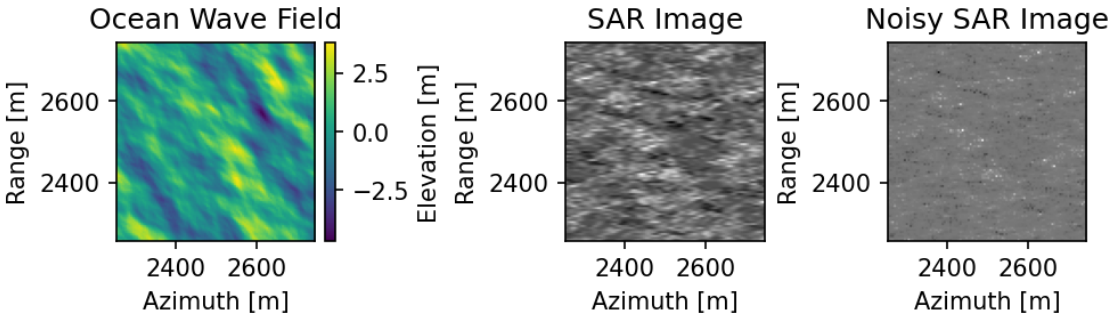

Figure A.45: Case A23 Ocean Surface with SAR Images

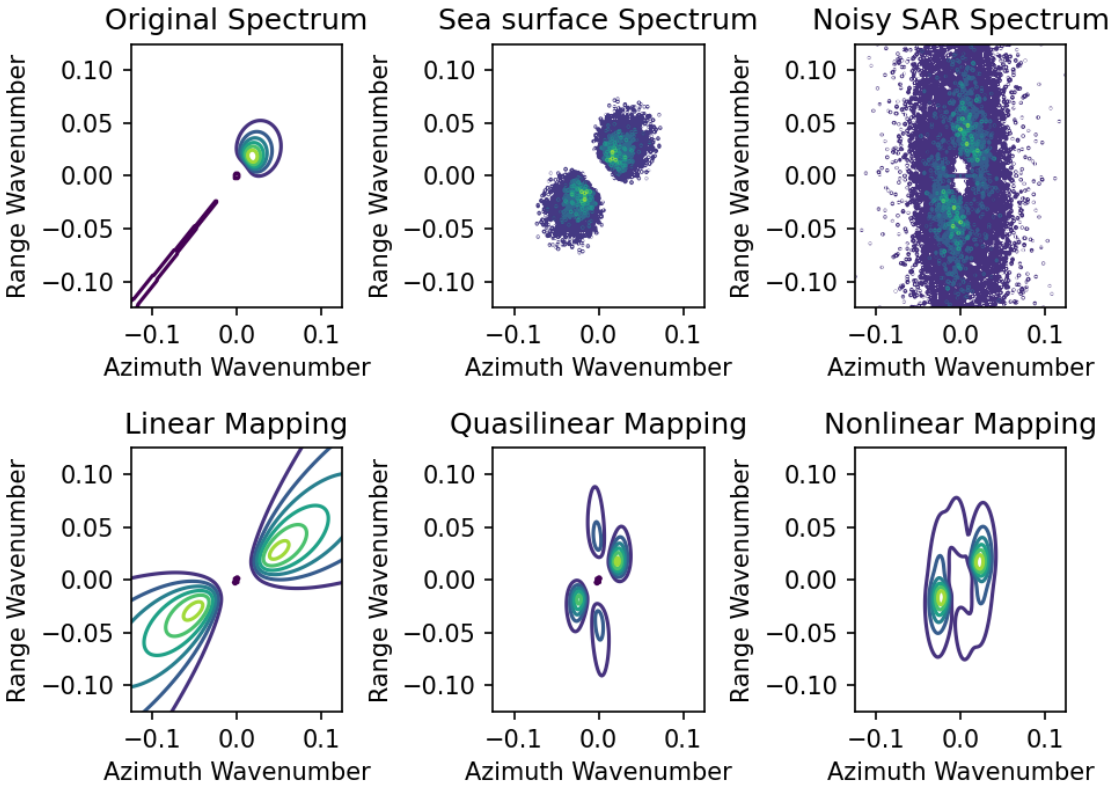

Figure A.46: Case A23 Plots of spectra

A.24 Case A24

Parameter	Value
Wind Speed	15 m/s
Wind Direction	45°
beta	100 s

Table A.24: Case A24 parameters

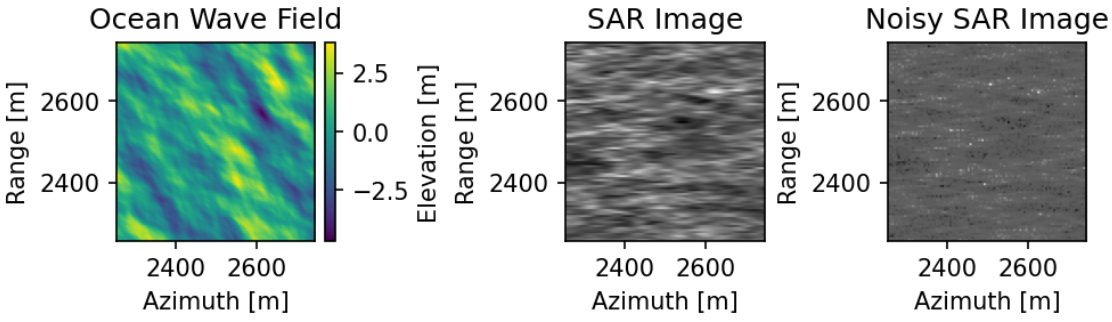

Figure A.47: Case A24 Ocean Surface with SAR Images

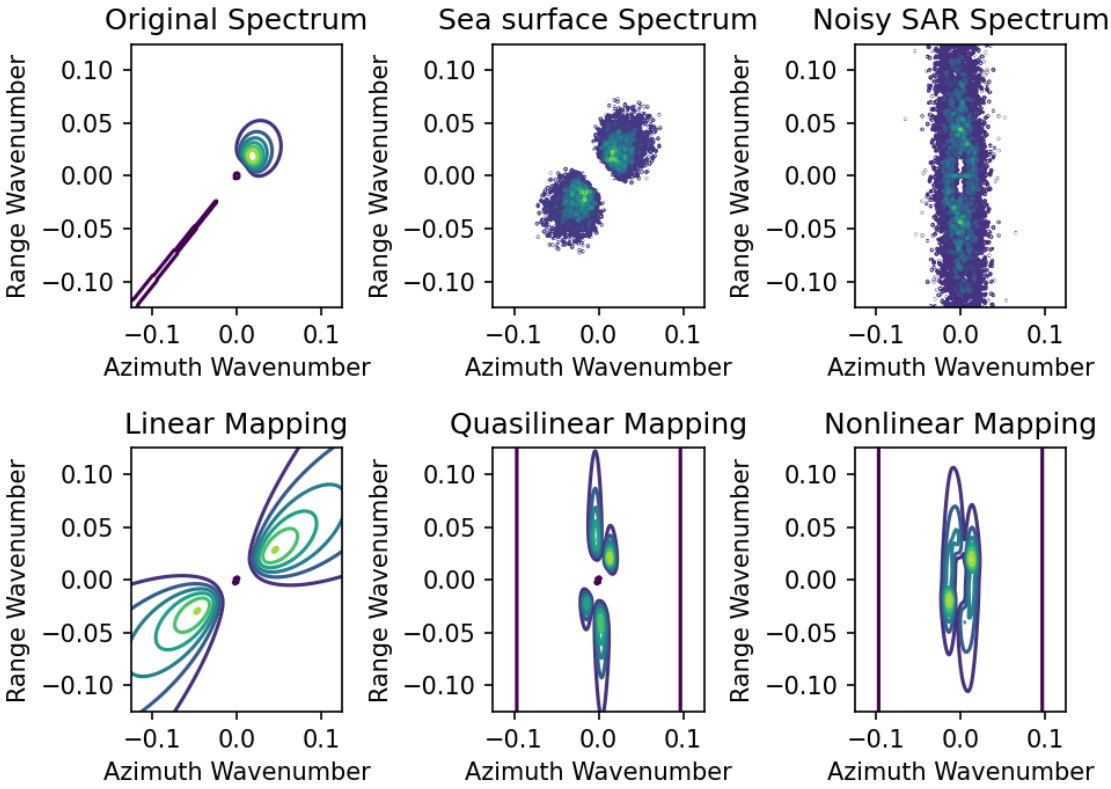

Figure A.48: Case A24 Plots of spectra

A.25 Case A25

Parameter	Value
Wind Speed	15 m/s
Wind Direction	90°
beta	10 s

Table A.25: Case A25 parameters

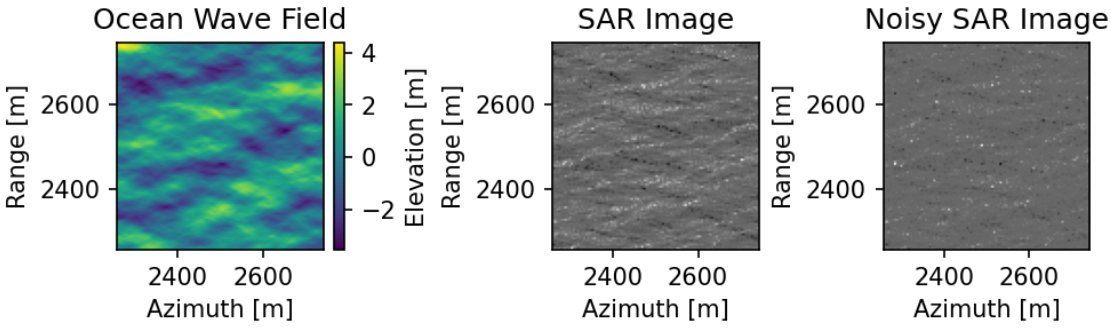

Figure A.49: Case A25 Ocean Surface with SAR Images

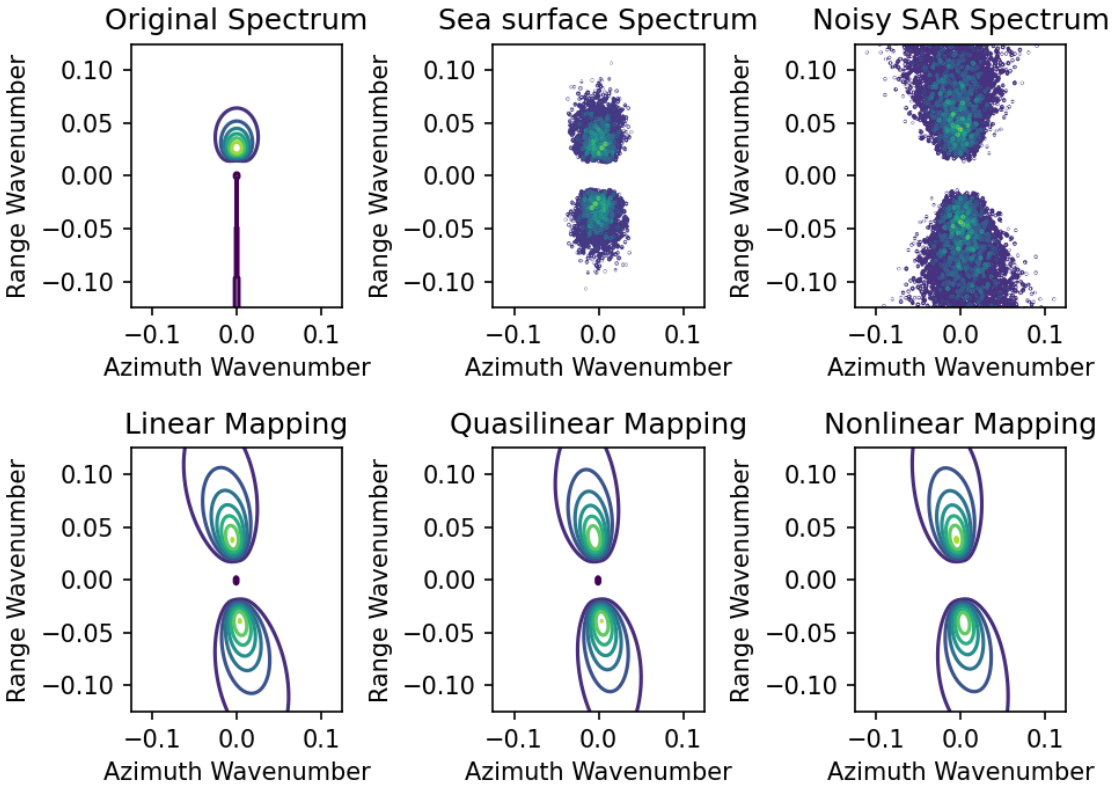

Figure A.50: Case A25 Plots of spectra

A.26 Case A26

Parameter	Value
Wind Speed	15 m/s
Wind Direction	90°
beta	50 s

Table A.26: Case A26 parameters

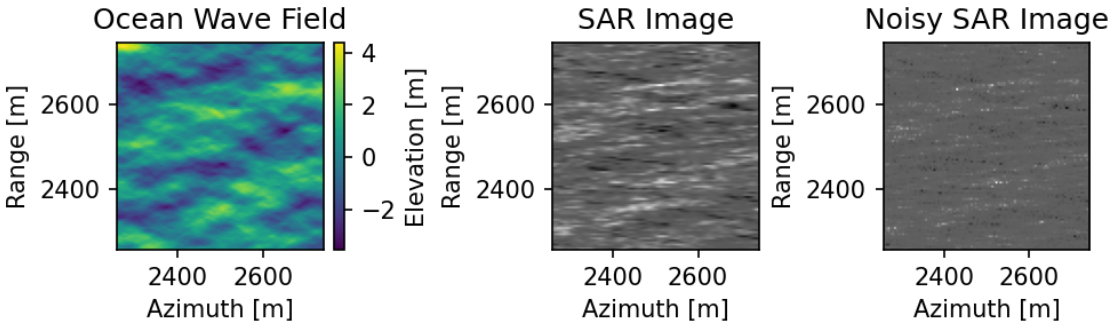

Figure A.51: Case A26 Ocean Surface with SAR Images

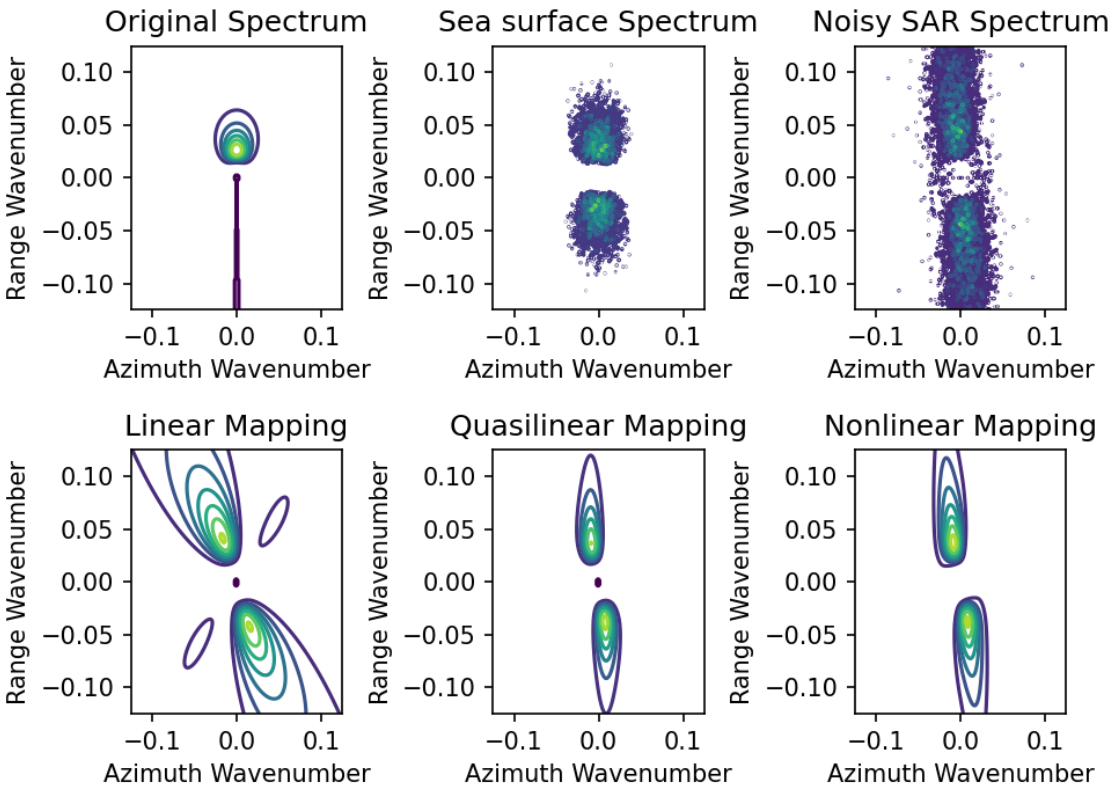

Figure A.52: Case A26 Plots of spectra

A.27 Case A27

Parameter	Value
Wind Speed	15 m/s
Wind Direction	90°
beta	100 s

Table A.27: Case A27 parameters

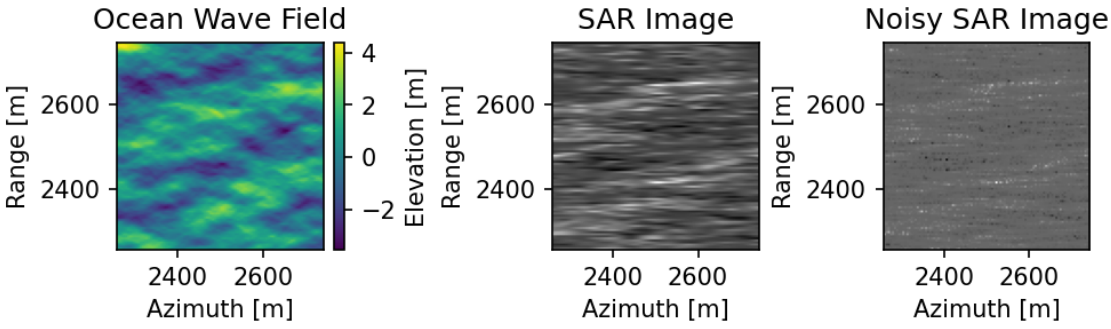

Figure A.53: Case A27 Ocean Surface with SAR Images

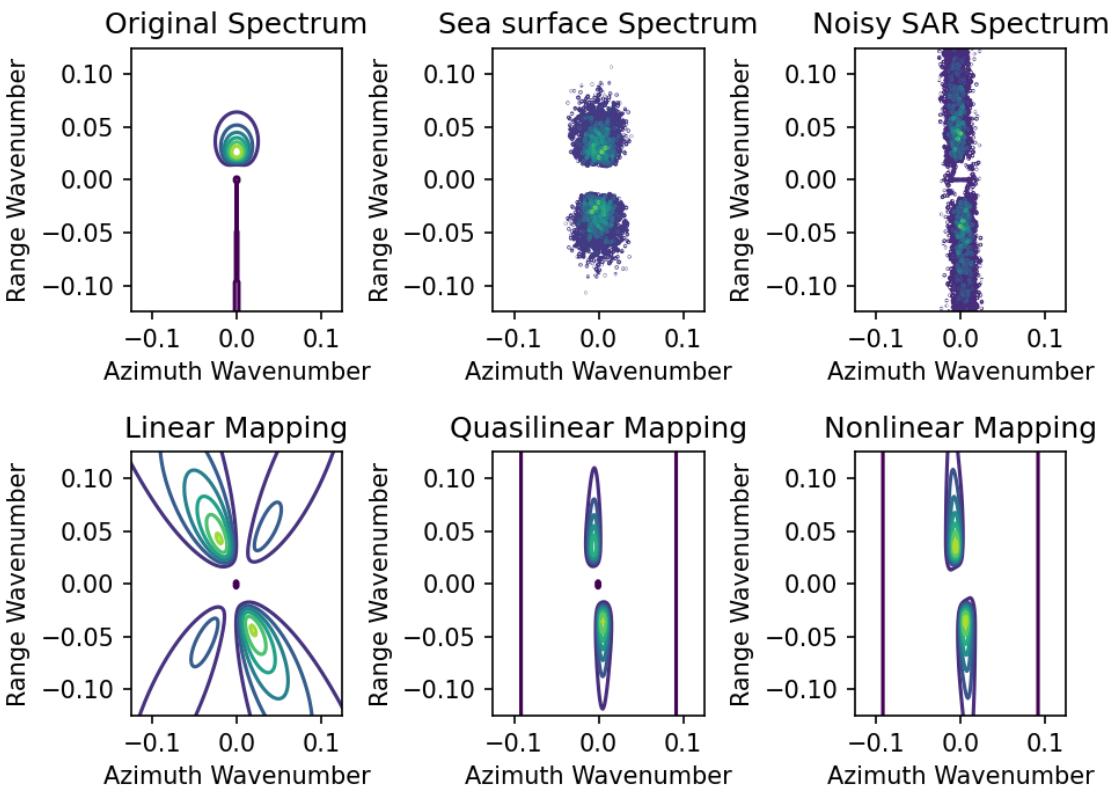

Figure A.54: Case A27 Plots of spectra

DEPARTMENT OF SPACE, EARTH AND ENVIRONMENT
CHALMERS UNIVERSITY OF TECHNOLOGY
Gothenburg, Sweden
www.chalmers.se

CHALMERS
UNIVERSITY OF TECHNOLOGY